Targeting ZAP-70 protein kinase in T-cell lymphoproliferative malignancies

Cristina Hernández Buñuel

UAB
Universitat Autònoma
de Barcelona

PhD in Medicine

Department of Medicine

Targeting ZAP-70 protein kinase in T-cell lymphoproliferative malignancies

Doctoral thesis presented by

Cristina Hernández Buñuel

To qualify for the degree of

Doctor

Supervisors

Dr. Francesc Bosch Albareda

Dr. Marta Crespo Maull

Tutor

Dr. Pere Barba Suñol

Barcelona, 2023

A mis padres. A mi hermana e Igor. A Hugo y David

‘If I die tomorrow, I will not regret it. I really did everything I could.’-

Freddie Mercury

Acknowledgements

Al reflexionar sobre las personas que han sido parte fundamental de esta etapa de mi vida, me encuentro profundamente agradecida por cada uno de ellos.

En primer lugar, quiero agradecer al Dr. Francesc Bosch y la Dra. Marta Crespo por haberme dado la oportunidad de formar parte del laboratorio de Hematología Experimental durante todos estos años. Gracias, Francesc, por haberme dado la oportunidad de trabajar en tu grupo de investigación. Gracias, Marta, por haberme enseñado que, con esfuerzo, dedicación y perseverancia, se puede conseguir todo lo que te propongas. Hoy estoy escribiendo estas palabras gracias a que me disteis una oportunidad.

En segundo lugar, quiero agradecer al Dr. Pau Abrisqueta, jefe del proyecto, por haber depositado su confianza en mí para formar parte de este proyecto, y al Dr. Pere Barba, mi tutor de tesis, por haber formado parte de este proyecto que me ha hecho crecer tanto personal como profesionalmente.

En cuarto lugar, quiero agradecer al grupo de Química Farmacéutica del IQS dirigido por el Dr. José Ignacio Borrel, especialmente a los Dr. Roger Estrada y Dr. Albert Gibert, porque sin vosotros no tendríamos los compuestos de mi tesis. Gracias por los consejos en las reuniones y por siempre querer ayudar. Gracias a Víctor, las manos que sintetizaron los compuestos y, a Ángel, por todo el trabajo en modelización.

Gracias a los compañeros del del servicio del módulo azul, CNAG, Luna y al Dr. Francesc Canals, por vuestra contribución al proyecto.

Pasamos ya a mis compañeros de batalla, mis compañeros del lab. En primer lugar, quiero agradecer a anteriores miembros del lab: Isabel, Juan, Lluis, Laura y Júlia. Ellos fueron los primeros mentores que tuve en el laboratorio. Sin duda, aprendí mucho de todos ellos. Especialmente quiero agradecer a Júlia por tu apoyo, escucha y consejo; eres un ejemplo de una gran compañera y persona. Gracias a Laura Palomo por siempre dar unos grandes consejos, por tu paciencia y escucha.

Entonces llegó Dani, para los amigos ¨Daliel¨, un gran compañero de trabajo, pareja de pádel, maestro de barbacoas...Hemos pasado por tantas cosas durante todos estos años. Estoy convencida de que algún día publicarás la lista de mis famosas frases, ¡quiero mi parte! Gracias por tu consejo, apoyo y por tantas risas.

Luego llegó Carlota, la reina de los ratolins y la más motomami del lab. Compañera de crio durante un tiempo, de risas, lloros, cafés (en vaso de cristal y con hielo en verano jaja). ¡Gracias por tantos buenos momentos!

Entonces hubo muchos cambios, mucha gente se fue, pero también vino gente maravillosa. Panagiota, even if you only stayed in the lab for a year, we learned a lot from you, personally and professionally. We are better friends with the Navios because of you. Thank you, Neha, for your clinical advice and for all the amazing candy you always brought to the lab. Soraya, gracias por tantas risas, por darnos nuestra dosis diaria de Wisi, lo echamos de menos por el lab.

Quiero agradecer especialmente a Gemma. No sé cómo agradecerte todo lo que me enseñaste con tus actos, tus palabras, siempre servicial, nunca una mala cara. Siempre con mil cosas, pero buscando un momento para ayudarnos a todos los del lab. ¡Qué suerte tuve de poder trabajar a tu lado y aprender tanto de ti! Eres una súper profesional y una super mamá.

Quiero también agradecer a antiguos estudiantes Oriol, Pablo, María, Belén, Jose, entre tantos otros, por haber formado parte de este camino. Especialmente quiero agradecer a Cecilia, mi estudiante de TFG, de ti aprendí lo que implica ser una mánager, lo que requiere organizar el trabajo de otra persona además del propio. Fuiste una gran estudiante. Nunca olvidaré el regalo de despedida que me hiciste, ZAPI ha crecido un montón. Gracias Marina por todos esos cafés que nos hemos tomado juntas, tantas risas y apoyo que nos hemos dado.

Y ya pasamos a los miembros actuales del lab: Patri, Iñaki, Mayte, Sofía, Claudia y Laura. Gracias Iñaki por tu consejo y escucha. Gracias a Patri, Mayte, Sofía y Claudia por vuestro apoyo, sin duda alguna, me siento mayor cuando os oigo hablar de redes sociales que no sabía ni que existiesen jajaj. Sois la próxima generación del lab, os deseo mucha suerte y que disfrutéis mucho de esta etapa.

Laura, Lauri, mi escucha incansable, consejera, compañera de risas, cenitas y esperemos que alguna excursión jajaj. Sin duda, tu apoyo durante este último año de tesis ha sido crucial para mi salud mental. Eres una gran compañera y amiga.

Quiero agradecer a la Dra. Teresa Palomero por haberme dado la oportunidad de hacer la estancia de tesis en su laboratorio y por haberme abierto las puertas de su laboratorio desde el primer momento. Gracias, Teresa, por tu escucha y consejo. Fueron tres meses, pero, sin duda, aprendí muchísimo de ti, tanto personal como profesionalmente.

I would also like to thank Anouchka, mi ride or die, and the proud owner of my furry nephew, baby Pongo. Meeting you was undoubtedly one of the highlights of my PhD journey, as you were incredibly welcoming from the very first

moment I sat behind you. Although three months were not sufficient to learn as much as I would have wanted from you, I know we have our whole lives as I am proud to call you a friend. Your invaluable advice guided me through some tough days. I miss our endless laughter during coffee breaks, in the TC room, or late in the evening leaving the lab.

Thank you, Hannah, for making daily life in the lab as smooth as possible. I miss our lunchtime discussions, whether it was going through TV shows episodes, sharing tourist recommendations, or simply talking about life. Gracias, Clara, una super mami y super científica, por tu amabilidad, paciencia, consejo y escucha. Thank you to the rest of the lab members, Bobby, Kalay, Ryan, Cindy, and Wendy, all of whom are excellent researchers. Thank you for explaining to me your projects and always being willing to help me.

A lo largo de estos años he tenido la suerte de compartir muchos momentos con grandes personas de otros grupos de investigación del VHIO, sin los cuales, no habría podido llegar donde estoy.

No puedo empezar esta parte si no es con Carlota. Sin duda, otro de los grandes descubrimientos de esta etapa profesional. Mi gran apoyo en el trabajo y en la vida, continuamente me demuestras que eres una gran amiga. Has estado a mi lado en los momentos más duros durante esta etapa, pero también en los mejores. ¡El viaje a NY lo recordaremos para siempre! Hemos vivido tantas cosas juntas… nuestra pasión por la pintura, las plantas, las plantas, (que quede claro que nos gustan las plantas jaja), la comida, las risas, cualquier plan es bueno a tu lado. Eres una gran profesional, ¡te admiro mucha amiga! Gracias a Ana y Alma por los momentos tan divertidos que hemos vivido, especialmente este año, con algunas lesiones en el humor amarillo y dándolo todo en el pádel.

Gracias a cada uno de los miembros del lab JVN, Mireia, Carla, Jose Ángel, Paula, Marina, y Joan por ser los mejores vecinos que se pueden tener, siempre ayudándonos con lo que necesitamos. Gracias Chiara, por todo el apoyo que me diste durante todos estos años, por todas las risas en cultis, consejos, hablando de todo y de nada. Gracias, Marta, por tantos cafés y risas que compartimos durante tu etapa en VHIO.

Gracias María por alegrarnos cada tarde con tu sentido del humor, eres de esas personas cuya ausencia se nota. Gracias por tu apoyo y cariño durante todos estos años.

Pasamos a nuestros otros vecinos, los ITAG. Gracias a todos los miembros del lab por haberme ayudado siempre que lo he necesitado. Especialmente quiero agradecer a Anna, Judit, María, Andrea y Albert. Anna, ¡amiga! Nos conocemos desde el máster y siempre has sido uno de mis pilares en VHIO. Siempre dispuesta a ayudarme y aconsejarme, gracias por todo, vales oro. Judit, te conozco desde el

primer día que llegaste a VHIO y, sin duda, has sido un gran apoyo. Gracias a María y Andrea, especialmente en este último año, por tantos consejos y escucha que me habéis dado. Albert, el rey de cultis, gracias por tantas risas por las tardes haciendo la crio.

A los antiguos miembros de la cuarta planta, los MAL, Elena, Olga, Marion, Alba, Iñaki, Emmanuela y Lluis, gracias por siempre estar dispuestos a ayudarme. Especialmente quiero mencionar a Alba y Marion, por tantos momentos compartidos mano a mano en cultis, la terapia estaba garantizada. Gracias por siempre escucharme y aconsejarme.

No me olvido de Andrea H, mi compi de aventuras, sin duda otro gran descubrimiento post-COVID. ¡Te admiro mucho, amiga! Tienes un corazón muy grande y lo compartes con todo el mundo y tu trabajo. Tengo la suerte de tenerte en mi vida y de tomar unos cafés muy divertidos poniéndonos al día, jaja. Gracias a Flami y Laia, por vuestro apoyo y ayuda durante esta etapa. No me olvido del resto de personas de la cuarta planta y de otras porque de una manera u otra habéis hecho de esta etapa, una muy especial.

Antes de agradecer individualmente a las personas más importantes de mi vida, mi familia, quiero que quien esté leyendo este texto sepa lo afortunada que soy de tener a cada uno de los miembros de mi familia, ya que cada uno me ha enseñado la importancia de estar presente, de ser generosa y de que todo sacrificio tiene su recompensa. No estaría donde estoy ahora sin todos vosotros.

A mis pilares, mi madre y mi padre, sin los cuales no sería como soy. Gracias por vuestro apoyo incondicional y escucha infinita. Para mí, sois un ejemplo que seguir en todos los aspectos. Gracias por enseñarme con vuestro ejemplo que, con trabajo y esfuerzo puedo conseguir todo lo que me proponga. A mi madre por ser mi roca, por todos los consejos que me has dado, por todo lo que he aprendido de ti y lo que me queda por aprender. Gracias por aguantar mis miles de llamadas en momentos duros, sin importar la hora. A mi padre, por enseñarme que, en la vida hay que ser como un junco, fuerte pero flexible frente a las adversidades. Vosotros me habéis mantenido a flote en los momentos más duros y habéis celebrado las mejores victorias. Os quiero mucho.

A mi hermana María, mi segunda madre y un ejemplo a seguir. Gracias por abrirme los ojos cuando más lo necesitaba y menos quería. Por siempre estar presente en mi vida, por lo cual soy una afortunada. A Igor, diría que uno de mis primeros recuerdos de la infancia fue cuando me enseñaste a leer la hora en un reloj, te conozco desde que tengo consciencia. Gracias a ambos por vuestro apoyo durante estos años, por siempre tener un consejo que darme o simplemente escucharme. No podía acabar este párrafo sin agradeceros el haberme dado el mejor regalo que jamás hubiera podido pedir, mis sobrinos Hugo y David.

A Hugo y David, mis amores, mis enanos, mis chicos. Ya son casi 9 años a vuestro lado. Vuestra tita Cris cambió mucho en cuanto vio vuestras caritas un 27 de noviembre de madrugada. Veros crecer, vuestros primeros pasos, primeras

sonrisas, la primera vez que dijisteis mi nombre. Son esos momentos que me enseñan lo importante en la vida, vosotros sois sin duda mi motor. Tal vez cuando seáis mayores os leeréis el libro de la tita Cris, aquí estaré para responderos a cualquier pregunta que tengáis. Os quiero infinito.

A mi tía Rosa, una mujer fuerte, una confidente, un gran ejemplo a seguir, me has enseñado que ser independiente significa ser feliz con una misma. Siempre tienes un buen consejo que me voy guardando en un baúl para cuando más los necesito. A mis primas Ana y Leticia, nos hemos criado juntas y no podemos ser más diferentes, pero sé que siempre estaremos presentes en la vida de las otras. A Yeison y Rubén, sin vosotros tampoco tendría otro de los mejores regalos de mi vida, mis sobrinas Anahí y Valentina. Espero ser un modelo que seguir para ellas cuando sean mayores. Gracias, Xabi y Arancha por vuestro apoyo durante estos años.

A mi abuela Pacita, la roca de la familia que nos crió a todas con esfuerzo, carácter y fuerza. Jamás probaré unas mejores croquetas ni tartas de nata de cumpleaños, como las que hacías, Yaya. A mi abuelo Pepe, por inculcarme el amor por los animales, inseparable de sus perritos Rex y Rudolf. A mis abuelos Josefina y Marcos, gracias por darme al mejor padre que nadie pudiera pedir. En este día tan especial, sé que todos estáis conmigo mirando desde arriba. Os echo de menos y os quiero mucho.

A José Manuel y Mercedes, no podía excluirlos de este apartado, vosotros sois familia elegida. Sois un gran ejemplo de humildad y excelencia, tanto en lo personal como en lo profesional. Me siento muy afortunada de teneros en mi vida. A Íñigo y Merceditas, vuestros hijos, los cuales son grandes personas y sé que llegarán muy lejos.

Me doy cuenta de que tengo a muchas Andreas en mi vida, pero ninguna como mi Andrius, mi amore, mi mejor amiga desde la universidad. La que ha estado en todas las etapas de mi vida. ¡Qué suerte tengo de tenerte en mi vida, amiga! La persona más generosa, cariñosa y paciente. ¡Te admiro mucho, amiga!

Sin duda otro de los grandes descubrimientos post-COVID ha sido Sara. ¡Qué afortunada soy de tenerte en mi vida! Cada vez que hablo contigo, me das una lección de vida. De mayor espero ser capaz de poder vivir con la misma libertad y pasión que me demuestras cada día. Gracias por escucharme siempre. Gracias a mi maño, mi amigo desde que tengo uso de razón. Gracias por apoyarme y siempre sacarme una sonrisa. A mis amigas Cris y Paloma, nos conocemos desde el máster y, aunque cueste vernos, siempre compartimos grandes momentos juntas. Gracias Marina por el apoyo, las risas que nos hemos echado durante los viajes, el pádel, conciertos.

Como podéis ver, esta tesis tiene muchos coautores. Me siento muy agradecida por cada uno de vosotros. ¡Ahora empieza una nueva etapa!

List of Abbreviations

0-9

6-MP	6-mercaptopurine

A

A+CHOP	Brentuximab vedotin, cyclophosphamide, doxorubicin, prednisone
ABL1	ABL proto-oncogene 1
ADAP	Adhesion- and degranulation-promoting adaptor protein
AITL	Angioimmunoblastic T-cell lymphoma
AKT	PI3K-serine/threonine kinase
ALCL	Anaplastic large cell lymphoma
ALK	Anaplastic lymphoma kinase
AP-1	Activator protein 1
APC	Antigen presenting cell
ASCT	Autologous stem cell transplant
AYA	Adolescent and young adult

B

BCL-xL	B-cell lymphoma extra-large
BCL11B	BCL11 transcription factor B
BCL2	B-cell lymphoma 2
BCR	B-cell receptor
BFM	Berlin-Frankfurt-Münster
BLI	Bioluminiscence
BM	Bone marrow
BR	Broad range

C

CAC	Clinical advisory committee
CAR	Chimeric antigen receptor
CCR7	C-C chemokine receptor type 7
CDK4/6	Cyclin-dependent kinase 4/6

CDKN2A/B	Cyclin-dependent kinase inhibitor 2A/B
CHIP	Clonal hematopoiesis of indeterminate potential
CHOP	Cyclophosphamide, doxorubicin, vincristine, prednisone
CLL	Chronic lymphocytic leukemia
CLP	Common lymphoid progenitor
CMP	Common myeloid progenitor
CNS	Central nervous system
COMPLETE	Comprehensive Oncology Measures for Peripheral T-cell lymphoma treatment
CTCL	Cutaneous T-cell lymphoma
CTLA-4	Cytotoxic T-lymphocyte-associated protein 4

D

DA-EPOCH	Dose-adjusted etoposide, prednisone, vincristine, cyclophosphamide, doxorubicin
DAG	Diacyl glycerol
DN	Double-negative
DNMT3A	DNA methyltransferase 3 alpha
DOR	Duration of response
DP	Double-positive
DFS	Disease-free survival
DUSP22	Dual specificity protein phosphatase 22

E

EBV	Epstein-Barr virus
EFGR	Epidermal growth factor receptor
EMA	European Medicines Agency
ER	Endoplasmic reticulum
ERK1/2	RAS-extracellular signal-regulated kinase 1/2
ETP	Early T-cell precursor
ETV6	ETS variant transcription factor 6

F

FBS	Fetal bovine serum
FBXW7	F-box and WD repeat domain containing 7
FDA	Food and Drug Administration

G

GADs	GRB-2 related adapter protein 2
GATA3	GATA 3 binding protein
GEP	Gene expression profile
GRB-2	Growth factor receptor-bound protein 2
GSEA	Gene set enrichment analysis
GSI	Gamma-secretase inhibitor
GTP	Guanosine triphosphate
GZB	Granzyme B

H

HDAC	Histone deacetylase
HLA	Human leukocyte antigen
HRP	Horseradish Peroxidase
HSC	Hematopoietic stem cell
HSPC	Hematopoietic stem and progenitor cell
HTLV-1	Human T-lymphotropic virus type-1
HyperCVAD	Cyclophosphamide, vincristine, doxorubicin, dexamethasone-alternating with methotrexate and cytarabine

I

ICC	International consensus classification
ICOS	Inducible T-cell co-stimulator
IDH2	Isocitrate dehydrogenase (NADP+) 2
IFNγ	Interferon gamma
IGHV	Immunoglobulin heavy chain
IgM	Immunoglobulin M
IHQ	Immunohistochemistry
IL	Interleukin
IP3	Inositol triphosphate
IPI	International prognostic index
ITAM	Immunoreceptor tyrosine-based activation motif
ITK	Interleukin-2-inducible T-cell kinase

J

JAK	Janus kinase

K

KDM6A	Lysine demethylase 6A
KHDRBS1	KH domain-containing, RNA binding, signal transduction-associated protein 1

L

LAT	Linker for activation of T cells
LCK	Lymphocyte cell-specific kinase
LT-HSC	Long-term hematopoietic stem cell

M

MALT	Mucosa-associated lymphoid tissue
MDACC	MD Anderson Cancer Center
MF	Mycosis fungoides
MHC	Major histocompatibility complex
MPP	Multipotent progenitor
MS	Mass spectrometer
mTOR	Mammalian target of rapamycin
MYO1F	Myosin 1F
m/z	Mass-to-charge ratio

N

NCK1	NCK adaptor protein 1
NF-κB	Nuclear factor kappa-light-chain-enhancer of activated B cells
NFAT	Nuclear factor of activated T cells
NHL	Non-Hodgkin lymphoma
NK	Natural killer
NKTCL	NK/T-cell lymphoma
NOTCH	Neurogenic locus homolog protein
NPM	Nucleophosmin
nTFHL-AI	Nodal T-follicular helper cell lymphoma, angioimmunoblastic-type
nTFHL-F	Nodal T-follicular helper cell lymphoma, follicular-type
nTFHL-NOS	Nodal T-follicular helper cell lymphoma, not otherwise specified
NUP214	Nucleoporin 214

O

OECD	Organization for Economic Cooperation and Development
ORR	Overall response rate
OS	Overall survival

P

PCA	Principal component analysis
PDK1	Pyruvate dehydrogenase kinase 1
PEI	Poliethyleneimine
PFS	Progression-free survival
PHF6	PHF finger protein 6
PI	Propidium iodide
PI3K	phosphatidylinositol-3-kinase
PIP2	Phosphatidylinositol 4,5-biphosphate
PIP3	Phosphatidylinositol 3,4,5-triphosphate
PLCγ1	Phospholipase gamma 1
PR	Partial response
PRC2	Polycomb repressive complex 2
PTCL, NOS	Peripheral T-cell lymphoma, not otherwise specified
PTEN	Phosphatase and tensin homolog

R

r/r	Refractory or relapsed
RAS	Rat sarcoma
RASGRP1	RAS guanyl nucleotide-releasing protein
REAL	Revised European-American Classification of Lymphoid Neoplasms
RHOA	Ras homology family member A
Ro	Romidepsin
ROS1	ROS proto-oncogene 1
RP-LC-MS	Reversed-phase liquid chromatography-tandem mass spectrometry
RUNX1	RUNX family transcription factor 1

S

SH2	Src homology domain
shRNA	Short-hairpin RNA

SLO	Secondary lymphoid organs
SLP-76	SH2 domain-containing leukocyte protein of 76 kDa
SOS	Son of sevenless
SP	Single-positive
Src	Src proto-onocogene
SS	Sézary syndrome
ST-HSC	Short-term hematopoietic stem cells
STAT3	Signal transducer and activator of transcription 3
STR	Short tandem repeat

T

T-ALL	T-cell acute lymphoblastic leukemia
TBX-21	T-box-21 protein
TCL	T-cell lymphoma
TCR	T-cell receptor
TET2	Tet methylcytosine dioxygenase 2
TFH	T-follicular helper
Th	T-helper CD4+ cell
TP53	Tumor protein 53
TP63	Tumor protein 63
TRAF3IP2	TRAF3 interacting protein 2
TYK2	Tyrosine kinase 2

V

VAV1	Vav guanine nucleotide exchange factor 1

W

WHO	World Health Organization

Z

ZAP-70	Zeta-chain-associated protein kinase 70

Index

Summary

The biological and clinical heterogeneity within T-cell malignancies presents a significant challenge in developing effective treatments, particularly given the limited efficacy of first-line anthracycline-based chemotherapy. These malignancies often exhibit epigenetic dysregulation and mutations in the T-cell receptor (TCR) signaling pathways. However, the rarity of these mutations has hindered the development of targeted therapies, necessitating more precise and effective therapies. Zeta-chain-associated protein kinase 70 (ZAP-70), a cytoplasmic tyrosine kinase predominantly expressed in T cells, plays a crucial role in proximal TCR signaling—an essential pathway for the survival and growth of T cells. Remarkably, heightened ZAP-70 expression has been detected in certain T-cell malignancies, and genetic ZAP-70 knockdown has been shown to impact malignant T-cell proliferation and induce apoptosis. Altogether, these results suggest a role of ZAP-70 in mediating T-cell malignancy progression.

Consequently, we aimed to develop pharmacological ZAP-70 inhibitors and evaluated their effect on malignant T-cell lines. After the *in vitro* screening of the kinase inhibition profile of 27 ZAP-70 candidate inhibitors against 26 kinases, we identified two promising small-molecule ZAP-70 kinase inhibitors, IQS117 and IQS141. These compounds demonstrated robust inhibition of approximately 90% of ZAP-70 kinase activity with off-targets residual kinase activity remaining above 20%. Subsequent *in vitro* studies in OCI-Ly13.2, Jurkat and T8ML-1 cell lines, representing distinct T-cell malignancy subtypes, unveiled a dose-dependent inhibition of both proliferation and viability, with cell lines tending to being more sensitive to IQS117. Additionally, both compounds exhibited dose-dependent inhibition of key TCR signaling molecules in Jurkat and OCI-Ly13.2 cell lines, including ZAP-70, LAT, SLP-76, PLCγ1, and ERK1/2. Notably, unlike IQS141, IQS117 also demonstrated inhibitory effects on AKT, potentially contributing to its enhanced effectiveness on decreasing cell proliferation and viability.

Our subsequent *in vivo* investigations with IQS117 and IQS141 in immunodeficient mice at a dose of 300 mg/kg, revealed no detectable acute toxicity effects through oral and intraperitoneal administration. Further pharmacokinetic analysis at a dose of 50 mg/kg indicated a prolonged half-life for

both ZAP-70 inhibitors following oral administration, establishing this as the best route for subsequent pharmacological assessment in xenograft models of malignant T-cell lines. Nonetheless, subcutaneous and intravenous xenograft models of malignant T-cells treated with IQS117 and IQS141 displayed no significant impact on tumor growth or survival. Additionally, transcriptome analysis of subcutaneous tumors following a seven-day treatment with IQS117 and IQS141 did not reveal specific ZAP-70 inhibition-associated changes, raising concerns about the delivery of these drugs to the tumor site and would require further validation.

Collectively, our results underscore the potential of ZAP-70 inhibition as a therapeutic approach for T-cell malignancies, while emphasizing the critical need for optimizing IQS117 and IQS141 drug delivery to the tumor site.

Resumen

La heterogeneidad biológica y clínica en las neoplasias linfoides de células T representa un desafío importante en el desarrollo de tratamientos efectivos, especialmente dada la limitada eficacia de la quimioterapia basada en antraciclinas de primera línea. Estas neoplasias a menudo muestran desregulación epigenética y mutaciones en las vías de señalización del receptor de células T (TCR). Sin embargo, la baja frecuencia de estas mutaciones ha obstaculizado el desarrollo de terapias dirigidas, lo que hace necesario buscar terapias más precisas y efectivas. La proteína quinasa 70 asociada a la cadena zeta (ZAP-70), una tirosina quinasa citoplasmática expresada predominantemente en células T, desempeña un papel crucial en la señalización proximal del TCR— una vía esencial para la supervivencia y crecimiento de las células T. Es relevante destacar que se ha detectado una expresión elevada de ZAP-70 en ciertos subtipos de neoplasias linfoides de células T, y que la supresión génica de ZAP-70 ha demostrado impactar la proliferación de células T malignas e inducir apoptosis. En conjunto, estos resultados sugieren un papel de la ZAP-70 en la progresión de las neoplasias de células T.

Por tanto, nuestro objetivo fue desarrollar inhibidores farmacológicos de la actividad quinasa de ZAP-70 y evaluar su efecto en líneas de células T malignas. Tras evaluar *in vitro* el perfil de inhibición de la actividad quinasa de 27 inhibidores candidatos de ZAP-70 frente a 26 quinasas, identificamos dos prometedores inhibidores de la quinasa ZAP-70, IQS117 e IQS141. Estos compuestos demostraron una sólida inhibición de aproximadamente el 90% de la actividad quinasa de ZAP-70, manteniendo una actividad quinasa residual superior al 20% para las demás quinasas del panel evaluado. Estudios *in vitro* posteriores en las líneas celulares OCI-Ly13.2, Jurkat y T8ML-1, que representan subtipos distintos de neoplasias linfoides de células T, revelaron una inhibición dependiente de la dosis tanto de la proliferación como de la supervivencia celular, habiendo una tendencia de las líneas celulares a ser más sensibles a IQS117. Además, ambos compuestos inhibieron de manera dependiente de la dosis la fosforilación de moléculas clave en la señalización del TCR en las líneas Jurkat y OCI-Ly13.2, incluyendo ZAP-70, LAT, SLP-76, PLCγ1 y ERK1/2. Notablemente, a diferencia de IQS141, IQS117 también

demostró efectos inhibidores sobre AKT, lo que podría contribuir a su mayor eficacia en la disminución de la proliferación y viabilidad celular.

Nuestras posteriores investigaciones *in vivo* con IQS117 e IQS141 en ratones inmunodeficientes a una dosis de 300 mg/kg no demostraron efectos tóxicos agudos detectables mediante administración oral e intraperitoneal. El análisis farmacocinético a una dosis de 50 mg/kg demostró una vida media prolongada en plasma para ambos inhibidores de ZAP-70 tras la administración oral, estableciendo esta como la mejor ruta para la posterior evaluación farmacológica de los compuestos en modelos de xenoinjerto de líneas de células T malignas. No obstante, el tratamiento con IQS117 e IQS141 en modelos de xenoinjerto subcutáneo e intravenoso de células T malignas, no mostró un impacto significativo en el crecimiento tumoral o en la supervivencia de los animales. Además, en el análisis del transcriptoma de los tumores subcutáneos tras ser sometidos a una semana de tratamiento con IQS117 e IQS141, no se identificaron cambios significativos asociados a la inhibición de ZAP-70, lo que plantea posibles dificultades en la distribución de los compuestos al tumor y requiere una validación adicional.

En resumen, nuestros resultados resaltan el potencial de la inhibición de ZAP-70 como un enfoque terapéutico prometedor para las neoplasias linfoides de células T, al tiempo que subrayan la necesidad de optimizar los mecanismos de distribución de IQS117 e IQS141 para llegar eficazmente al tumor.

1. Introduction

1.1. Origin and development of T lymphocytes

1.1.1. Hematopoiesis

Hematopoiesis refers to the intricate process of generation, development and maturation of all blood cells, originating from a population of long-lived and self-renewing cells known as hematopoietic stem cells (HSC) (1). This process initiates during embryonic development within blood islands present in the yolk sac, subsequently transitioning temporarily to the liver before ultimately establishing in a special microenvironment within the bone marrow (BM), called HSC niches (2). Following birth, hematopoiesis takes place within the bones throughout the skeleton and, by the time of puberty, it becomes primarily confined to the BM of flat bones such as the sternum, vertebrae, iliac bones and ribs (1).

The classical stepwise hematopoietic hierarchy postulates a hierarchical three-branched process of cellular differentiation **(Figure 1A)**. At the apex of this hierarchy are HSCs, which possess the capacity to progressively differentiate into all blood cell lineages. HSCs can be classified into two groups based on their expression of CD34: CD34-negative long-term HSCs (LT-HSCs) and CD34-positive short-term HSCs (ST-HSCs). LT-HSCs undergo differentiation into ST-HSCs which, subsequently give rise to multipotent progenitors (MPPs). These MPPs have the capability to differentiate into either common myeloid progenitors (CMPs) or common lymphoid progenitors (CLPs). CMPs possess the potential to generate myeloid, erythroid and megakaryocytic lineages whereas CLPs exclusively possess lymphoid potential (3).

Significant progress in the field of single-cell transcriptomics has unveiled the existence of heterogeneity in the most primitive HSCs populations (4). A more recent model proposes that lineage-restricted cells originate from a continuum of low-primed undifferentiated hematopoietic stem and progenitor cells (HSPCs), achieved through the suppression of cell proliferation-related genes and the upregulation of lineage-specific genes **(Figure 1B)** (3,4).

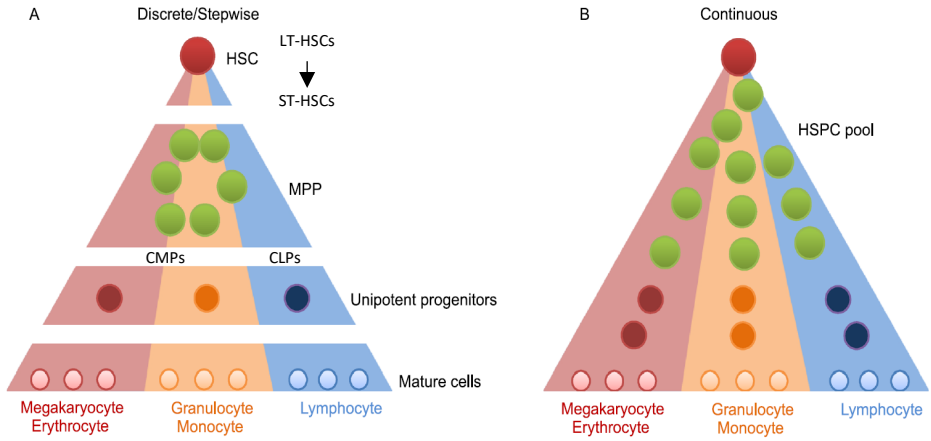

Figure 1. The evolution of hematopoietic models. (A) In the classical hematopoietic hierarchy model, hematopoietic stem cells (HSCs) at the apex give rise to various blood cell types. HSCs differentiate into long-term HSC (LT-HSCs) and short-term HSC (ST-HSCs). ST-HSCs further differentiate into multipotent progenitors (MPP), which can give rise to either common myeloid progenitors (CMPs) or common lymphoid progenitors (CLPs), leading to myeloid or lymphoid lineages, respectively. **(B)** Hematopoiesis is described as a continuum of less-differentiated hematopoietic stem and progenitor cells (HSPCs) differentiation, leading to the generation of lineage-restricted cells. Adapted from Cheng H. *et al.* Protein Cell. 2020.

1.1.2. Development and differentiation of T lymphocytes

T lymphocytes, also known as T cells, play a pivotal role in the adaptive immune system's response, serving as a critical component in the eradication of pathogens and tumor surveillance. T cells originate from BM progenitors that migrate to the thymus at an early stage as thymocytes. Within the thymus, these thymocytes undergo a series of maturation steps prior to ultimately migrating to peripheral tissues. The main characteristic of T-cell lymphopoiesis is the rearrangement of the T-cell receptor (TCR) genes prior to exposure to antigens, resulting in the generation of a diverse repertoire of more than 10^8 unique TCRs, each capable of recognizing distinct antigens (5).

1.1.2.1. T cells maturation in the thymus

The thymocytes that enter the thymus are considered double-negative cells (DN) as they do not express the coreceptors CD4 or CD8 (**Figure 2**). As they progress through the outer cortex of the thymus, thymocytes encounter cortical epithelial cells to proliferate and they can further be divided into different subpopulations (DN1-DN4) based on the expression of specific surface markers (CD44 and CD25): DN1 cells (CD44+ CD25-), DN2 cells (CD44+ CD25+), DN3 (CD44-CD25+) and DN4 (CD44-CD25-) (6,7).

The transition from DN1 to DN3 cells occurs independently of the TCR as the cells primarily interact with the thymic environment to proliferate. At the DN3 stage, cell proliferation ceases, and TCR gene rearrangement of the TCR β chain takes place (8). Thymocytes at this stage express the pre-TCR complex on the cell membrane, consisting of the TCR β chain paired with a surrogate TCR α chain and CD3 subunits **(Figure 2)**. The pre-TCR complex plays a crucial role in β selection, where the functionality of the TCR β chain is evaluated. Only thymocytes that express a functional β-subunit progress beyond this checkpoint. However, those thymocytes that successfully rearrange TCR γ and δ chains instead of β chains are selected as γδ T cells, representing less than 10% of T cells. Thymocytes expressing a functional β-subunit at DN3 will proliferate and proceed to the DN4 stage, ultimately expressing CD4 and CD8 to become double-positive cells (DP) (8,9)**.**

At the DP stage, thymocytes rearrange their TCR-α chain to form the cell-surface TCR-αβ complex (**Figure 2**). DP thymocytes then undergo two rigorous consecutive selection checkpoints to ensure the responsiveness of the TCR to foreign antigens (positive selection) while also establishing central tolerance to autoantigens (negative selection) (5) **(Figure 2)**. During positive selection, TCRs interact with self-antigens presented by the major histocompatibility complex (pMHC), also known as human leukocyte antigens (HLA) class I (pHLA-I) or II (pHLA-II) molecules. If the signal strength is strong enough to promote T-cell survival and maturation, cells mature into single-positive (SP) CD8+ or CD4+ T

cells, respectively. Thymocytes not recognizing self-antigens with sufficient affinity undergo death by neglect. In the subsequent negative selection, thymocytes with TCRs that strongly interact with self-antigens presented by antigen presenting cells (APCs) are eliminated by apoptosis (10). Those thymocytes with weak interactions survive to become CD4+ or CD8+ naïve T cells. Intermediate or high interactions will divert CD4+ T cells towards regulatory T cells that maintain immunological tolerance (11).

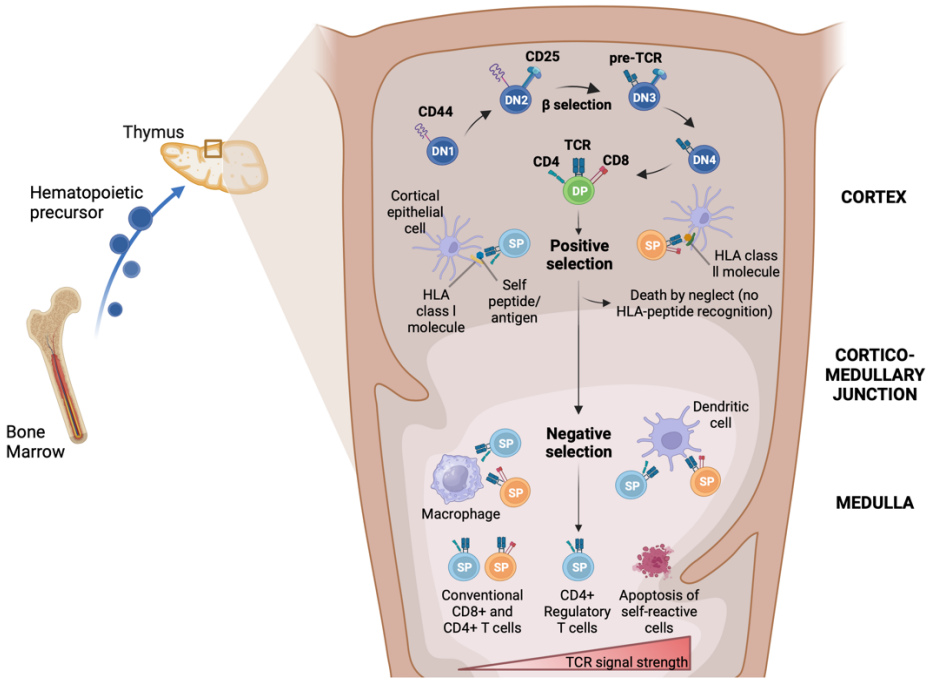

Figure 2. T-cell development in the thymus. Bone marrow progenitors migrate to the thymus as thymocytes. Thymocytes enter the thymus as double-negative (DN) cells and undergo a series of developmental stages, from DN1 to DN4. Transition from DN1 to DN3 is independent of T-cell receptor (TCR) and involves proliferation, while DN3 cells express the pre-TCR complex for β-selection. Thymocytes expressing a functional β-subunit progress to the DN4 stage. TCR-α chain rearrangement and coexpression of CD4 and CD8 lead to the double-positive (DP) stage. DP thymocytes undergo positive selection based on TCR interactions with self-antigens, leading to maturation into CD4+ or CD8+ single-positive (SP) T cells if signal strength is adequate, and negative selection, eliminating thymocytes with strong self-antigen interactions through apoptosis. Weak interactions result in the development of mature SP CD4+ or CD8+ naïve T cells, while intermediate or high interactions result in regulatory T cells, maintaining immunological tolerance. HLA, human leukocyte antigen. Image adapted from 'T-Cell Development in Thymus 2' by BioRender.com and Magali I. *et al.* Annu. Rev. Immunol. 2022.

1.1.2.2. T cells antigen recognition in the periphery

Mature naïve T cells, which have successfully undergone TCR rearrangement and possess functional, non-self-reactive TCRs, exit the thymus and migrate to secondary lymphoid organs (SLOs) such as lymph nodes, tonsils, spleen, Peyer's patches, and mucosa-associated lymphoid tissue (MALT) to identify and recognize foreign antigens presented by self-HLA molecules (12).

The two major classes of T cells, CD4+ and CD8+ T cells, exert different effector functions and recognize epitopes in a different manner. CD8+ T cells recognize short peptides (around 8-10 amino acids) derived from endogenous proteins (e.g., viral particles, intracellular pathogens, or tumor antigens) previously partially degraded by the proteasome and presented on the cell membrane on HLA-I molecules **(Figure 3)**. HLA-I molecules are present on almost all nucleated cells and activate CD8+ effector T cells, leading to a cytotoxic response that directly kills the recognized cells (13).

CD4+ T cells typically recognize longer peptides (12-20 amino acids) derived from extracellular proteins. These proteins are endocytosed, transported to endosomes, and then presented on the cell-surface on HLA-II molecules **(Figure 3)** (13). HLA-II molecules expression is restricted to APCs (monocytes, macrophages, B cells, and dendritic cells). However, certain inflammatory stimuli can induce HLA-II expression on some epithelial cells and endothelial cells. Peptides presented by HLA-II molecules are recognized by CD4+ T cells, which in turn activate other immune cells and help amplify the immune response (13,14).

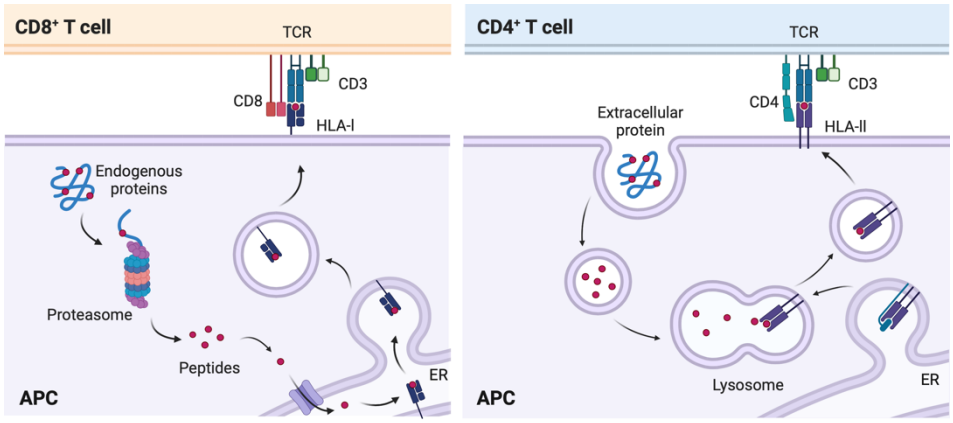

Figure 3. Antigen recognition by CD4+ and CD8+ T cells. Both CD8+ and CD4+ T cells recognize peptides bound to HLA molecule on the surface of target cells via their TCRs. CD8+ T cells identify short peptides originating from cytoplasmic proteins, which are partially digested through proteasomal activity and then presented by HLA-I molecules. In contrast, CD4+ T cells recognize longer peptides derived from extracellular proteins that were previously endocytosed, loaded and presented on HLA-II molecules. ER, endoplasmic reticulum. Image adapted from 'MHC class I and II Pathways' by BioRender.com

1.2. T-cell lymphoid malignancies

1.2.1 Definition and Classification

T-cell lymphoid malignancies constitute a heterogeneous group of rare disorders that can be indolent or aggressive, characterized by the abnormal growth of clonal, dysfunctional immature or mature T-cells. These entities can be broadly categorized into precursor and mature T-cell neoplasms, delineating distinct stages of T-cell development (15).

In 1994, the first international consensus system known as the 'Revised European-American Classification of Lymphoid Neoplasms' (REAL) classification included over 11 distinct entities within the category of 'T-cell and Putative Natural Killer (NK)-Cell neoplasms' (16).

Since then, the World Health Organization (WHO) has been instrumental in providing a standardized global reference for the classification of T-cell lymphoid malignancies since the release of its 3rd edition in 2001. This edition

expanded upon the REAL classification and described 2 precursor T-cell neoplasms arising from maturing thymocytes and 14 mature T-cell and NK-cell neoplasms derived from post-thymic T cells. This classification was based on their clinical presentation and histological morphology, under the unified category of 'T-cell and NK-cell neoplasms' (17).

Over the years, the WHO, and other Clinical Advisory Committees (CACs) have continually updated the classification of T-cell malignancies, incorporating major advances in the understanding of the genetic landscape of these diseases. The most recent updates to the classification of T-cell neoplasms were released in 2022 by two different institutions: the WHO and a multidisciplinary group of international haematologists, oncologists, and scientists through joint CACs (15,18). In this fifth edition of the WHO classification, T-cell and NK-cell neoplasms are organized into 9 families, categorized based on their cell of origin/differentiation state, disease localization, clinical presentation, and cytomorphology (**Table 1**) (15). It is important to note that the classification released by CACs, namely 'The International Consensus Classification (ICC) of Mature Lymphoid Neoplasms', solely focuses on mature T-cell and NK-cell neoplasms, classifying them in a manner that aligns with the WHO classification (18). For this thesis, we will focus on describing the WHO classification.

The 2022 WHO classification of Hematolymphoid tumors categorizes T-cell neoplasms into two major groups based on their cell of origin: precursor T-cell neoplasms and mature T-cell neoplasms (**Table 1**) (15). Notably, this updated classification introduces a third major group termed 'Tumor-like lesions with T-cell predominance', which will not be further elaborated upon as it falls beyond the scope of this thesis.

This doctoral thesis will primarily be focused on discussing the precursor T-cell neoplasm, T-cell acute lymphoblastic leukemia (T-ALL), as well as the three most common subtypes of mature T-cell lymphomas: peripheral T-cell lymphoma, not otherwise specified (PTCL, NOS), nodal T-follicular helper cell lymphoma, angioimmunoblastic-type (nTFHL-AI), and anaplastic large cell lymphoma (ALCL).

Table 1. List of T-cell lymphoid malignancies based on the 2022 WHO classification

WHO Classification, 5th edition	
Precursor T-cell neoplasms	
T-lymphoblastic leukemia/lymphoma	T-lymphoblastic leukemia/lymphoma, not otherwise specified (NOS) Early T-precursor lymphoblastic leukemia/Lymphoma
Mature T-cell and NK-cell neoplasms	
Mature T-cell and NK-cell leukemias	T-prolymphocytic leukemia T-large granular lymphocytic leukemia NK-large granular lymphocytic leukemia Adult T-cell leukemia/Lymphoma Sézary Syndrome Aggressive NK-cell leukemia
Primary cutaneous T-cell lymphomas	Primary cutaneous CD4-positive small or medium T-cell lymphoproliferative disorder Primary cutaneous acral CD8-positive lymphoproliferative disorder Mycosis fungoides Primary cutaneous CD30-positive T-cell lymphoproliferative disorder: Lymphomatoid papulosis Primary cutaneous CD30-positive T-cell lymphoproliferative disorder: Primary cutaneous anaplastic large cell lymphoma Subcutaneous panniculitis-like T-cell lymphoma Primary cutaneous gamma/delta T-cell lymphoma Primary cutaneous CD8-positive aggressive epidermotropic cytotoxic T-cell lymphoma Primary cutaneous peripheral T-cell lymphoma, NOS
Intestinal T-cell and NK-cell lymphoid proliferations and lymphomas	Indolent T-cell lymphoma of the gastrointestinal tract Indolent NK-cell lymphoproliferative disorder of the gastrointestinal tract Enteropathy-associated T-cell lymphoma Monomorphic epitheliotropic intestinal T-cell lymphoma Intestinal T-cell lymphoma, NOS
Hepatosplenic T-cell lymphoma	Hepatosplenic T-cell lymphoma
Anaplastic large cell lymphoma	ALK-positive anaplastic large cell lymphoma ALK-negative anaplastic large cell lymphoma Breast implant-associated anaplastic large cell lymphoma
Nodal T-follicular helper (TFH) cell lymphoma	Nodal TFH cell lymphoma, angioimmunoblastic-type Nodal TFH cell lymphoma, follicular-type Nodal TFH cell lymphoma, NOS
Other peripheral T-cell lymphomas	Peripheral T-cell lymphoma, not otherwise specified
EBV-positive NK/T-cell lymphomas	EBV-positive nodal T- and NK-cell lymphoma Extranodal NK/T-cell lymphoma
EBV-positive T- and NK-cell lymphoid proliferations and lymphomas of childhood	Severe mosquito bite allergy Hydroa vacciniforme lymphoproliferative disorder Systemic chronic active EBV disease Systemic EBV-positive T-cell lymphoma of childhood

1.2.2 Epidemiology

The American Cancer Society estimates that in 2023, there will be approximately 80.550 new cases of non-Hodgkin lymphomas (NHLs) diagnosed in the USA, with approximately 15% of these cases being attributed to T-cell lymphoid malignancies (19,20).

The incidence of T-cell lymphomas (TCL) displays significant geographical disparities worldwide. In Western countries, TCLs constitute merely 5-10% of all NHL, whereas in regions such as Asia, the Caribbean, Africa, and South America, their incidence escalates to 15-20% of all NHL cases (21). This disparity can be attributed, in part, to the exposure to viral infections, such as human T-lymphotropic virus type-1 (HTLV-1) and Epstein-Barr virus (EBV), both implicated in the pathogenesis of adult T-cell leukemia/lymphoma and EBV+ NK/T-cell lymphomas (NKTCL), respectively (20). Most TCL subtypes are more prevalent in males, with an increase in incidence correlating with advanced age (typically diagnosed between the ages of 49-75) (21,22).

Although the 2022 WHO classification of Hematolymphoid tumors describes a total of 35 distinct entities, approximately 30% of TCL cases in North America and Europe, along with 21% in Asia, remain unclassifiable due to not meeting the existing criteria for any classification. Consequently, these cases receive a diagnosis of exclusion called PTCL, NOS (21). The second most common subtype is nTFHL-AI, accounting for 16% of cases in North America and approximately 29% in Europe (21). The third most prevalent subtype is the ALCL, contributing to 15% of the TCL cases (20). In Asia, the most common subtypes are NKTCL (28,6% cases), followed by the nTFHL-AI (approximately 25% cases) and PTCL,NOS (approximately 21% cases) (23).

Regarding the precursor T-cell neoplasms, T-ALL arises from early T-cell progenitors and represents 10-15% of pediatric and 20-25% of adult acute lymphoblastic leukemia (ALL) cases (24). It is more frequent in males than females and predominantly affects younger age groups, being commonly considered an adolescent and young adult-affecting (AYA) disease. Survival

outcomes in ALL are profoundly influenced by age, evidenced by a 5-year overall survival (OS) of 80% for individuals younger than 50 of age, in contrast to a less favorable rate under 35% for those aged 50 years or older (24,25).

1.2.3 Clinical presentation and diagnosis

T-cell malignancies exhibit a wide range of symptoms that vary across their distinct types. Both immature and mature forms of T-cell leukemia are characterized by the circulation of malignant T cells leading to lymphocytosis, generalized lymphadenopathy, and hepatosplenomegaly (26,27). Malignant T-cell colonization of the BM can lead to anemia with neutropenia and thrombocytopenia (27).

Mature TCL typically exhibit an aggressive clinical behavior at the time of diagnosis. Among these, two of the better-known subtypes, the ALCL and nTFHL-AI, are frequently present with generalized lymphadenopathy, systemic B symptoms (night sweats, fever, and weight loss) and can involve extranodal sites (28). Primary cutaneous T-cell lymphomas (CTCL) present various manifestations on the skin. The most common subtype, mycosis fungoides (MF), initially presents as skin patches that can evolve to plaques and, in some cases, tumors. The second most common, the leukemic Sézary syndrome (SS), is characterized by peripheral blood involvement, erythroderma, and lymphadenopathy (29).

Extranodal subtypes are localized diseases without nodal involvement, whose names reflect their predilection for a specific anatomic site. These subtypes include intestinal T-cell and NK-cell lymphoid proliferations and lymphomas, as well as hepatosplenic T-cell lymphomas (30).

Lastly, PTCL, NOS, the most heterogeneous subtype, primarily involves nodal sites, yet extranodal involvement can also occur in the liver, BM, gastrointestinal tract, and skin. Patients with PTCL, NOS may display a range of symptoms, including systemic B symptoms and hepatosplenomegaly (31).

Given the rarity and heterogeneity of T-cell malignancies, precise differential diagnosis of T-cell malignancies strongly depends on the histopathological features of the disease. Among these malignancies, the Anaplastic lymphoma kinase (ALK)-positive ALCL stands as the only subtype with a unique diagnostic genetic marker—the t(2;5) translocation involving *ALK* and nucleophosmin (*NPM*). In contrast, the diagnosis for other major subtypes greatly relies on morphologic traits. Notably, nTFHL-AI is identified by partial or total effacement of the lymph node structure, infiltrated by polymorphous small to medium-size T cells clustered around high endothelial venules and follicular dendritic cells (28). In the case of ALCL, it is characterized by a diffuse proliferation of large cells exhibiting abundant cytoplasm and characteristic horseshoe- or kidney-shaped nuclei (32).

Emerging research reveals the distinct clinical nature of each subtype of T-cell malignancies, emphasizing the need for tailored therapeutic strategies based on their specific pathogenesis. The ideal approach to reach a more accurate diagnosis would involve integrating the clinical, morphological, immunophenotyping, cytogenetic, and molecular characteristics of tumor cells (33). The rarity and heterogeneity of these diseases, the complex diagnostic criteria, and incomplete biological understanding contribute to the difficulties in achieving an accurate diagnosis and treatment.

1.2.4 Genetic landscape

Genomic and transcriptomic investigations on T-cell malignancies have advanced our comprehension of the complex molecular alterations that underlie the pathogenesis of these uncommon and diverse malignancies. These studies have unveiled the potential for a more precise molecular subtyping and the development of targeted therapies tailored to specific subtypes that would lead to better clinical outcomes (34). The subsequent sections discuss our current insight into the genetic landscape of several prevalent T-cell malignancies.

1.2.4.1 Nodal T_{FH} cell lymphoma, angioimmunoblastic-type (nTFHL-AI)

The nTFHL-AI subtype, formerly recognized as angioimmunoblastic T-cell lymphoma (AITL), is characterized by the presence of clonal malignant CD4+ T_{FH} cells. CD4+ T_{FH} cells reside in the lymph node germinal center and support B cell responses (35). The most frequently mutated genes in nTFHL-AI involve epigenetic regulators, the Ras homology family member A (*RHOA*) and TCR signaling genes.

Genetic alterations affecting epigenetic regulators including Tet methylcytosine dioxygenase 2 (TET2), DNA methyltransferase 3 alpha (DNMT3A) and isocitrate dehydrogenase (NADP+) 2 (IDH2) are prevalent in hematological malignancies. Although initially identified in myeloid malignancies, their mutations are particularly high within the Nodal T_{FH} cell lymphomas family, comprised of nodal T_{FH} cell lymphoma, follicular type (nTFHL-F), nodal T_{FH} cell lymphoma, NOS (nTFHL-NOS) and nTFHL-AI (36–38).

TET2 encodes a 2-oxoglutarate/Fe^{2+}-dependent oxygenase that participates in the epigenetic control of gene expression by catalyzing the oxidation of DNA 5'-methylcytosine to 5-hydroxymethylcytosine. *TET2* loss-of-function mutations have been identified in 40-80% nTFHL-AI (**Figure 4**). These mutations are frequently identified as the initial event in malignant transformation and are correlated with advanced-stage disease and unfavorable clinical outcomes (34,39–42). Studies in animal models demonstrated that *TET2* loss contributes to heightened self-renewal and repopulation of HSCs (43). Interestingly, *TET2* mutations are commonly detected in the blood of healthy elderly individuals without accompanying indications of an ongoing or prior hematological malignancy, a phenomenon termed clonal hematopoiesis of indeterminate potential (CHIP) (44). Studies in mice models have proven that *TET2* mutations alone are insufficient to induce nTFHL-AI malignant transformation; a secondary genetic alteration is required to drive this process (45).

DNMT3A encodes a DNA methyltransferase that controls cytosine methylation. Loss-of-function mutations have been described in 10-40% nTFHL-AI. These mutations are considered an initial event in malignant transformation and frequently co-occur with *TET2* mutations (**Figure 4**) (46).

IDH2, a metabolic mitochondrial enzyme, participates in the generation of 2-oxoglutarate. Mutations in *IDH2*, specifically at the R172 position, have been exclusively described in nTFHL-AI, with a prevalence of 30-40%. *IDH2* R172 mutation is considered a second hit and often co-occurs with *TET2* mutations (**Figure 4**) (34,38). Recent studies in mouse models suggest that the presence of *IDH2* R172 mutation in *TET2*-deleted T_{FH} cells can modify the cross-talk between malignant T cells and their surrounding microenvironment, potentially contributing to the establishment of the characteristic nTFHL-AI microenvironment (47).

The RHOA small GTPase, encoded by the *RHOA* gene, plays a role as a molecular switch activated upon guanosine triphosphate (GTP) binding. This binding is finely regulated by guanine exchange factors (GEFs), including Vav guanine nucleotide exchange factor 1 (VAV1). *RHOA* regulates numerous biological processes, most notably in actin polymerization, cytoskeleton formation, adhesion, migration and cytokinesis (48).

The heterozygous missense *RHOA* G17V mutation, present in up to 70% cases of nTFHL-AI (**Figure 4**), has become a molecular diagnostic biomarker for nTFHL-AI (39,40,49). This mutation results in an inactive RHOA that functions as a dominant-negative form, interfering with the wild-type RHOA signaling (39,40,49). Furthermore, *RHOA* G17V frequently coincides with mutations in epigenetic regulators, particularly *TET2* (39,40). Mice models carrying the *RHOA* G17V mutation in CD4+ T cells exhibited an expanded CD4+ T_{FH} cell population. When coupled with *TET2* loss, these models demonstrated the expansion of CD4+ T cells and the development of TCL with features of human nTFHL-AI (50,51).

(a)

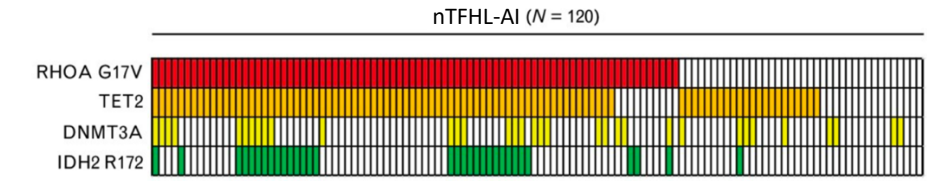

(b)

Co-occurrence (*n* (%))

	RHOA G17V	*TET2*	*DNMT3A*	*IDH2 R172*	Cases
RHOA G17V	n/a	72 (88)	30 (36.5)	31 (37.8)	82
TET2	72 (76.6)	n/a	29 (30.8)	29 (30.8)	94
DNMT3A	30 (83)	29 (80.5)	n/a	15 (41.6)	36
IDH2 R172	31 (97)	29 (90.6)	15 (46.8)	n/a	32

Figure 4. Co-ocurrence of frequent mutations in nTFHL-AI. (A) Mutational status analysis of RHOA G17V, TET2, DNMT3A, and IDH2 in a cohort of 120 patients. Each row represents mutations in each of the genes of interest and each column represents a patient sample. **(B)** Quantification of the co-occurrence of mutations in RHOA G17V and epigenetic regulators. The column of the right shows the total number of cases mutated for RHOA G17V, TET2, DNMT3A, and IDH2 R172; the rest of the columns display the mutational co-occurrence for the mutations indicated by the number (n) of cases and the percentage of co-occurrence calculated from the total of cases [(%)]. DNMT3A, DNA methyltransferase 3 alpha; IDH2, isocitrate dehydrogenase (NADP+) 2; RHOA, Ras homology family member A; TET2, Tet methylcytosine dioxygenase 2. Adapted from Cortés J. *et al.* Curr. Opin. Hematol. 2016.

1.2.4.2 Anaplastic large cell lymphoma (ALCL)

ALCL comprises three aggressive subtypes, all characterized by the consistent expression of CD30 and often defective expression of T-lineage markers (15). In this section we will focus on the most frequent subtypes, ALK-positive ALCL and ALK-negative ALCL.

ALK-positive ALCL subtype is distinguished by chromosomal translocations that lead to *ALK* constitutive activation. The most prevalent is the t(2,5) translocation, which fuses the *ALK* gene in chromosome 2 with nucleophosmin (*NPM*), resulting in a constitutive active kinase that aberrantly activates downstream signaling pathways as Janus kinase (JAK)-signal transducer and activator of transcription 3 (STAT3) (52). The *ALK-NPM* was the first recurrent genetic abnormality identified in TCL (53).

In contrast, ALK-negative ALCL differs from the ALK-positive ALCL by the absence of *ALK* translocations (32). Numerous genomic mechanisms lead to oncogenic activation of STAT3 signaling in ALK-negative ALCL. Mutations in *JAK1* and *STAT3* are identified in approximately 20% ALK-negative ALCL cases (54). Recurrent gene translocations involving the ROS proto-oncogene 1 (*ROS1*) and the tyrosine kinase 2 (*TYK2*) also exert oncogenic effects by activating the JAK/STAT signaling pathway. This suggests that constitutive STAT3 activation is a prevalent mechanism of malignant transformation of ALCL, irrespectively of the ALK status (54,55).

Recurrent chromosomal rearrangements in ALK-negative ALCL involve the dual specificity protein phosphatase 22 (*DUSP22*) and the tumor protein 63 (*TP63*). These rearrangements are mutually exclusive and are related to different survival outcomes; rearrangements in *DUSP22* are associated with a better prognosis compared to *TP63* rearrangements (56,57).

1.2.4.3 Peripheral T-cell lymphoma, Not otherwise specified (PTCL, NOS)

PTCL, NOS is the most common subtype of TCL. Early transcriptional profiling studies unveiled the intricate diversity within PTCL, NOS, exhibiting subsets resembling other subtypes as ALK-negative ALCL and nTFHL-AI, while others diverge from them completely (58,59). Notably, recent transcriptional studies identified that approximately 15% of cases exhibited a transcriptional profile that resembled nTFHL (60). The current WHO classification recognizes them as a distinct entity called, nodal T_{FH} cell lymphoma, NOS (nTFHL-NOS), defined by the expression of CD4 and at least two T_{FH}-associated antigens and a lack of morphologic features of other nodal T_{FH} lymphomas (15,41).

Recurrent genetic alterations identified in nTFHL-AI are also present in nTFHL-NOS in varying frequencies. Epigenetic mutations involving *RHOA* G17V (25-50% cases) (39,40,61), *TET2* (50-75% cases) and *DNMT3A* (7-18% cases) loss (39,40,61), as well as TCR signaling mutations.

Immunohistochemistry (IHQ) and gene expression profile (GEP) studies demonstrated that PTCL, NOS could be subdivided into two different subgroups, distinguishable by the opposing expression of two distinct transcriptional factors: T-box-21 (*TBX-21*) and GATA 3 binding protein (*GATA3*). *TBX-21* regulates the differentiation and function of T-helper CD4+ type 1 (Th1) and cytotoxic T-cell (CTL), regulating the expression of interferon-gamma (*IFNG*) and granzyme B (*GZB*). Conversely, *GATA3* is implicated in T-helper CD4+ type 2 (Th2) differentiation and regulates interleukin-4 (*IL-4*), *IL-5*, and *IL-13* expression (60,62).

A study encompassing the profiling of 121 of PTCL, NOS cases delineated two principal subtypes. The PTCL-GATA3 subtype, representing 33% of cases, exhibited high expression of *GATA3* and its target genes and correlated with poor prognosis (60). The loss or mutations in the cyclin dependent kinase inhibitor 2A/B (CDKN2A/B)-tumor protein 53 (TP53) and phosphatase and tensin homolog (PTEN)- phosphatidylinositol-3-kinase (PI3K) signaling pathways are a key feature of PTCL-GATA3. In contrast, the PTCL-TBX-21 subtype constituted 49% of cases, characterized by high expression of *TBX-21* and its target genes, and was associated with a better outcome. This signature is associated with nuclear factor kappa-light-chain-enhancer of activated B cells (NF-κB) activation and a more inflammatory microenvironment in comparison to the PTCL-GATA3 signature. The remaining 18% were unclassifiable (60,63). A minor subgroup within PTCL-TBX-21, marked with a high cytotoxic signature, exhibited a more adverse clinical outcome than the rest of PTCL-TBX21, highlighting the heterogeneity within the PTCL-TBX21 subtype (59). Despite these distinct genetic landscapes being uncovered, the current WHO and ICC classifications have not incorporated them as a distinct subclassification (15,18).

1.2.4.4 T-cell acute lymphoblastic leukemia (T-ALL)

T-ALL arises from the accumulation of genetic alterations that disrupt the precise control of cellular growth, proliferation, survival, and differentiation

within different stages of T-cell development. A hallmark of T-ALL is the intricate interplay between oncogenic signaling pathways and critical regulators of early T-cell development associated with T-ALL (64).

Recurrently altered genes in T-ALL disrupt multiple essential cellular processes, including deregulation of the cell cycle (e.g., deletions of *CDKN1AB* or *TP53*), the activation of several signaling pathways, including neurogenic locus notch homolog protein (NOTCH) signaling, rat sarcoma (RAS) pathway, IL-7 receptor (IL7R)-JAK-STAT signaling, PI3K-serine/threonine kinase (AKT) signaling, and the ABL proto-oncogene 1 (ABL1)-Src proto-oncogene (Src) family kinases. Additionally, inactivating mutations or deletions affecting epigenetic modulators such as PHD finger protein 6 (*PHF6),* lysine demethylase 6A *(KDM6A),* *DNMT3A,* and members of the polycomb repressive complex 2 (*PRC2)*, along with alterations in tumor suppressor genes including ETS variant transcription factor 6 (*ETV6),* RUNX family transcription factor 1 *(RUNX1), GATA3,* and the BCL11 transcription factor B *(BCL11B*), collectively contribute to the pathogenesis of leukemia (65,66).

A prominent genetic hallmark of T-ALL involves gain-of-function mutations in NOTCH receptor 1 (*NOTCH1)*, a key regulator of thymocyte development. These mutations are present in more than 60% of T-ALL cases and drive the constitutive activation of NOTCH1, resulting in aberrant thymocyte proliferation and survival (67). Additionally, the NOTCH pathway can be activated by loss-of-function mutations or deletions of F-box and WD repeat domain containing 7 (*FBXW7)*, a gene encoding a ubiquitin protein that mediates NOTCH1 degradation, observed in up to 24% T-ALL cases. Notably, *NOTCH1* and/or *FBXW7* mutations can co-occur in approximately 60% of T-ALL cases (68).

Another recurrent genetic alteration involves deletions within the *CDKN2A* locus, present in more than 70% of T-ALL patients (69). *CDKN2A* encodes two distinct tumor suppressor proteins, P16/INK4 and P14/ARF. While P16/INK4 inhibits cell cycle progression from G1 to S phase, P14/ARF mediates cell cycle arrest and apoptosis. The inactivation of *CDKN2A* promotes cell cycle

progression and resistance to apoptosis, significantly contributing to leukemia progression (70).

Chromosomal translocations affecting oncogenic genes is another distinctive trait of T-ALL, resulting in the abnormal expression of a diverse group of oncogenic transcription factors (**Figure 5**). These alterations disrupt the typical progression of thymocyte development, ultimately leading to a stage-specific blockage in cellular differentiation (65). Notably, the early T-cell precursor (ETP) subtype of T-ALL experiences an early block in thymocyte development at the DN stage. This subtype exhibits a transcriptional program characterized by the overexpression of *HOXA, MEF2C* or *BCL11B*, alongside the expression of markers associated with HSCs and myeloid progenitors as CD34. In contrast, T-ALL with an early cortical phenotype present overactivation of *TLX1/3, NKX2.1*, or *NKX2.2* transcription factors. Lastly, T-ALL with a late cortical thymocyte phenotype is associated with the dysregulation of TAL and LMO transcription factors (71). Each T-ALL subtype is associated with specific alterations in signaling pathways as shown in **Figure 5**.

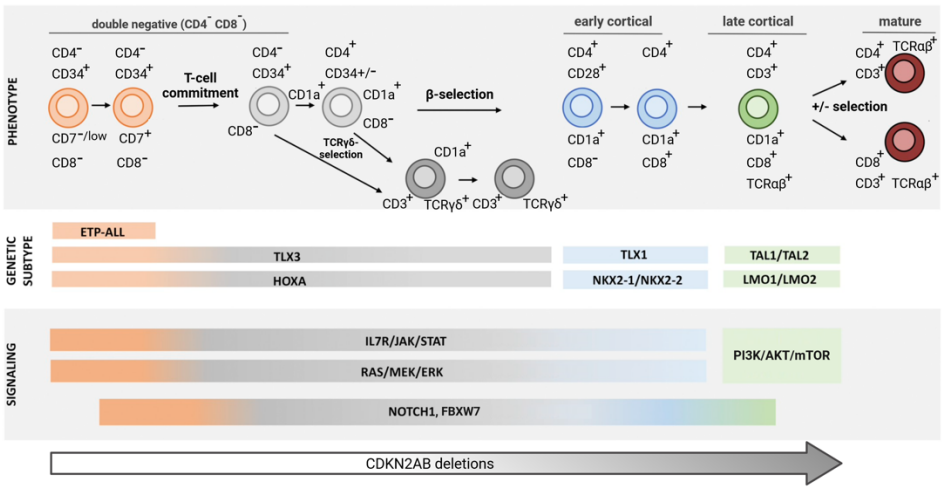

Figure 5. Schematic representation of the different molecular genetic subtypes of human T-ALL in relation to normal T-cell differentiation. Genetic subtypes are categorized based on T-cell phenotype, the unequal distribution of mutations that activate specific oncogenic signaling pathways, and CDKN2A/B deletions. Early T-cell precursor ALL, ETP-ALL. Adapted from De Smedt R. *et al.* Blood Rev. 2019.

1.2.5 Treatment options and outcome

1.2.5.1 First-line treatment in T-cell lymphomas

In T-cell malignancies, first-line anthracycline-based chemotherapy regimens have been adapted from effective strategies employed in the treatment of aggressive B-cell NHLs, being CHOP (cyclophosphamide, doxorubicin, vincristine, and prednisone) or CHOP-like combination chemotherapy the standard first-line treatment regimen in T-cell malignancies (**Figure 6**) (72). However, these approaches have yielded suboptimal responses in TCL, with notable differences in the 5-year overall survival (OS) and 5-year progression-free survival (PFS) rates. ALK-positive ALCL demonstrates better survival outcomes (70% and 60%), compared to other prevalent subtypes like PTCL, NOS (32% and 20%) and nTFHL-AI (32% and 18%) (21,73,74). These findings have been substantiated by additional retrospective studies. Within a cohort of 181 ALCL cases treated with CHOP-like therapies, individuals with ALK-positive ALCL exhibited enhanced 5-year OS (70% vs 49%) compared to those with ALK-negative ALCL (75).

Consolidation therapy after achieving first complete remission with autologous stem cell transplant (ASCT) is commonly employed for young patients with chemotherapy-sensitive disease (**Figure 6**). A report from the Comprehensive Oncology Measures for Peripheral T-Cell Lymphoma Treatment (COMPLETE) initiative, a multicenter prospective cohort, estimated an improved 2-year OS and PFS among patients with nTFHL-AI who underwent ASCT, compared to their non-ASCT counterparts (93,3% vs 52,9% and 68,8% vs 41,2%, respectively). However, no significant benefits were observed for ALCL and PTCL, NOS patients (76). A more recent retrospective study from the Netherlands Cancer Registry reported that patients under 65 years old who underwent ASCT exhibited a 5-year OS of 81%, in contrast to 39% for non-ASCT patients in ALK-negative ALCL, nTFHL-AI, and PTCL, NOS (77). It is important to consider that the observed

benefits may be influenced by patient selection, especially considering that many patients are ineligible for ASCT due to early progression or relapse of the disease (78).

Given the unfavorable prognosis associated with first-line treatment in T-cell malignancies, there is an urgent need for the development of innovative therapeutic strategies (79,80). Efforts to combine CHOP with targeted therapies in the front-line treatment (**Table 2**), such as the addition of the anti-CD52 monoclonal antibody (alemtuzumab) or the histone deacetylase (HDAC) inhibitor romidepsin (Ro) to CHOP, have not demonstrated improved survival in phase III clinical trials, possibly due to increased treatment-related toxicity (81,82). Nonetheless, exploratory analysis indicate a potential prolongation of PFS for Ro-CHOP in nTFHL compared to the CHOP alone (19,5 vs 10,6 months) (82). These observations are consistent with prior research demonstrating extended duration of response in patients with relapsed/refractory (r/r) nTFHL-AI treated with Ro, as well as recent retrospective report finding a benefit of HDAC inhibitors in TCL exhibiting a TFH phenotype (83,84).

The phase III randomized trial (ECHELON-2) assessed the impact of combining Brentuximab vedotin, an antibody-drug conjugate targeting CD30, with cyclophosphamide, doxorubicin, and prednisone (A+CHP), compared to CHOP, in a cohort of 452 patients with previously untreated systemic ALCL and other CD30-positive TCL (CD30 expression defined as ≥10% of cells) (85). After a median follow-up of 5 years, the median OS remained indeterminate, while the median PFS was 63 months for A+CHP and 24 months for CHOP. The estimated 5-year PFS and 5-year OS rates were 51% and 69% for A+CHOP, and 43% and 60% for CHOP. The survival advantage of A+CHP therapy was more pronounced for ALCL, which constituted 70% of participants in the trial. Consequently, these outcomes lead to the approval of A+CHP by the Food and Drug Administration (FDA) as a first-line treatment for patients with untreated systemic ALCL and other CD30-expressing subtypes, including PTCL, NOS and nTFHL-AI. Additionally, the European Medicines Agency (EMA) approved A+CHP for front-line therapy and r/r systemic ALCL.

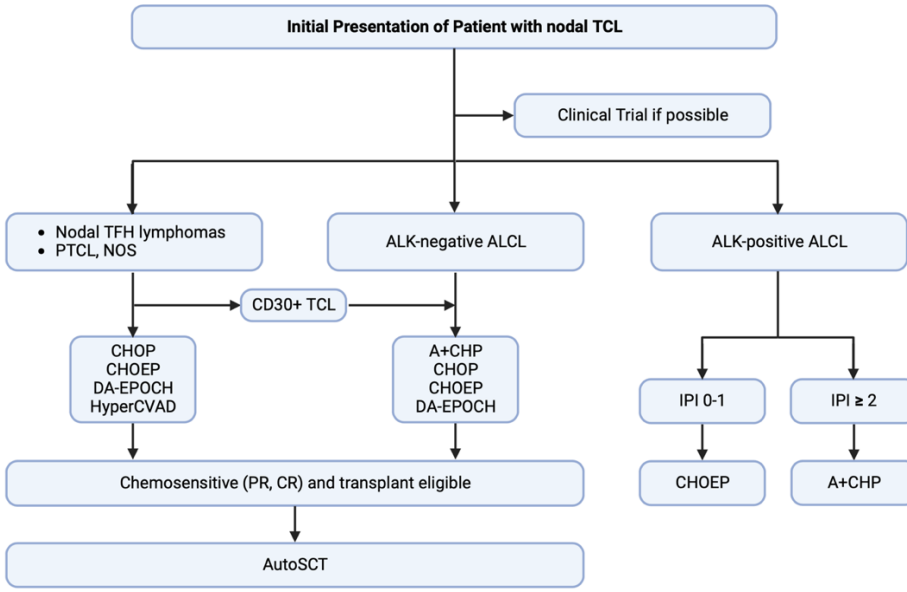

Figure 6. Treatment algorithm for initial presentation of nodal T-cell lymphomas. A+CHP, brentuximab vedotin + cyclophosphamide + doxorubicin + prednisone; ALCL, anaplastic large cell lymphoma; ALK, anaplastic lymphoma kinase; AutoSCT, autologous stem cell transplant; CHOP, cyclophosphamide + doxorubicin + vincristine + prednisone; CHOEP, cyclophosphamide + doxorubicin + vincristine + etoposide + prednisone; CR, complete response; DA-EPOCH, dose-adjusted etoposide + prednisone + vincristine + cyclophosphamide + doxorubicin; HyperCVAD, cyclophosphamide + vincristine + doxorubicin + dexamethasone –alternating with methotrexate + cytarabine; IPI, International prognostic index; PR, partial response; PTCL, NOS, peripheral T-cell lymphoma, not otherwise specified; TCL, T-cell lymphoma; TFH, T-follicular helper. Adapted from Zing N. *et al.* Oncology (Williston Park) 2018 and Sibon D. *et al.* Cancers 2022.

Table 2. Phase III randomized studies in treatment-naïve T-cell lymphomas

Clinical Study	Study Size	Therapies being studied	Age for Inclusion	Results
ACT2 (NCT00725231)	116	Alemtuzumab + CHOP vs CHOP	61-80 years	No significant difference in PFS or OS. Alemtuzumab-derived increased toxicity
LYSA (NCT01796002)	421	Ro+CHOP vs CHOP	18-80 years	No significant difference in PFS or OS. Romidepsin-derived increased toxicity
ECHELON-2 (NCT01777152)	452	A+CHP vs CHOP	≥18 years	Median PFS: 63 mo in A-CHP vs 24 mo CHOP

A+CHP, brentuximab vedotin + cyclophosphamide + doxorubicin + prednisone; CHOP, cyclophosphamide + doxorubicin + vincristine + prednisone; mo, months; OS, overall survival; PFS, progression-free survival; Ro+CHOP, romidepsin + cyclophosphamide + doxorubicin + vincristine + prednisone.

1.2.5.2 First-line treatment in T-ALL

The treatment algorithm for T-ALL involves several stages and differs between AYA patients (approximately 15-39 years old) and adults (40 years or older), as well as for different T-ALL subtypes. Variations of multiagent chemotherapy regimens, such as those formulated by the Berlin-Frankfurt-Münster (BFM) group and the hyper-CVAD regimen from MD Anderson Cancer Center (MDACC), form the core of T-ALL treatment strategy. The treatment phases involve induction, consolidation, and maintenance of therapy, with all regimens incorporating central nervous system (CNS) prophylaxis at specific points (**Figure 7**) (86–88).

The induction phase (**Figure 7**) employs combination therapy involving vincristine, anthracyclines (such as doxorubicin), and corticosteroids (dexamethasone or prednisone), often with L-asparaginase and/or cyclophosphamide. This aims to eliminate the bulk of the disease. Under the BFM regimen, AYA patients receive a 4-drug induction regimen including vincristine, anthracycline, corticosteroid, and L-asparaginase. In contrast, adults receive a 5-drug regimen by adding cyclophosphamide (72). Studies like AIEOP-BFM ALL 2000 and UK MRC ALL97 demonstrated the benefits of dexamethasone over prednisone for pediatric T-ALL, including reduced risk of CNS relapse, potentially due to its enhanced penetration into the CNS, although concerns about toxicities remain (89,90).

Following successful CR, consolidation therapy (**Figure 7**) aims to further reduce risk of relapse using drugs similar to those used in the induction phase, such as corticosteroids, cyclophosphamide, vincristine, and L-asparaginase and can include methotrexate, cytarabine or 6-mercaptopurine (6-MP). After consolidation phase, Allo/autoASCT may be considered and tailored based on individual patient disease characteristics. Lastly, maintenance therapy aims to prevent disease relapse, often involving daily 6-MP and weekly methotrexate administration for 2 to 3 years (72).

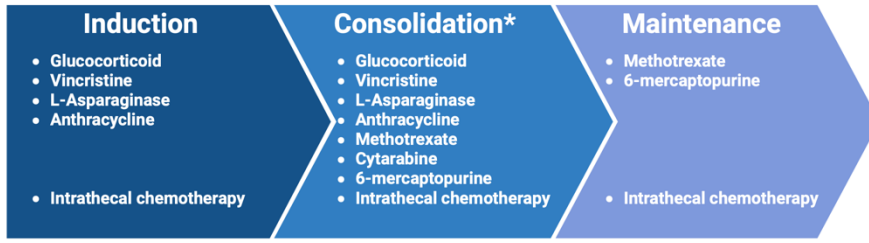

Figure 7. Front-line treatment of T-acute lymphoblastic leukemia. T-ALL treatment involves multiple phases: induction to reduce disease burden, consolidation to reduce the risk of relapse, and maintenance to prevent progression of disease. Different drug combinations are used for each phase. Adapted from Malard F. & Mohty M. The Lancet 2020 and NCCN Acute Lymphoblastic leukemia guidelines (Version 2.2023). Intrathecal chemotherapy consists of methotrexate alone or combined with cytarabine and corticosteroids. *Allogeneic HSCT transplantation is optional after consolidation.

1.2.5.3 Approved therapies in relapsed/refractory T-cell lymphomas

Approximately 70% patients with TCL will experience relapse or develop refractory disease in response to chemotherapy, resulting in a dismal clinical outcome (91). Patients with r/r TCL have a median PFS of 3,1 months and a median OS of 5,5 months (91). Notably, the FDA has granted approval to five agents for r/r TCL (**Table 3**). The first agent that received approval was the anti-folate pralatrexate. This decision followed the promising results observed in the prospective phase II study (PROPEL) conducted in pre-treated patients with r/r TCL in 2009 (92). In 2011, the HDAC inhibitor romidepsin obtained FDA approval for r/r TCL, based on its efficacy in 130 patients (93). However, in August 2021, the FDA withdraw the approval of romidepsin. This decision was made in response to the results of the phase III trial comparing Ro-CHOP versus CHOP, where, after a median follow-up of 28 months, there was not a significant improvement in ORR, CR, or PFS. Moreover, there was an increase in adverse effects within the Ro-CHOP group (82).

In 2011, the FDA granted approval to Brentuximab vedotin for the treatment of r/r ALCL (**Figure 8**). This decision was based on the high response rate of 86% observed in a phase II study focused on r/r CD30+ ALCL after prior

therapy (94). More recently, in 2014, the FDA approved the pan-HDAC inhibitor Belinostat based on the outcomes of the phase II BELIEF trial in r/r TCL, which demonstrated a similar ORR of 26% to other HDAC inhibitors, along with a favorable toxicity profile (95). Lastly, in 2021, the FDA approved the ALK inhibitor, crizotinib, for use in pediatric and young adults with r/r ALK-positive ALCL after at least one prior line of therapy (**Figure 8**) (96).This approval was based on the results from the ADVL0912 trial, where 26 patients with r/r ALK-positive ALCL were treated with crizotinib, observing an ORR of 88% and a CR rate of 81% (97).

Table 3. FDA-approved novel agents for relapsed/refractory T-cell lymphomas

Agent	Mechanism of Action	Phase	Indication	Outcomes (ORR, CR, DOR)
Pralatrexate	Anti-folate	II (PROPEL)	TCL and transformed MF	29%, 11%, 10,1 mo
Romidepsin[a]	HDAC inhibitor	II	TCL	25%, 15%, 28 mo
Brentuximab Vedotin	α-CD30 linked to auristatin (antitubulin agent)	II	ALCL	86%, 57%, 13,2 mo
Belinostat	HDAC inhibitor	II (BELIEF)	TCL	26%, 11%, 13,6 mo
Crizotinib	ALK inhibitor	II	ALK-positive ALCL	88%, 81%, –[b]

Abbreviations: ALK, anaplastic lymphoma kinase; ALCL, anaplastic large cell lymphoma; CR, complete response; DOR, duration of response; HDAC, histone deacetylase; mo, months; MF, mycosis fungoides; ORR, objective response rate; TCL, T-cell lymphoma.
[a]Phase III study romidepsin plus CHOP lead to withdrawal of romidepsin for relapsed/refractory TCL in the USA in 2022.
[b]DoR assessment not provided.

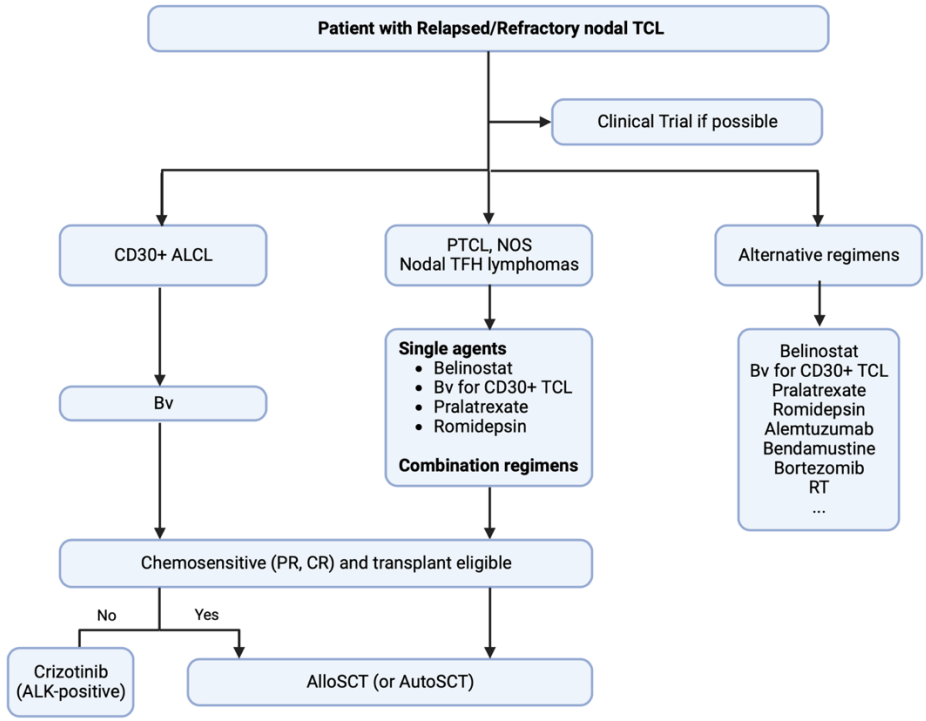

Figure 8. Treatment algorithm for relapsed/refractory nodal T-cell lymphomas. Bv, brentuximab vedotin; ALCL, anaplastic large cell lymphoma; AlloSCT, allogenic stem cell transplantation; ALK, anaplastic lymphoma kinase; AutoSCT, autologous stem cell transplant; CR, complete response; PR, partial response; PTCL, NOS, peripheral T-cell lymphoma, not otherwise specified; RT, radiotherapy; TCL, T-cell lymphoma; TFH, T-follicular helper. Adapted from Zing N. *et al.* Oncology (Williston Park) 2018.

Considering the need for more effective therapies within these diseases, several new targeted agents are currently under investigation as monotherapies in the context of r/r TCL (**Figure 8**). The recurrent TET2 alterations identified in PTCL, NOS and nTFHL-AI is a promising therapeutic target. A retrospective study involving 12 nTFHL-AI patients treated with the hypomethylating agent azacytidine reported an impressive ORR of 75% and a CR of 50%. These patients exhibited TET2 mutations and, in some cases, additional mutations in DNMT3A, IDH2, and RHOA (98). This compelling outcome lead to multiple clinical trials testing combinations involving azacytidine for TCL treatment. One ongoing phase III trial (NCT03593018) compares azacytidine against the investigator-selected choice of romidepsin, bendamustine or belinostat in r/r nTFHL-AI. Additionally, a randomized phase IIb trial (NCT04747236) has incorporated romidepsin

alongside azacytidine to assess its efficacy in comparison to the investigator-selected choice of romidepsin, pralatrexate, bendamustine or belinostat for r/r TCL. No results have been published yet.

Several early-phase studies have demonstrated the clinical efficacy in TCL. Given that JAK/STAT pathway mutations are observed in several TCL subtypes, two ongoing trials are evaluating the therapeutic potential of the oral JAK inhibitor ruxolitinib. The first trial, a completed phase II study (NCT01431209), enrolled 71 patients of B-cell NHL and TCL concluding in 2021. The second ongoing phase II trial (NCT02974647) has enrolled 82 patients so far. No results have been published so far.

Ongoing and recently completed single-agent trials in TCL are summarized in **Table 4**.

Table 4. Single-agent therapies under investigation for relapsed/refractory T-cell lymphomas

Single-Agent	Route of administration	Mechanism of Action	Phase	Clinical Trial ID
Avelumab	Intravenous	Anti-PDL1 antibody	II	NCT03046953
AZD4205	Oral	JAK inhibitor	II	NCT04105010
Ruxolitinib	Oral	JAK inhibitor	II	NCT01431209
HBI-8000	Oral	HDAC inhibitor	IIb	NCT02953652
Valemetostat Tosylate	Oral	EZH1/2 inhibitor	II	NCT04703192
Tipifarnib	Oral	Farnesyltransferase inhibitor	II	NCT02464228
CD7 CAR-T	Intravenous	Humanized CD7 CAR-T	II	NCT05059912
Chidamide	-	HDAC inhibitor	II	NCT05833724
Venetoclax	Oral	BCL2 inhibitor	II	NCT03552692
Carfilzomib	-	Proteasome inhibitor	I	NCT01336920
ONO-4685	-	CD3-PD1 bispecific antibody	I	NCT05079282

BCL2, B-cell lymphoma 2; CAR-T, chimeric antigen receptor T-cell; EZH1/2, enhancer of zeste homolog; HDAC, histone deacetylase; JAK, janus kinase; PD1, programmed cell death 1; PDL1, programmed cell death ligand 1.

1.2.5.4 Approved therapies in relapsed/refractory T-ALL

Both children and adults with r/r T-ALL have dismal outcomes. The OS in children and adults is approximately 25% (99,100). Nelarabine, a purine nucleoside analogue with cytotoxic effects on T lymphoblasts, is the only FDA-approved therapy (in 2005) for the treatment of r/r T-ALL (101). Initial early-phase trials demonstrated its efficacy as a monotherapy in paediatric r/r T-ALL cases, achieving a response rate over 50%, with neurotoxicity being the most prevalent dose-limiting adverse effect (102). In a study involving 26 adult patients with r/r T-ALL, Nelarabine achieved an ORR of 41% accompanied by mild neurotoxicity (103).

The AALL0434 trial evaluated Nelarabine in the upfront setting among children and young adults in combination with different methotrexate regimens. This integration led to an improved 5-year disease-free survival (DSF) rate of 88% and a reduced CNS relapse rate without an associated increase in toxicity, leading to consider it as standard of care in paediatric T-ALL (104). The ongoing phase III UKALL 14 trial (NCT01085617) is currently evaluating the impact of chemotherapy with or without Nelarabine in adults with T-ALL in the front-line setting.

At present, there are no other FDA-approved therapies for T-ALL. Early-phase studies are exploring several novel agents as chimeric antigen receptor (CAR) T-cell therapy and small-molecule compounds targeting NOTCH-1 signaling, cell cycle (such as Palbociclib), or apoptosis [such as B-cell lymphoma 2 (BCL2) inhibitors] (**Table 5**). Given that over 50% T-ALL present activating NOTCH-1 mutations, targeting this pathway has been appealing. γ-secretase inhibitors (GSIs), initially developed for Alzheimer's disease, prevent NOTCH-1 cleavage and activation. However, in T-ALL, they exhibited limited antileukemic effects and gastrointestinal toxicity (105,106).

In a phase I multicenter trial (NCT03181126), the combination of the selective BCL2 inhibitor Venetoclax with the B-cell lymphoma extra-large (BCL-

xL)/BCL2 inhibitor, navitoclax, demonstrated promising results in pediatric and adult patients with r/r T-ALL, achieving a 52,6% CR rate (107). Daratumumab, a CD38 monoclonal antibody approved for multiple myeloma, demonstrated antileukemic effects in preclinical T-ALL models (108,109). A phase II study is currently evaluating the safety of Daratumumab in combination with conventional chemotherapy for pediatric and young r/r T-ALL patients (NCT05289687). Additionally, a phase I clinical trial (NCT05038644) is investigating the safety of XmAb18968, a bispecific antibody targeting CD3 and CD38. Regarding the cell cycle, the cyclin-dependent kinase 4/6 (CDK4/6) inhibitor Palbociclib, which disrupts G1/2 cell cycle phase, is undergoing phase I evaluation in r/r T-ALL (NCT03792256).

In light of the approval of several CAR-T therapies for the treatment of several r/r B-cell malignancies, efforts have been directed towards adapting CAR-T therapy for T-ALL (110). However, one of the major challenges is that normal T cells share antigens with malignant T cells, leading to fratricide and T-cell aplasia upon CAR-T treatment (111). Despite this challenge, potential targets have been identified, leading to the initiation of several phase I and/or II clinical trials of CAR-T therapy in T-ALL (112). An early-phase clinical trial investigating CD7 CAR-T treatment for r/r T-ALL demonstrated safety and efficacy, achieving a 90% CR among the 20 participants (113). These promising results led to an ongoing phase II study (NCT04689659). There are currently 15 active clinical trials employing CAR-T targeting CD7 for r/r T-ALL (**Table 5**). Additionally, other clinical trials in r/r T-ALL are exploring CAR-T therapy targeting CD4 or CD5. Nonetheless, there are currently no phase III or phase IV clinical trials utilizing CAR-T therapy in r/r T-ALL.

Table 5. Ongoing or recently completed clinical trials for relapsed/refractory T-ALL

Agent	Mechanism of Action	Phase	Clinical Trial ID
Daratumumab	CD38 monoclonal antibody	II	NCT05289687
Alemtuzumab	CD52 monoclonal antibody	II	NCT00199030
XmAb18968	CD3-CD38 bispecific antibody	I	NCT05038644
Venetoclax + Navitoclax	BCL2 inhibitor + BCL-xL/BCL2 inhibitor	I	NCT03181126
Palbociclib	CDK4/6 inhibitor	I	NCT03792256
CAR-T	CD7 CAR-T	II	NCT04689659
		I/II	NCT04984356 NCT04762485 NCT05909527 NCT05212584
		I	NCT05127135 NCT03690011 NCT05716113 NCT05043571 NCT05907603 NCT04823091 NCT05397184 NCT04599556 NCT05290155 NCT04572308
	CD4 CAR-T	I	NCT03829540
	CD5 CAR-T	I	NCT04594135 NCT05487495 NCT05596266 NCT05032599

BCL2, B-cell lymphoma 2; BCL-xL, B-cell lymphoma extra-large; CAR-T, chimeric antigen receptor T-cell.

1.3. TCR signaling in T-cell malignancies

T-cell activation is a meticulously regulated process that requires three sequential signals. The first signal involves antigen recognition presented by APCs through the TCR on the naïve T cell, thereby activating the TCR signaling pathway. To achieve full T-cell activation, a second signal is required, known as co-stimulation, originated from the interaction of costimulatory receptors on the T cell and their ligands on APCs. An essential interaction for T-cell activation is the binding of CD28 on T cells with CD80/86 on APCs. The lack of the second signal leads to T-cell anergy, a state of T-cell unresponsiveness where T cells are refractory to restimulation. The third signal involves T-cell response to the cytokines present in the environment, orchestrating T-cell differentiation and functionality (114).

1.3.1. Overview of TCR signaling pathway

The TCR signaling pathway plays a crucial role in various aspects of T-cell biology, including development, homeostasis, activation, and tolerance. Physiological activation of TCR signaling occurs when T cells recognize specific peptides presented by APCs (115). This recognition leads to the recruitment of signaling molecules to the plasma membrane near the activated TCR. Subsequently, multiple downstream pathways are activated, resulting in the induction of specific cellular functions, such as cytoskeletal reorganization, gene transcription and cytokine production. The connection between the proximal and the distal signaling is mediated by adaptors, which act as scaffolds to assemble complexes of multiple signaling molecules, known as signalosomes (116,117). Under physiological conditions, TCR activation is a tightly regulated process to control foreign agents and prevent autoimmunity, contributing to the immune homeostasis. Abnormal function can contribute to autoimmunity, inflammation, or malignant pathogenesis (116).

1.3.1.1. Physiologic role of TCR signaling in T cells

The TCR is a membrane-bound receptor expressed on the surface of T cells (**Figure 9**). It consists of a heterodimer composed of two transmembrane polypeptide chains: TCR α and β, expressed in more than 90% T cells, or TCR γ and δ, found in less than 10% T cells (118). While the intracellular and transmembrane regions of the TCR lack enzymatic activity, signal transduction relies on the assembly of the TCR with the CD3 proteins (consisting of δ, γ, ε and ζ chains). The TCR chains recognize antigen fragments presented by APCs, transmitting this signal through the cytosolic domains of the CD3ζ chains that contain the immunoreceptor tyrosine-based activation motifs (ITAMs). Each ITAM consists of two tyrosine residues flanked by leucine/isoleucine, spaced by six to eight amino acids, forming a consensus sequence of YxxL/I-(x)6-8- YxxL/I (Y: tyrosine, L/I:

leucine/isoleucine). CD3δ, ε, γ have one ITAM each, while each CD3ζ has three tandem ITAMS. In total, each TCR-CD3 complex has 10 ITAMS (119).

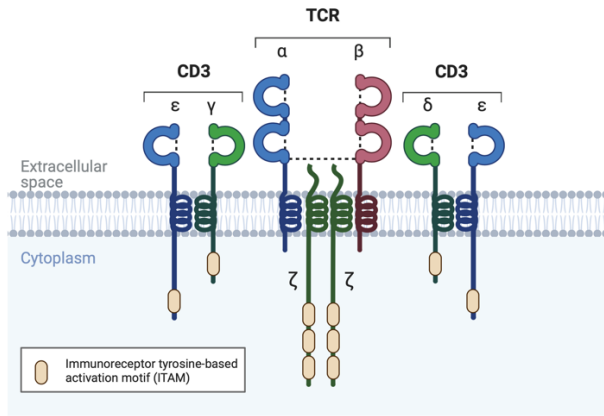

Figure 9. TCR α/β complex structure. The α/β chains of the TCR are non-covalently linked to CD3 chains in the plasma membrane of T cells. Citoplasmic domains of CD3δ, ε, γ chains contain one ITAM each, while each ζ chain contains three ITAMs. Image adapted from 'TCR/CD3 subunit structure' by BioRender.com

Upon antigen recognition, early TCR signaling occurs in a matter of a few seconds (**Figure 10**) (120). One of the initial events is the phosphorylation of the tyrosine residues in the ITAMS by the Src family of tyrosine kinases, mainly lymphocyte cell-specific kinase (LCK) and to some extent FYN, although FYN expression is not essential for T-cell development (121,122). This prompts the recruitment of ZAP-70 kinase to the phosphorylated ITAMs and its further activation through LCK-mediated phosphorylation and autophosphorylation. ZAP-70 proceeds to phosphorylate its substrates, the adaptor proteins linker for activation of T cells (LAT) and SH2 domain-containing leukocyte protein of 76 kDa (SLP-76), which serve as docking sites for multiple signaling molecules (123). Phosphorylated LAT recruits phospholipase C gamma 1 (PLCγ1), as well as the adaptors proteins growth factor receptor-bound protein 2 (GRB-2) and GRB-2 related adapter protein 2 (GADs). GRB2 is constitutively associated with a GEF, son of sevenless (SOS). Importantly, GADs plays a crucial role in expanding the signalosome by recruiting SLP-76 (124). ZAP-70 also phosphorylates SLP-76 at multiple tyrosine residues, leading to the recruitment of several molecules, including IL2 inducible T-cell kinase (ITK), VAV1, NCK adaptor protein 1 (NCK1) or

adhesion- and degranulation-promoting adaptor protein (ADAP), a key regulator of T-cell cytoskeletal rearrangement (118).

The association of PLCγ1 with SLP-76 serves to further strengthen the dual-scaffolded signalosome. Following the recruitment of ITK to SLP-76 and its activation by LCK, ITK interacts and phosphorylates PLCγ1. Activated PLCγ1 catalyzes the hydrolysis of membrane-bound phosphatidylinositol 4,5-biphosphate (PIP2) to generate the secondary messengers: inositol triphosphate (IP3) and diacyl glycerol (DAG) that lead to the activation of major downstream pathways fundamental for T-cell biology (125).

IP3 binds to its receptors located in the endoplasmic reticulum, triggering Ca^{2+} release and calcineurin activation. This activation of calcineurin leads to the dephosphorylation and nuclear translocation of nuclear factor of activated T cells (NFAT) (126). Membrane-bound DAG activates the GTPase RAS guanyl nucleotide-releasing protein (RASGRP1), initiating the RAS-extracellular signal-regulated kinase 1/2 (ERK1/2)-activator protein 1 (AP-1) cascade. Nuclear NFATs form a complex with AP-1 transcription factor to induce the expression of genes fundamental for T-cell activation, such as the pro-inflammatory cytokine IL-2 (127).

DAG can also activate protein kinase C-theta (PKCθ), which stimulates the inhibitor of kappa B kinase (IKK)-induced release of activated NF-κB and its nuclear translocation leading to T-cell activation, survival and effector function (115,127). NF-κB signaling can be further promoted through CD28 signaling.

CD28 signaling complements and extends the pathways initiated by TCR ligation. Upon the recruitment of PI3K to CD28, PI3K converts PIP2 into phosphatidylinositol 3,4,5-triphosphate (PIP3), which facilitates the recruitment of pyruvate dehydrogenase kinase 1 (PDK1) that subsequently activates PKCθ, thereby prolonging NF-κB signaling. Moreover, PDK1 can also activate AKT and downstream mammalian target of rapamycin (mTOR) pathway, critical for T-cell proliferation and survival. Additionally, activated AKT can enhance NF-κB signaling, although it is not essential for NF-κB signaling in T cells. Furthermore,

AKT can prolong the nuclear localization of NFAT, thereby influencing IL-2 transcription (118,127).

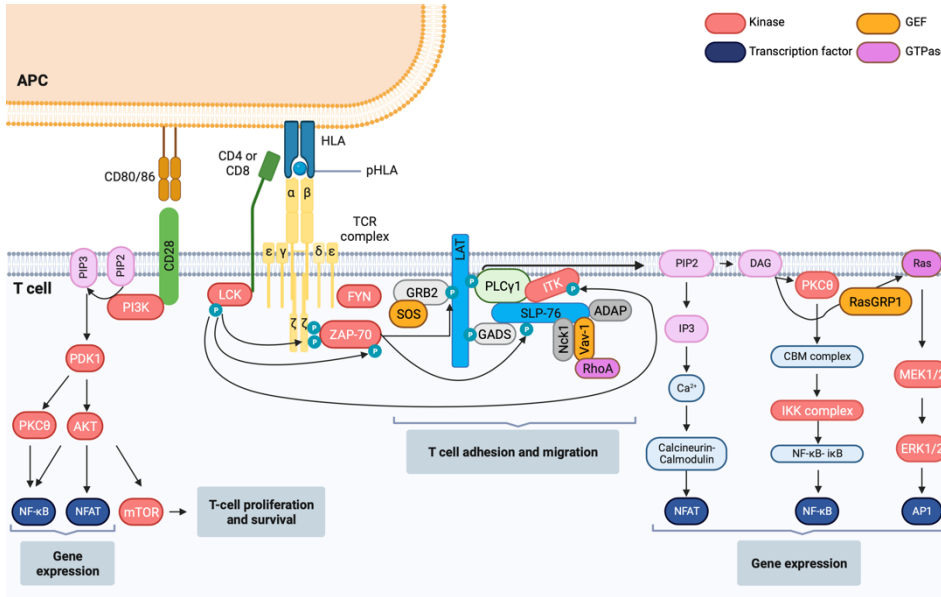

Figure 10. T-cell receptor signaling. Schematic of the TCR signaling cascade with a simplified representation of the downstream signaling mediators. Briefly, TCR engagement leads to the activation of LCK and FYN that phosphorylate the tyrosine residues in ITAMs, recruiting ZAP-70 kinase, which is further activated through LCK-mediated phosphorylation and autophosphorylation. ZAP-70 then phosphorylates adaptor proteins LAT and SLP-76, serving as docking sites for signaling molecules. This leads to the recruitment of PLCγ1, GRB-2, GADS, SOS and other molecules, expanding the signalosome. PLCγ1 catalyzes the hydrolysis of PIP2 to generate IP3 and DAG, activating downstream pathways. IP3 triggers Ca^{2+} release and NFAT activation, while DAG initiates the RAS-ERK1/2-AP-1 cascade. Additionally, DAG activates PKC*θ*, stimulating NF-*κB* signaling, complemented, and extended by CD28 signaling through PI3K, PDK1, AKT, and mTOR pathways, influencing T-cell activation, survival, and effector function. GEF, guanine exchange factor; Adapted from Shah K. et al. Signal Transduct. Target. Ther. 2021.

1.3.1.2. Pathogenic role of TCR signaling in T-cell lymphoid malignancies

Recurrent mutations and fusions affecting genes associated with proximal TCR signaling have been reported in several T-cell malignancies. In the following section, I will focus on genetic alterations that impact proximal TCR signaling, significantly contributing to the pathogenesis of T-cell malignancies (**Figure 11**).

In addition to the widely prevalent *RHOA G17V* mutation observed in AITL and PTCL, NOS, studies on gene expression profiling studies within TCL have identified several mutations in other genes regulating the TCR signaling pathway (128). Genetic alterations within the most proximal TCR signaling kinases, *FYN* and *LCK*, have been reported. Mutations occurring within the autoinhibitory loop of the *FYN* tyrosine kinase lead to its constitutive activation. These mutations are detected in 3% of cases of nTFHL-AI and PTCL, NOS (39,61). Furthermore, a gene fusion involving *FYN* and the TRAF3 interacting protein 2 (*TRAF3IP2*), a cytoplasmic adaptor signaling downstream of the IL-17 receptor (IL-17R), results in aberrant NF-κB signaling (129,130). Notably, within a cohort of 30 patients, the FYN-TRAF3IP2 fusion was identified in 20% cases (4/30 nTFHL-AI and 2/30 PTCL, NOS) (130).

A less common fusion involving *LCK* and KH domain-containing, RNA-binding, signal transduction associated 1 (*KHDRBS1*) was identified in 1/15 patient of PTCL, NOS. Importantly, the ectopic expression of LCK-KHDRBS1 in murine CD4+ T cells triggered the chronic activation of various TCR signaling branches and resulted in increased LCK phosphorylation compared to the empty vector in mice (129). Around 5-10% of T-ALL cases exhibit a fusion involving nucleoporin 214 (*NUP214*) and *ABL1*, which leads to the epigenetic amplification of ABL1. The NUP215-ABL1 fusion protein promotes proliferation and survival of T-lymphoblasts in a LCK-dependent manner (131).

Genomic alterations in *VAV1* encompass in-frame deletions in its negative regulatory domain, resulting in the disruption of the autoinhibitory conformation of the protein, leading to an enhanced NFAT and NF-κB signaling. These mutations are detected in approximately 11% of ALCL, 6-11% of PTCL, NOS and 5% of nTFHL-AI (132–135). Additionally, gene fusions involving the C-terminal domain of *VAV1* lead to aberrant activation of VAV1 downstream signaling (133). Notably, the VAV1 and myosin 1F (*MYO1F*) fusion protein strongly activates VAV1-dependent signaling cascades, including ERK1/2 and NFAT pathways. A mouse model with a conditional knock-in of VAV1-MYO1F fusion protein, selectively

expressed in CD4+ T cells, resulted in the development of PTCL,NOS mimicking traits of the human GATA3 subtype (132,133,136,137).

Activating mutations within the PLCγ1 gene are detected in approximately 14% nTFHL-AI and 6% in PLCγ1 of PTCL, NOS, contributing to enhanced NFAT signaling (61). Another notable translocation involves *ITK* and spleen tyrosine kinase (*SYK*), often abnormally expressed in TCL. This fusion is described in approximately 18% of nTFHL-F and leads to the over-expression of SYK, a component of the B-cell receptor (BCR) signaling (138). The ITK-SYK fusion gene in mice leads to persistent activation of TCR signaling and induced lymphomagenesis (139,140).

Mutations in the co-stimulatory receptor CD28 signaling have been documented in TCL. A subset of patients with nTFHL-AI, ranging from 4% to 12%, exhibit mutations within *CD28* that prolong ligand-receptor interactions, thereby amplifying TCR signaling (61,137). Additionally, *CD28* gene fusions are common. Cytotoxic T-lymphocyte-associated protein 4 (*CTLA-4)-CD28* fusions are detected in approximately 58% of cases, and inducible T-cell co-stimulator (*ICOS)-CD28* fusions are identified in around 5% of cases (54). Upon TCR stimulation, the expression of *CTLA4* and *ICOS* increases, while *CD28* expression is downregulated. These CD28 fusions are believed to sustain CD28 co-stimulatory signaling pathway (141).

Furthermore, mutations in PI3K have been identified in 7% of nTFHL-AI, as well as other nTFHL. These mutations likely enhance the catalytic subunit activity or strengthen the binding of the PI3K regulatory subunit 1 (PI3K1R) to CD28 (61). The negative regulation of the PI3K signaling highly depends on the PTEN, a phosphatase responsible for dephosphorylating PIP3, thereby preventing AKT activation (142). PTEN mutations or deletions are described in 20% of T-ALL patients, leading to the PI3K hyperactivation and subsequent enhancement of proliferation and survival of malignant T-ALL cells (143). Lastly, PDK1, a pivotal mediator of PI3K-AKT signaling, displays mutations in 5,9% of nTFHL-AI, potentially contributing to enhanced downstream signaling activation (61,144).

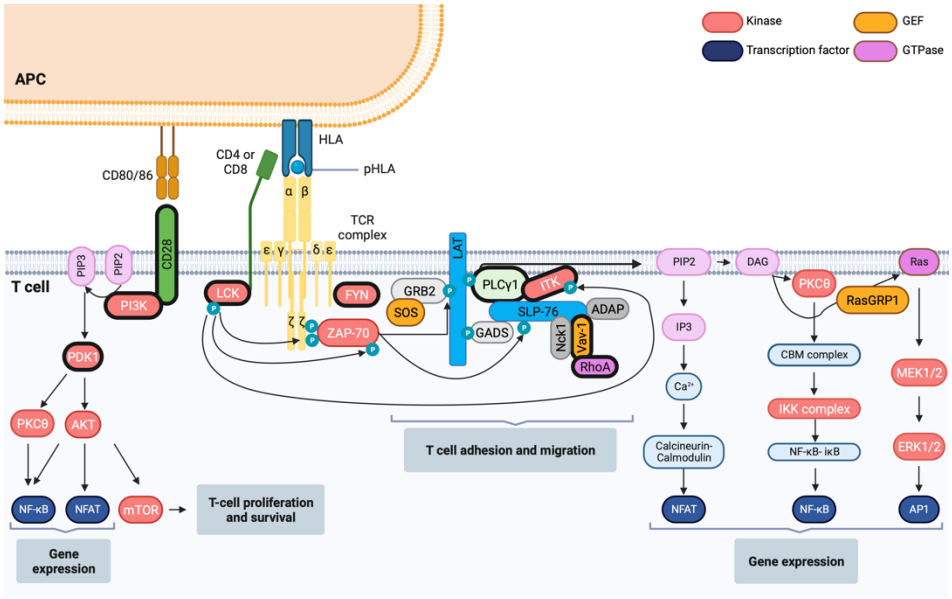

Figure 11. Recurrent alterations in the TCR signaling pathway in T-cell malignancies. Genes that are frequently altered are indicated with bold black borders. Adapted from Shah K. et al. Signal Transduct. Target. Ther. 2021.

1.3.2. Therapeutic targeting of TCR signaling

A few early-phase studies in TCL have demonstrated the clinical potential of targeting pivotal kinases in the TCR signaling cascade. Notably, a phase II trial (NCT03372057) assessing Duvelisib, an orally administered PI3K-gamma, delta inhibitor, in 78 patients with r/r TCL. unveiled an ORR 50% and CR of 32% during the expansion phase (145). Another phase II study (NCT04705090) exploring the safety and efficacy of YY-20394, a small molecule PI3K-delta inhibitor, in r/r TCL is currently underway.

Dasatinib, an oral small molecule inhibitor targeting the ABL1 kinase and the Src family kinases, in synergy with CHOEP, exhibited enhanced chemotherapy efficacy *in vitro* and efficacious tumor growth inhibition in murine TCL models (146). Dasatinib has been used for the treatment of Philadelphia-positive B-cell ALL, which is characterized by the presence of the BCR-ABL1 oncoprotein, and T-ALL patients expressing the NUP215-ABL1 fusion protein, suggesting the utility and application of dasatinib in the clinic (147,148). Interestingly, emerging research elucidated the reliance of NUP215-ABL1-driven T-ALL cells on LCK

expression and activity to proliferate and survive, which can also be targeted by dasatinib (131). Nevertheless, dasatinib single-drug treatment often leads to drug-resistant mutations within BCR-ABL1 or activates Ras and PI3K/AKT/mTOR signaling pathways as compensatory mechanisms (149,150). Further exploring the potential benefits of LCK inhibition in T-ALL, a preclinical study identified a potent synergistic effect between dasatinib and AKT/mTOR1 inhibitors, validated in human T-ALL cell lines and murine models (151).

Another member of the Src family of kinases, FYN can also be targeted in TCL. Given the aberrant activation of NF-κB signaling by the FYN-TRAF3IP2 fusion protein, a preclinical study with the IKK inhibitor, BMS-345541, induced strong dose-dependent anti-lymphoma effects with *in vitro* and *in vivo* (130).

While the expression of the ITK-SYK fusion protein is predominantly observed in nTFHL-F, heightened ITK expression has been detected in diverse subtypes, including nTFHL-AI (152). Preclinical studies highlighted the potential role of ITK in chemotherapy resistance in malignant T cells, with ITK inhibition showing promise in overcoming this resistance and suppressing tumor growth in TCL models (152,153). Cerdulatinib, a small-molecule inhibitor targeting both SYK and JAK family members, demonstrated favorable tolerability in a phase IIa trial for r/r TCL patients (154). However, a subsequent phase IIb trial (NCT04021082) was withdrawn. Presently, an ongoing phase I trial (NCT03952078) is evaluating the selective ITK inhibitor CPI-818 in r/r TCL patients.

1.4. Zeta-Chain Associated Protein Kinase 70 (ZAP-70)

In 1991, Chan A. et al aimed to identify molecules interacting with the ζ chain of the TCR complex, crucial for TCR signal transduction (155). In their investigation, they successfully discovered a 70 kDa protein that co-precipitated with the ζ chain following TCR stimulation, which they designated as ZAP-70 (155,156).

ZAP-70 is a crucial kinase in the transduction of proximal TCR signaling, whose expression is predominantly confined to T cells and NK cells (157). ZAP-70 belongs to the SYK-family of tyrosine kinases, along with its B-cell homologue, SYK kinase, that is primarily expressed in B cells. Interestingly, it has been reported that ZAP-70 is expressed in pro/pre B cells of both mice and humans, but not in mature B cells (158). Both ZAP-70 and SYK have essential roles in the signaling pathways of TCR and B-cell receptor (BCR), crucial for the functionality and development of these respective cell types (159).

1.4.1. ZAP-70 Structure

The ZAP-70 protein is organized into three domains and two interdomains (**Figure 12**). The N-terminal region of the protein contains two Src homology (SH2) domains, linked by the interdomain A (160). The C-terminal SH2 domain is connected to the kinase domain via interdomain B (161). The total length of the five segments accounts for 619 amino acids (162).

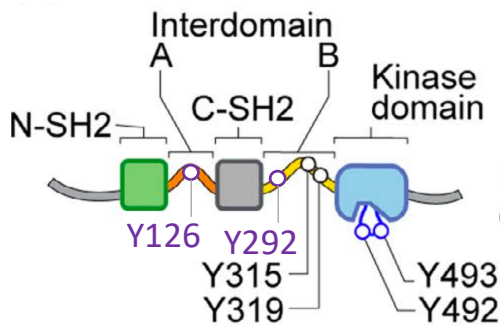

Figure 12. ZAP-70 domain structure. Schematic representation of ZAP-70 structural domains, including the N-terminal and C-terminal SH2 domains, interdomain A, interdomain B and the kinase domain. Positive regulatory tyrosines are depicted in black while negative regulatory tyrosines are represented in purple. Adapted from Ashouri J. *et al.* Immunol Rev. 2022.

- SH2 domains

SH2 domains are renowned for their specific binding capability to phosphorylated tyrosine residues on other proteins. In the case of ZAP-70, they are responsible for recruiting ZAP-70 to the TCR complex by interacting with the

diphosphorylated ITAMs located on the cytoplasmatic ζ chain dimers of the TCR complex (123).

- Interdomain A

Interdomain A confers flexibility and facilitates communication between the two SH2 domains. Mutations in the Tyrosine 126 (Y126) residue of the interdomain A have been shown to reduce the binding affinity of ZAP-70 to phosphorylated ITAMS (123). The phosphorylation of Y126 promotes the release of ZAP-70 from ITAMs, enabling its interaction with more distantly located LAT molecules, thereby amplifying the TCR signal during early stages of TCR stimulation (123,163).

- Interdomain B

Interdomain B contains three critical tyrosine residues, namely Y292, Y315 and Y319. Upon phosphorylation by LCK, these Tyr residues facilitate the interaction of ZAP-70 with other proteins, therefore contributing to the propagation of downstream signaling events (161). Mutational studies have demonstrated that the phosphorylation of Y292 allows the binding of negative regulators, as the ubiquitin ligase c-Cbl, that inactivate ZAP-70 kinase activity (164). Conversely, the phosphorylation of Y315 facilitates the recruitment of the guanine exchange factor VAV and the phosphorylation of Y319 facilitates the interaction with LCK, respectively, that positively regulate ZAP-70 kinase activity (161).

- Kinase Domain

The kinase domain is responsible for the catalytic activity of ZAP-70. Following TCR stimulation, two critical tyrosine residues, Y492 and Y493, undergo phosphorylation by LCK or autophosphorylation of ZAP-70 itself. The phosphorylation of both residues, particularly Y493, is imperative for the full kinase activity of ZAP-70 (165).

1.4.2. Recruitment of ZAP-70 to the TCR

In the absence of ligand binding to the TCR complex, 'the non-ligand bound state' (**Figure 13A**), ZAP-70 resides in the cytoplasm of the T cell, adopting an autoinhibited conformation (**Figure 13A**). In this state, two regulatory tyrosine residues, Y315 and Y319, located within interdomain B, engage with interdomain A and the kinase domain, respectively. These interactions effectively prevent the SH2 domains from engaging with the ITAMs at the TCR complex (**Figure 13B**) (123).

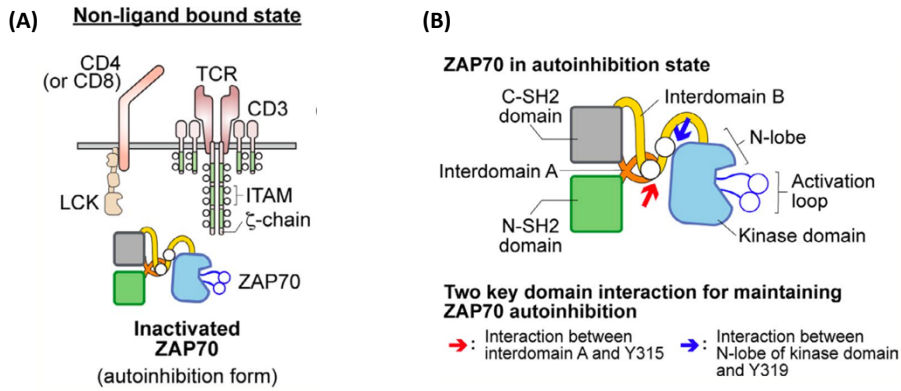

Figure 13. Schematic reprsentation of ZAP-70 location and conformational state in resting state. (A) In resting T cells in the absence of interaction between the TCR and any pHLA, ITAMs are not phosphorylated and ZAP-70 is located in the cytoplasm in an autoinhibited state. **(B)** The red and blue arrows indicate key interactions among different structural domains of ZAP-70 that maintain the autoinhibitory state of ZAP-70. From Ashouri J. *et al.* Immunol Rev. 2022.

Upon recognition of self-antigens (self-pHLA), the 'self-ligand-bound state', the membrane bound LCK kinase phosphorylates both tyrosines within ITAMs (**Figure 14A**). Subsequently, the tandem SH2 domains of ZAP-70 establish high affinity and specific interactions with these phosphorylated tyrosines. This binding induces a conformational change in interdomain A, leading to a partial release from the autoinhibited state of ZAP-70. However, self-antigen recognition does not lead to full activation of ZAP-70, mainly because the self-pHLA-TCR interaction is transient, and does not endure long enough for LCK to

phosphorylate the essential ZAP-70 residues required for complete autoinhibition relief and consequent activation (123,160).

Conversely, when foreign antigens (agonist pHLA) are recognized, the 'agonist-bound state' (**Figure 14B**), the prolonged interaction between the agonist pHLA-TCR and the sustained association of the CD4 or CD8 coreceptors, which are linked to active LCK, results in the phosphorylation of specific residues. LCK phosphorylates Y315 and Y319 within interdomain B, as well as Y493 within the ZAP-70 kinase domain. The phosphorylation within the kinase domain leads to the stabilization of its active conformation, a pivotal step for ZAP-70 catalytic function. Subsequently, ZAP-70 is able to phosphorylate its targets, LAT and SLP-76 (160).

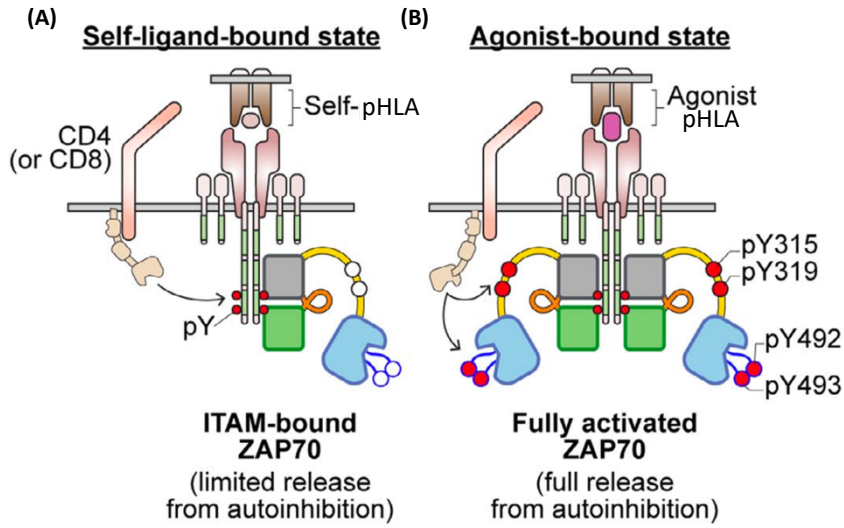

Figure 14. Schematic reprsentation of ZAP-70 location and conformational state during TCR recognition of self-pHLA or agonist pHLA antigens. (A) Upon antigen recognition of a self-pHLA, the interaction delivers a sufficient tonic signal to lead ITAM phosphorylation by LCK. This results in the recruitment of ZAP-70 to the phosphorylated ITAMs but ZAP-70 is not further phosphorylated. **(B)** Upon recognition of an agonits pHLA, coreceptor-associated LCK is recruited to the proximity of engaged TCR and CD3 complexes long enough to phosphorylate ITAMs and recruit as well as phosphorylate ZAP-70 that is bound to phosphorylated ITAMs. Further phosphorylation of ZAP-70 by LCK on Y315, Y319 and Y493 leads to its activation. From Ashouri J. *et al.* Immunol Rev. 2022.

1.4.3. Role of SYK family kinases in T-cell development

The two constituents of the SYK family of tyrosine kinases, namely SYK and ZAP-70, are expressed at various stages of thymic ontogeny, featuring an inverse expression pattern and play distinct functions (**Figure 15**) (166).

SYK is predominantly expressed during the early stages of DN1-DN3 populations, after which it experiences downregulation. During the intermediate developmental stages, there is an overlapped expression of both kinases at DN3 and DN4 stages (**Figure 15**). Notably, studies in mice thymocytes deficient in either ZAP-70 or SYK do not exhibit any apparent abnormalities at the β-selection stage. Intriguingly, when both kinases are simultaneously knocked out, a complete blockage at this stage is observed. This observation suggests that SYK and ZAP-70 can functionally compensate for each other during pre-TCR signaling in the DN3 stage (166,167).

In contrast, ZAP-70 expression exhibits an upward trend, increasing from the DN3 population and continuing to promote sustained pre-TCR/TCR signaling from DN4 to SP stages. This sustained signaling orchestrated by ZAP-70 contributes to the promotion of cell survival and cell-cycle progression (168,169).

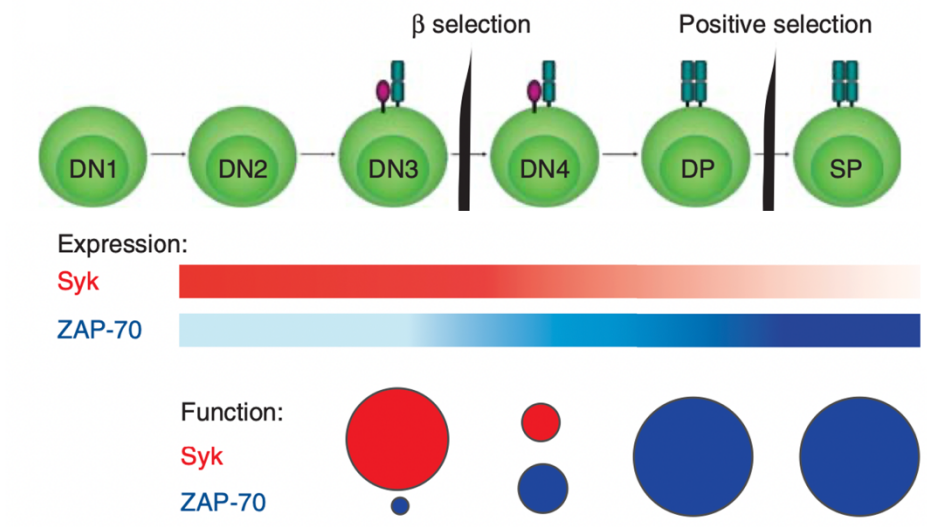

Figure 15. Expression and function of SYK family kinases throughout T-cell development. SYK is primarily expressed in early-stages of T-cell development (DN1-DN3), whereas the expression of ZAP-70 increases from DN3 onwards, promoting survival of mature T cells. Adapted from Wang H. *et al.* Cold Spring Harb. Perspect. Biol. 2010.

1.4.4. ZAP-70 and disease

ZAP-70 expression has been identified across various subtypes of B cell malignancies (170). Nevertheless, the central emphasis of this chapter will be on chronic lymphocytic leukemia (CLL), since it was the first B cell malignancy where ZAP-70 expression was identified and has been extensively studied (171). Furthermore, I will discuss the role of ZAP-70 in T-cell lymphoid malignancies.

1.4.4.1. Chronic lymphocytic leukemia (CLL)

CLL is a lymphoproliferative malignancy characterized by the clonal expansion of mature CD5+ B cells in peripheral blood, BM, lymph nodes and the spleen. To date, this disease is still incurable (172). Early investigations unveiled a distinct prognostic significance in CLL linked to the mutational status of the immunoglobulin heavy chains (IGHV). Specifically, patients with unmutated

IGHV genes exhibit a more aggressive disease and an unfavorable prognosis compared to those with mutated IGHV genes (173).

The aberrant expression of ZAP-70 in CLL B cells has emerged as a surrogate marker for determining the IGHV mutational status. The detection of at least 20% ZAP-70-positive malignant B cells through flow cytometry correlates with the presence of unmutated IGHV genes (174,175).

However, the strict segregation of SYK to B cells and ZAP-70 commonly seen in healthy cells, is less evident in lymphoid malignancies. In CLL, ZAP-70 expression is associated with unfavourable outcomes due to heightened BCR signaling, increased proliferation, and migration of CLL cells to the tumor microenvironment (123). Early investigations indicated that ZAP-70 enhanced Immunoglobulin M (IgM) BCR signaling within ZAP-70 positive CLL B cells (176). Importantly, this enhancement was independent of ZAP-70 kinase activity, as its phosphorylation levels within CLL B cells were inefficient and negligible compared to those of SYK (177). Induced mutations in the kinase domain of ZAP-70 did not abolish IgM-mediated BCR signaling activation. This implies that ZAP-70 assumes a more prominent role as an adaptor protein within CLL cells (178).

Recent research has shown that ZAP-70 plays pro-survival roles in CLL that are independent of BCR signaling. ZAP-70 positive CLL B cells exhibit enhanced surface C-C chemokine receptor type 7 (CCR7) expression, enabling increased migration to its chemokine ligands CCL19 and CCL21 towards the lymph nodes, where they can encounter CD4+ T cells, promoting CLL B cells survival (179,180). Besides, ZAP-70 is involved in the assembly of protein complexes between itself and ribosomal proteins. This interaction ultimately leads to elevated MYC expression and protein synthesis. Additionally, ZAP-70 enhances the production of the chemokines CCL3 and CCL4. These chemokines facilitate the accumulation of CD4+ T cells within the CLL microenvironment and can further induce CLL B cell proliferation via CD40 activation (181).

The expression of ZAP-70 has also been described in other B cell malignancies. In cases where ZAP-70 and SYK are co-expressed aberrantly in B

cells, ZAP-70 competes with SYK at the BCR signalosome. This rewires BCR signaling, shifting it from negative selection to tonic PI3K signaling. Consequently, B cells are able to escape anergy and negative selection, thereby promoting B cell survival (182).

1.4.4.2. T-cell malignancies

ZAP-70 expression is preserved in the majority of nTFHL, AI and PTCL, NOS cases (183–185). However, systemic ALCL commonly exhibits the lack of expression of TCR, CD3 proteins or ZAP-70 (183,186). In a prospective study involving 12 paired nTFHL-AI samples treated with CHOP or CHOP-like therapy, newly identified ZAP-70 missense mutations were detected in 41,7% of patients by whole exome sequencing. However, the biological implications of these mutations remain uncertain. Moreover, the phosphorylation status of crucial regulators in the proximal TCR signaling pathway was assessed in tumor tissues from 38 nTFHL-AI. IHQ analysis demonstrated ZAP-70 phosphorylation in 68,4%, ITK phosphorylation in 73,7% and PLCγ1 phosphorylation in 52,6% of cases (152). Besides, the knockdown of ZAP-70 by short-hairpin RNA (shRNA) led to a pro-apoptotic effect, compromised proliferation, adhesion, invasion, migration and G2/M cell cycle arrest of malignant T-cell lines (187). Conversely, a separate article focused on ZAP-70 expression mainly in NKTCL cell lines. Interestingly, ZAP-70 knockout exhibited no advantageous effect on cell viability or apoptosis induction. Furthermore, treatment with Gefitinib, an epidermal growth factor receptor (EGFR) inhibitor of which ZAP-70 is an off-target, showed no significant differences between ZAP-70 overexpressing or knockdown cell lines (188).

1.4.5. Therapeutic targeting of ZAP-70

Given its crucial role in TCR signaling transduction and its relevance in lymphoid malignancies pathogenesis, targeting ZAP-70 holds compelling potential in these diseases. Despite not achieving the same level of success of SYK-specific inhibitors, limited selective ZAP-70 inhibitors have emerged, with none progressing to clinical trials so far. Various strategies for ZAP-70 inhibition have

been explored, leading to the development of potential inhibitors like 2-phenylaminopyrimidines or imidazo[1,2-c]pyrimidine scaffolds (162). A recent publication presented a pyrimidine covalent inhibitor of ZAP-70 kinase domain, impacting CD4+ T-cell proliferation, division and cytokine production *in vitro*, along with promising results in a psoriasis mouse model (189,190).

An alternative approach seeks to prevent ZAP-70 from binding to doubly phosphorylated ITAMs while promoting its autoinhibited conformation. Biophysical screenings identified small organic compounds, mainly sulfone and sulphonamide compounds, that could covalently modify tSH2 of ZAP-70, consequently impeding their binding to ITAMs (191).

The third described strategy for ZAP-70 inhibition involves an allele-specific approach, achieved by replacing a specific M414 residue within the ZAP-70 kinase domain. This modification preserved kinase activity while creating a unique binding pocket sensitive to analogues of the broad kinase inhibitor PP1. This strategy hinders downstream signals, including the rise in cytosolic free Ca^{2+}, prior to TCR stimulation. Notably, this technique demonstrates specificity by lacking inhibition effects on wild-type ZAP-70 and having negligible effect on SYK-dependent BCR signal transduction (192).

In a recent study, a dual small molecule-gated ZAP-70 signaling switch was introduced. This design fuses the analogue-sensitive ZAP-70 allele with the engineered ligand binding domain of the estrogen receptor ERT2. The activity of ERT2 can be upregulated to a certain degree by a tamoxifen metabolite, and diminished by an ATP analogue, 3-MB-PP1. This system also allows the modulation of early TCR signaling by adjusting the concentration of activator or inhibitor. However, the fusion of ERT2 with ZAP-70 seems to alter ZAP-70 downstream effector function, necessitating further exploration (193). This approach holds promise for potentially managing overreactions in CAR-T therapy, offering a means to regulate their activity and limit their effects (171).

These diverse approaches for ZAP-70 inhibition collectively hold the promise of advancing therapies for lymphoid malignancies and fine-tuning

immune responses in novel ways, paving the path towards more effective treatments.

2. Hypothesis

Hypothesis

T-cell malignancies are a heterogeneous group of highly aggressive diseases that currently lack effective treatments. Despite recent advancements in the understanding of T-cell malignancy biology, the standard approach of using front-line anthracycline-based chemotherapy, originally adapted from studies in more prevalent B-cell lymphomas, leads to limited response rates, high relapse rates and dismal survival outcomes. These suboptimal clinical responses underscore the need to develop new highly selective and more effective drugs that target specific molecular and genomic vulnerabilities in T-cell malignancies.

Similar to B-cell lymphoproliferative syndromes, where the B-cell receptor (BCR) plays a central role in pathogenesis, multiple somatic mutations and gene translocations have been identified in crucial genes within the TCR signaling pathway, suggesting its critical role in the survival and proliferation of malignant T cells. Within the TCR signaling pathway, ZAP-70, a tyrosine kinase protein that belongs to the SYK/ZAP-70 family and is predominantly expressed on T cells, plays a pivotal role in proximal TCR signaling. Upon TCR stimulation, ZAP-70 undergoes phosphorylation and participates in signal transduction, essential for the survival and proliferation of T cells and, to date, no specific inhibitors targeting ZAP-70 have been translated to clinic use.

Based on this observation, we hypothesized that ZAP-70, due to its major function in the TCR signaling pathway, is a potential main effector to target to decrease the proliferation and survival of malignant T cells and represents a novel therapeutic approach for the treatment of T-cell malignancies.

3. Objectives

Objectives

The **main objective** of this thesis is:

To assess the preclinical therapeutic potential of pharmacological inhibitors targeting the tyrosine kinase ZAP-70 in T-cell malignancies.

The **secondary objectives** are the following:

1. To determine the *in vitro* efficacy and specificity of novel ZAP-70 kinase inhibitors against a panel of kinases using a biochemical kinase assay.

2. To analyze *in vitro* the impact of the most efficient and specific ZAP-70 kinase inhibitors on the proliferation, viability, and TCR signaling of human malignant T-cell lines.

3. To characterize *in vivo* the acute toxicity profile and pharmacokinetic properties of the most efficient and specific ZAP-70 inhibitors in immunodeficient mice.

4. To assess the *in vivo* anti-tumor efficacy of the most efficient and specific ZAP-70 kinase inhibitors in subcutaneous and intravenous T-ALL and ALK-negative ALCL xenograft models of malignant T-cell lines.

4. Material and Methods

4.1. Compounds

The 27 small-molecule ZAP-70 kinase domain inhibitors, IQS117 and IQS141, are pyrido[2,3-d]pyrimidine derivatives that were designed, synthesized, and provided by the Pharmaceutical Chemistry group led by Dr. José Ignacio Borrell (Chemistry Institute of Sarrià, Barcelona, Spain). The reference compounds, TAK-659, a SYK/FLT3 inhibitor, was obtained from Takeda Pharmaceutical International Co., while the BTK inhibitors, Ibrutinib and Acalabrutinib, were acquired from Selleckchem.

4.2. Kinase Inhibition profiling

The kinase inhibition profile of the ZAP-70 kinase domain inhibitor candidates was evaluated at Reaction Biology (Freiburg, Germany) using a radiometric protein kinase assay (^{33}PanQinase® Activity Assay). The kinase residual activity (in %) of each compound was evaluated at 10 µM in duplicates against a panel of 26 kinases relevant to T-cell and B-cell biology, particularly in TCR and BCR signaling, and kinases structurally related to ZAP-70 (see **Supplementary table 1** for the complete list of kinases). Briefly, the reaction cocktail for each kinase (10 µL of non-radioactive ATP solution; 25 µL of assay buffer/ [γ-33P]-ATP mixture; 5 µL of each test compound in 10% DMSO; and 10 µL of enzyme/substrate mixture) was added in duplicates in a 96-well FlashPlatesTM (Perkin Elmer) plate and incubated at 30ºC for 60 min. The reaction was stopped with 50 µL of 2 % (v/v) H_3PO_4, wells were aspirated, and washed two times with 200 µL of 0.9 % (w/v) NaCl. All assays were performed with a BeckmanCoulter Biomek 2000/SL robotic system. The incorporation of ^{33}Pi was determined with a microplate scintillation counter (Microbeta, Wallac). Commercial drugs TAK-659, Ibrutinib and Acalabrutinib were used as internal quality controls.

The residual kinase activity was calculated as follows: Residual activity (%) = 100 x [(signal of compound – low control)/(high control – low control)], where 'low control' defines the unspecific binding of radioactivity to the plate only

in the presence of the substrate and 'high control' reflects the maximum kinase activity of each kinase in the presence of the substrate in the absence of any inhibitor. The difference between the high and low control of each enzyme was taken as 100% activity.

4.3. Cell lines

The T-ALL cell line Jurkat and the Burkitt lymphoma B-cell line Ramos were purchased from the American Type Culture Collection (ATCC, Manassas, VA, USA). The ALK-negative ALCL cell line OCI-Ly13.2 was kindly provided by Dr. David M. Weinstock (Dana-Farber Cancer Institute, Harvard Medical School, Boston, MA, USA). The PTCL, NOS cell lines SMZ-1, OCI-Ly12 and T8ML-1 were provided by Dr. Adolfo Ferrando (Irving Cancer Research Center, University of Columbia, NY, USA). Ramos, Jurkat, OCI-Ly12 and OCI-Ly13.2 were cultured in RPMI (#L0500, Biowest) supplemented with 2 mM L-glutamine (#X0550, Biowest), 10% heat-inactivated fetal bovine serum (FBS) (#10270-106, Gibco) and 50 µg/mL penicillin/streptomycin (#L0022, Biowest). SMZ-1 was cultured in RPMI supplemented 2 mM L-glutamine, 20% FBS and 50 µg/mL penicillin/streptomycin. T8ML-1 was cultured in RPMI containing 2 mM L-glutamine, 20% heat-inactivated FBS, 50 µg/mL penicillin/streptomycin and 10 µg/mL recombinant human IL-2 (#200-02, Peprotech). Cell lines were maintained at 37ºC in a humidified atmosphere under 5% CO_2. Cell lines were routinely tested for mycoplasma contamination and cell lines authenticity was validated by short tandem repeat (STR)-profiling.

4.4. Flow cytometry analysis

To immunophenotype malignant human T-cell lines by flow cytometry, an extracellular and intracellular panel of human-specific antibodies was designed (**Table 6**). Briefly, T cells were stained with surface marker antibodies for 15 min at room temperature. Then, cells were resuspended in staining buffer [PBS with 1% bovine serum albumin (#A7906-100G, Merck) and 0.1% sodium azide (#S2002-5G, Merck)] and acquired in the flow cytometer. For the staining of

intracellular markers, cells were fixed and permeabilized for 30 min at 4ºC using the IntraPrep Permeabilization reagent (#A07803, Beckman Coulter) and incubated with the corresponding antibodies for 30 min at room temperature.

Table 6. List of monoclonal antibodies used for flow cytometry staining and their applications

Target	Conjugate	Clone	Application	Supplier	Catalog number
CD2	FITC	39C1.5	Cell lines phenotyping (s.s.)	BD Biosciences	A07743
CD3	ECD	UCHT1	Cell lines phenotyping (s.s.)	BD Biosciences	A07748
CD3	AA750	UCHT1	Cell lines phenotyping (i.s.)	BD Biosciences	A94680
CD4	AA750	13B8.2	Cell lines phenotyping (s.s.)	BD Biosciences	A94682
CD5	APC	BL1A	Cell lines phenotyping (s.s.)	BD Biosciences	A60790
CD7	PB	8H8.1	Cell lines phenotyping (s.s.)	BD Biosciences	B06499
CD8	AA700	B9.11	Cell lines phenotyping (s.s.)	BD Biosciences	B49181
CD10	PC5.5	ALB1	Cell lines phenotyping (s.s.)	BD Biosciences	B16490
CD19	PC7	J4-119	Cell lines phenotyping (s.s.)	BD Biosciences	IM3628
CD25	PC7	B149.9	Cell lines phenotyping (s.s.)	BD Biosciences	A52882
CD27	APC	1A4CD27	Cell lines phenotyping (s.s.)	BD Biosciences	B09983
CD28	PC7	CD28.2	Cell lines phenotyping (s.s.)	BD Biosciences	B23313
CD30	APC	HRS4	Cell lines phenotyping (s.s.)	BD Biosciences	A87939
CD45	KrO	J.33	Cell lines phenotyping (s.s.)	BD Biosciences	A96416
CD45RA	PB	2H4LDH11LDB9	Cell lines phenotyping (s.s.)	BD Biosciences	A82946
CD45RO	FITC	UCHL1	Cell lines phenotyping (s.s.)	BD Biosciences	IM1247U
CD197	PE	G043H7	Cell lines phenotyping (s.s.)	BD Biosciences	B30632
CD279	PE	PD1.3	Cell lines phenotyping (s.s.)	BD Biosciences	B30634
TCRαβ	PE	BMA	Cell lines phenotyping (s.s. and i.s.)	BD Biosciences	B49177
TCRγδ	PC5.5	IMMU510	Cell lines phenotyping (s.s.)	BD Biosciences	A99021
HLA-DR	PB	IMMU-357	Cell lines phenotyping (s.s.)	BD Biosciences	B36291
CD3	APC/A750	UCHT1	T-cell lines xenografts	BD Biosciences	A94680
CD45	V500	HI30	T-cell lines xenografts	BD Biosciences	560777

s.s., surface staining; i.s., intracellular staining

To identify malignant human T cells in processed mouse organs from intravenous xenograft models of malignant T-cell lines, the list of monoclonal antibodies used for flow cytometry staining is detailed in **Table 1**. After single-cell suspension obtention from each mouse organ (explained in 'Tissue dissociation

for flow cytometry analysis' below), cells were washed with ice-cold PBS 1X and erythrocytes were lysed using ACK lysing buffer (#A10492-01, Gibco). To minimize non-specific antibody binding, cells were blocked with 1 µg rat serum IgG per 10^6 cells (#I8015-10MG, Merck) for 10 min at 4ºC before the 30 min incubation with LIVE/DEAD™ Fixable Violet Dead Stain Cell kit (#L34964, Invitrogen) to stain dead cells. Cells were washed in PBS 1X and stained with the antibodies shown in **Table 1**. Human T cells were identified as CD45+ CD3+.

Cells from both experiments were acquired by a Navios™ cytometer (Beckman Coulter, Brea, CA, USA) and data were analyzed using the FlowJo v10 software (TreeStar).

4.5. Western blot

To initially select malignant human T-cell lines exhibiting functional TCR signaling, tyrosine phosphatase inhibition was induced by treating cell lines with 300 mM hydrogen peroxide (H_2O_2) and 100 mM sodium pervanadate (Na_3VO_4) for 5 min at 37ºC. To assess the impact of ZAP-70 kinase domain inhibitors upon TCR signaling activation, $3x10^6$ cells/well were seeded in a 24-well plate and treated for 6 h at 37ºC with 1, 10 or 25 µM of each compound. Cells were treated for 1 min with 5 µg/mL human anti-CD3 antibody (#130-093-387, Miltenyi) and 1 µg/mL human anti-CD28 antibody (#130-093-375, Miltenyi) to stimulate TCR signaling. Stimulation was stopped by the addition of ice-cold 1X PBS. In this experiment, Jurkat and OCI-Ly13.2 cells treated with 300 mM H_2O_2 and 100 mM Na_3VO_4 were included as positive controls for phospho-proteins. Whole-cell protein extracts were prepared using lysis buffer [20 mM Tris pH 7.4, 1 mM EDTA, 140 mM NaCl, 1% NP-40, 2% Na_3VO_4 and 1X proteases inhibitor cocktail (#P8340-1ML, Sigma-Aldrich)] for 30 min at 4ºC. Equal amounts of denatured protein were resolved by 10% SDS-PAGE and transferred to Immobilon-P membranes (#IPVH00010, Millipore). Membranes were blocked for 1 h at room temperature in 5% non-fat milk/TBST (Tris-Buffered Saline Tween 20) and incubated overnight at 4ºC with the following primary antibodies: phospho-Akt^{Ser473} (#9271), phospho-ERK1/2$^{Thr202/Tyr204}$ (#9101), phospho-LAT^{Tyr171} (#3581), phospho-PLCγ1^{Tyr783} (#2821),

phospho-ZAP-70^{Tyr319} (#2717), Akt (#9272), ERK1/2 (#9102), LAT (#4533), PLCγ1 (#2822) and SLP-76 (#4958) from Cell Signalling Technology; phospho-SLP76^{Tyr128} (#PA540272) and phospho-ZAP-70^{Tyr493} (#MA5-28073) (Invitrogen), ZAP-70 (#05-253) from Sigma-Aldrich and GAPDH (#sc-32233, Santa Cruz Biotechnology) or β-actin (#ab8226, Abcam) as loading control. Immunodetection was done with the corresponding IgG horseradish peroxidase (HRP)-linked secondary antibodies swine anti-rabbit (#P0399) or rabbit anti-mouse (#P0260) (Dako North America). The Immobilon Classico Western HRP substrate (WBLUC0100, Millipore) was used to detect protein-antibody complexes through chemiluminescence in an Amersham™ Imager 600 (GE Healthcare Life Sciences).

4.6. Cell proliferation assay

The effect of ZAP-70 kinase inhibitor candidates on cell proliferation was evaluated by measuring the metabolic reduction of the tetrazolium salt MTS. This was done using the CellTiter96™ Cell Proliferation Assay (#G3582, Promega) following the manufacturer's instructions to determine IC50 values. A total of $5x10^5$ cells/well were seeded in a 24 well-plate and treated with increasing concentrations of each ZAP-70 inhibitor candidate (IQS117 or IQS141) from 1-30 µM. We analyzed drug treatment responses following 48 h incubation. Absorbance was measured in a Spark 10M plate reader (Tecan) at 490 nm after MTS conversion. The IC50 values were calculated with GraphPad Prism 8 (GraphPad Software).

4.7. Assessment of apoptosis

Apoptosis was determined by analyzing the binding of Annexin V-APC (#BMS306APC, Invitrogen) and the incorporation of Propidium Iodide (PI) (#556463, BD Biosciences) staining by Flow cytometry. Annexin V/PI double-negative cells were considered viable cells. A total of $5x10^5$ cells/well were seeded in a 24 well-plate and treated with increasing concentrations of each ZAP-70 inhibitor candidate (IQS117 or IQS141) from 1-30 µM. After 48h, cells were stained

and acquired in a Navios cytometer (Beckman Coulter), and results were evaluated using FlowJo v10 software (TreeStar).

4.8. Plasmids

For human cell line lentiviral infection, we obtained FUW-mCherry-Puro-Luc (194), pCMV ΔR8.91 vector (195) and pMD2.G VSVG (#12259, Addgene) from Dr. Adolfo Ferrando (Irving Cancer Research Center, University of Columbia, NY, USA).

4.9. Virus production and cell lines infection

To generate infectious viral particles, 293FT cells (kindly provided by Dr. Alena Gros, Vall D'Hebron Institute of Oncology, Barcelona, Spain) were transfected with lentiviral constructs FUW-mCherry-Puro-Luc, pCMV ΔR8.91 and pMD2.G VSVG using polyethyleneimine (PEI) (#24765-1, Polysciences) as a transfecting agent. To transduce Jurkat and OCI-Ly13.2 cell lines, lentiviral supernatants were harvested at 48 h after transfection and malignant T-cell lines were infected by spinoculation. After infection, transfected cells were selected for 1 week in medium containing 1 µg/mL puromycin (#A1113802, Gibco). Cells bioluminescence was quantified using bioluminescence imaging (BLI), measured as total photons per second (ph/s), utilizing the IVIS® Spectrum system and Living Image software (PerkinElmer).

4.10. Animal models

NOD.CB17-Prkdc^{scid}/J (NOD/SCID) mice and NOD.Cg-Prkdc^{SCID}Il2rg^{tm1Wjl}/SzJ (NSG) mice were purchased from Charles River (Charles River Laboratories, France). NOD/SCID mice were used to evaluate the *in vivo* acute toxicity and pharmacokinetic profile of ZAP-70 inhibitor candidates. For *in vivo* therapeutic studies, NSG mice were used to develop subcutaneous and intravenous xenograft models of Jurkat and OCI-Ly13.2 cells lentivirally transfected to express luciferase.

All animals were maintained in filter-topped cages on autoclaved food and water in specific pathogen-free facilities at Vall D'Hebron Institute of Oncology. All animal procedures were approved by the Ethics Committee of Animal Research of the Vall D'Hebron Institute of Research and by the Catalan Government.

4.10.1. Acute toxicity

To assess the potential acute toxic effects resulting from a single-dose of our ZAP-70 inhibitors (IQS117 and IQS141), we adhered to the guideline outlined in the Organization for Economic Cooperation and Development (OECD) Fixed Dose Procedure Guideline for Single-dose Acute Toxicity (196). In this approach, the death of animals as an endpoint is avoided, and relied on the observation of clear signs of toxicity within a predefined range of fixed doses (5; 50; 300; 2000 mg/kg), leading to a decrease in the number of animals tested. The initial choice of 300 mg/kg dose is suggested in the absence of prior *in vivo* drug information. Given so, eight-week-old NOD/SCID mice were randomized into 6 groups, with each group comprising 2 males and 2 females. Prior to drug administration, mice were subjected to a 2 h fasting period. Then, one mouse from each group received a dose of 300 mg/kg of IQS117, IQS141 or vehicle (5% DMSO, 0.5% methylcellulose and 0.1% Tween80) via either oral gavage (p.o.) or intraperitoneal injection (i.p.). Following drug administration, mice were carefully monitored for signs of distress and toxicity for 30 min post-administration. If no critical conditions were observed during this initial observation period, the remaining mice were treated as planned, and the fasting period was resumed 1 h after compound administration. Mice weight and general condition were recorded every 3-4 days for two weeks. Animals were sacrificed 14 days after treatment and major organs (bone marrow, liver, lung, inguinal lymph node, kidney, small intestine, and spleen) were histologically examined at necropsy.

4.10.1.1. Histopathology and immunohistochemistry

Mouse tissues were dissected and fixed in 10% buffered formalin and paraffin-embedded at the Pathological Anatomy department at Vall D'Hebron Hospital. Tissue sections were subjected to hematoxylin-eosin staining using standard procedures. Microscopic images were captured with a light microscope (Nikon Eclipse Ci).

4.10.2. Single-dose pharmacokinetics

Seven- to eight-week-old NOD/SCID mice were randomized into eight groups (2 males and 2 females per group) for each drug. A single-dose of 50 mg/kg of IQS117 or IQS141 was administered via p.o. or i.p. and intracardiac blood was obtained at various time points after drug administration over 24 h (basal, 30 min, 2 h, 4 h, 6 h, 8 h, 16 h and 24 h). Plasma samples were obtained by centrifugation of individual blood samples at 2000g for 10 min at 4ºC and stored at -80ºC until drug concentration could be analyzed using reversed-phase liquid chromatography-tandem mass spectrometry (RP-LC-MS). Proteins were precipitated from 10 µL plasma samples by adding two volumes of acetonitrile. After vigorous vortexing, the samples were centrifuged for 5 min at 16.000 g. The supernatant was separated and diluted 40-fold in a solution containing 15% acetonitrile and 0.1% formic acid in water before LC-MS analysis. These samples were analyzed using a Maxis Impact high-resolution Q-TOF spectrometer (Bruker, Bremen), coupled to a nano-HPLC system (Proxeon, Denmark).

In the first step, 10 µL of each diluted sample was loaded onto a trapping column (Acclaim PepMap 100 nanoviper), which was 2 cm long with an inner diameter of 75 µm packed with C18 material (5 µm particle size, from Thermo Fisher Scientific) at a flow rate of 4 mL/min. Then, the samples were separated on the analytical column (Acclaim PepMap 100), which was 15 cm long with an inner diameter of 75 µm and packed with C18 (3 µm particle size, from Thermo Fisher).

Chromatography was performed using a gradient of 0.1% formic acid - acetonitrile (ranging from 0% to 80% over 30 min) at a flow rate of 300 nL/min. The column was coupled to the mass spectrometer (MS) inlet through a Captive Spray (Bruker) ionization source.

The MS acquisition was configured to 3 s cycles of mass spectra (2 Hz), followed by intensity dependent MS/MS scans at a variable rate between 2-20 Hz, depending on the intensity of the most intense precursor ions. A minimum intensity threshold of 2500 counts was applied, with a dynamic exclusion time of 1 min. All spectra were acquired on the range 150-2200 Da.

The LC-MS data was first processed using Data Analysis 4.1 (Bruker) and then quantified using Skyline Software (MacCoss Lab) to filter and integrate precursor signals of the target compounds. Using a HR-XIC Skyline template, extracted ion chromatograms for the mass-to-charge ratio (m/z) corresponding to the main isotope and charge state signal for each target compound were used for quantification. Plasma inhibitor concentrations were calculated using a standard curve constructed through the analysis of plasma samples spiked with known amounts of each drug. Pharmacokinetic parameters were calculated using the noncompartmental analysis tool of the software PCModfit V7.1.

4.10.3. Subcutaneous xenografts

Six-to seven-week-old NSG mice were subcutaneously injected with $5x10^6$ cells in 100 uL PBS (Jurkat-Luc) or PBS+Matrigel (1:1 ratio) (OCI-Ly13.2-Luc) into the right flank of each mouse. Two experiments were developed, a survival experiment and an acute drug treatment to further evaluate potential drug-related changes in the tumor transcriptome by RNA sequencing.

For the survival experiment, tumor growth was weekly measured by BLI, starting on day 14 post-injection until the end of the experiment. In parallel, tumor size was measured twice a week using a Vernier caliper and tumor volume was calculated using the following formula: volume=length x width^2/2. At day 15 post-injection, mice were randomized into 3 groups per cell line (4 females and 4 males

per group) and treatments were initiated: vehicle control (5% DMSO + 0.5% Methyl Cellulose + 0.1% Tween80 + 5% D-sucrose), IQS117 and IQS141 (50 mg/kg). Drugs were administered in the drinking water until the end of the experiment. Mice were euthanized when endpoint criteria were met, including tumor size (≥1500 mm^3), tumor ulceration, and significant weight loss (20% body weight loss or ≥10% over a week). Survival analysis used the Kaplan-Meier log-rank (Mantel-Cox) test using GraphPad Prism 8 (GraphPad Software).

For the acute treatment experiment, at day 28-post-injection, mice were randomized into 3 groups per cell line (4 males and 4 females): vehicle control (5% DMSO + 0.5% Methyl Cellulose + 0.1% Tween80 + 5% D-sucrose), IQS117 and IQS141 (50 mg/kg). Drugs were administered in the drinking water for a week. At day 35-post-injection, all mice were sacrificed, and tumors were snap-frozen in liquid nitrogen and kept at -80ºC until RNA extraction.

4.10.3.1. Bioluminiscence imaging

Mice were anesthetized with isoflurane (1-2%) before i.p. injection of luciferin at a dosage of 150 mg/kg. Images were acquired in an IVIS® Spectrum system, and the resulting data were processed with the Living Image software (PerkinElmer). The analysis involved determining the average radiance, expressed in units of photons per second per square centimeter per steradian (p/s/cm^2/sr), for each individual mouse.

4.10.3.2. RNA sequencing and data processing

Subcutaneus tumors were disaggregated using the hard tissue homogenizing CK28-2 mL kit (#P000916-LYSKO-A, Bertin Technologies) following standard procedures in a Precellys® Evolution Homogeniser (Bertin Technologies). Total RNA from tumors was isolated using the RNeasey mini kit (#74104, Qiagen). Total RNA was quantified by Qubit® RNA Broad Range (BR) Assay kit (Thermo Fisher Scientific) and the RNA integrity was estimated by using RNA 6000 Nano Bioanalyzer 2100 Assay (Agilent).

The RNASeq libraries were prepared with KAPA Stranded mRNA-Seq Illumina® Platforms Kit (Roche) following the manufacturer´s recommendations starting with 500 ng of total RNA as the input material. The library was quality controlled on an Agilent 2100 Bioanalyzer with the DNA 7500 assay.

The libraries were sequenced on a NovaSeq 6000 sequencing system (Illumina) with a read length of 2x51bp, following the manufacturer's protocol for dual indexing. Image analysis, base calling and quality scoring of the run were processed using the manufacturer's software Real Time Analysis (RTA 3.4.4).

RNA-seq reads were mapped against a combined reference genome of human (GRCh38) and mouse (GRCm39), using STAR aligner version 2.7.8a (197) with ENCODE parameters. Annotated genes were quantified using a combined annotation of human GENCODE v42 and mouse GENCODE version M31, with software RSEM (198) version 1.3.0 and default parameters. Subsequently, counts belonging to mouse genes were filtered out.

Differential expression analysis was performed independently for each cell line, using limma v3.6.1 R package (199). Counts were normalized with TMM (200) and transformed with the 'voom' function into logCPM. The linear models were fitted with the voom-transformed counts adjusting for the sex covariate and contrasts were extracted. A gene set enrichment analysis (GSEA) was perfomed on the list of pre-ranked genes by the limma moderated t-statistic, with the R package fgsea v1.12 (201), against the Reactome database (202).

4.10.4. Intravenous xenografts

Six-to seven-week-old NSG mice were intravenously injected with $5x10^6$ Jurkat-Luc cells or $2.5x10^6$ OCI-Ly13.2-Luc via tail vein in 100 uL PBS. Tumor engraftment was evaluated weekly by BLI, as described in section 4.10.3.1, starting at day 14 post-injection (Jurkat-Luc) and day 21 post-injection (OCI-Ly13.2-Luc) until the end of the experiment. At day 15 post-injection (Jurkat-Luc) and day 22 post-injection (OCI-Ly13.2-Luc), mice were randomized into 3 groups per cell line

(3 females and 3 males per group) and treatments were initiated: vehicle control (5% DMSO + 0.5% Methyl Cellulose + 0.1% Tween80), IQS117 and IQS141 (50 mg/kg). Drugs were administered daily via oral gavage. Mice were euthanized when endpoint criteria were met, including paraplegia, significant weight loss (20% body weight loss or ≥10% over a week) or general bad condition. Spleen and the left femur (Jurkat-Luc) or spleen and liver (OCI-Ly13.2-Luc) were collected in cold RPMI-1640 medium immediately after euthanasia and destined for flow cytometry analysis. Survival analysis was done using the Kaplan-Meier method and applied the log-rank (Mantel-Cox) test using GraphPad Prism 8 (GraphPad Software).

4.10.4.1. Tissue dissociation for flow cytometry analysis

Femur. The left femur from each mouse was cleaned after obtention with a scalpel and gentle rolling of the tissue between the fingers with paper towels. Each femur was placed inside of a mortar containing 5 mL of cold RPMI-1640 medium and the bone was crushed with a pestle. Cells were harvested with a Pasteur pipette and filtered through a 70 µm cell strainer (#352350, Falcon). This process was repeated three times to maximize the number of cells gathered.

Spleen. Half of the spleen from each mouse was placed in a 70 µm cell strainer. The organ was minced using the flat end of a plunger by crushing the spleen 5 times in gentle circular motions. 3 mL of RPMI-1640 were flushed through the filter to ensure maximizing cell harvesting. This process was repeated three times.

Liver. Half of the liver from each mouse was placed in a 10 mm petri dish containing 5 mL cold RPMI-1640. The organ was minced with a scalpel, cells were harvested with a Pasteur pipette and filtered through a 70 µm cell strainer. This process was repeated three times.

Single-cell suspensions were stained and analyzed in the flow cytometer as described in section 4.4.

4.11. Statistical Analysis

We conducted statistical analyses using Prism software v8.0 (GraphPad Software, La Jolla, CA, USA). Results are expressed as the mean ± SEM (standard error of the mean) or mean ± SD (standard deviation) of three independent experiments or replicates. The statistically significant differences between groups were analyzed using the Mann-Whitney test or two-way ANOVA and Bonferroni post-hoc test, and $P < 0.05$ was considered significant. For mouse survival experiments, we represented the results as Kaplan-Meier curves and determined the significance using Log-rank test. Representative images correspond to experiments repeated at least twice.

4.12. Data sharing statement

RNA-seq data is deposited at GEO under GSE243897.

5. Results

5.1. Design and synthesis of ZAP-70 kinase inhibitors

In our pursuit of developing novel ZAP-70 kinase domain inhibitors for preclinical evaluation in the context of T-cell malignancies, we focused on developing nitrogen-containing heterocyclic compounds, specifically pyrido[2,3-d]pyrimidine derivatives. This particular chemical structure is considered a privileged heterocyclic scaffold for drug discovery, due to their well-known activity as tyrosine kinase inhibitors (203). In this context, our collaborators from the Pharmaceutical Chemistry group at IQS had previously synthesized pyrido[2,3-d]pyrimidine compounds that demonstrated significant activity against BTK, effectively suppressing BCR signaling in B-cell lymphoid malignancies (204).

While several classes of ZAP-70 inhibitors have been reported (192,205), most display limited potency against ZAP-70 and a lack of selectivity, particularly in comparison to its structurally homologous protein, SYK. To develop ZAP-70 kinase domain inhibitors for our research project, our collaborators utilized structure-based design methods, conducting an in-depth analysis of ZAP-70 kinase domain. This comprehensive analysis identified crucial residues in the ATP-binding site for selective inhibition through pocket analysis and pharmacophore modelling. Subsequently, we identified compounds establishing critical interactions with ZAP-70, assessing their binding affinity through docking, and refining this process via molecular dynamics simulations. These efforts ultimately led to the synthesis of the most promising candidates (206).

5.2. Kinase inhibition profile of ZAP-70 kinase inhibitors

Our initial assessment involved the evaluation of the efficacy and selectivity of 27 novel pyrido[2,3-d]pyrimidine compounds against a panel of 26 kinases (complete list is provided in Appendix Figure 1). This panel included ZAP-70, along

with other kinases implicated in TCR and BCR signaling, including its structurally homologous kinase, SYK. As internal controls for the assay, we used three commercial tyrosine kinase inhibitors that target the BCR signaling pathway in B-cell malignancies. These included TAK-659, a dual SYK/FLT3 inhibitor currently undergoing phase I clinical studies for r/r diffuse large B-cell lymphoma (207) and r/r acute myeloid leukemia (208). We additionally included two BTK inhibitors, Ibrutinib and the more selective BTK inhibitor Acalabrutinib, both of which are approved therapies for several B-cell malignancies (209–211).

Among the 27 compounds tested, IQS117 and IQS141 primarily targeted ZAP-70 kinase activity, reducing it to 17% ± 1.6 and 11% ± 0.5, respectively, at a 10 µM dose (**Table 7**). Furthermore, IQS117 and IQS141 exhibited moderate inhibition of SYK kinase activity, with both compounds displaying approximately three-fold greater selectivity for ZAP-70 over SYK. Regarding off-targets effects on other relevant proximal signaling kinases, IQS117 reduced kinase residual activity to 21-50% for BTK and kinases within the Src family (LYN, LCK and YES), which are relevant in BCR and TCR signaling. Conversely, IQS141, exhibited off-target effects on SYK, BTK, and kinases in the Src family (LYN, LCK and FYN).

Interestingly, TAK-659 demonstrated potent inhibition on SYK and FLT3 kinase activity but also targeted other kinases like ZAP-70, BTK, LYN, LCK, YES, FYN and ITK, exhibiting low selectivity at 10 µM dose (**Table 7**). In contrast, Ibrutinib and Acalabrutinib effectively suppressed BTK kinase activity, with Ibrutinib also inhibiting other kinases, as its well-known off-target, ITK (212). As expected, these BTK inhibitors had minimal impact on ZAP-70 activity (**Table 7**).

These findings highlight the distinctive efficacy and selectivity of IQS117 and IQS141 in inhibiting ZAP-70 kinase activity among the tested candidates, making them promising candidates for targeting TCR signaling pathways in T-cell malignancies.

Table 7. Kinase inhibition profiles of the most potent and selective ZAP-70 inhibitors, IQS117 and IQS141, and commercial drugs (Ibrutinib, Acalabrutinib and TAK-659) at 10 µM. Residual kinase activity (%) for selected kinases (including off-targets) classified as significantly inhibited (<20%), moderately inhibited (21-50%), and low-inhibited (>50%). Results reported as mean ± SEM.

Residual Activity @ 10 µM (%)*	Compound (target)				
	IQS117	**IQS141**	**Ibrutinib (BTK/ITK)**	**Acalabrutinib (BTK)**	**TAK-659 (SYK/FLT3)**
ZAP70	17 ± 1.6	11 ± 0.5	76 ± 0	95 ± 2	7 ± 0.6
SYK	62 ± 3.3	41 ± 9.2	81 ± 0.8	92 ± 5.3	1 ± 0.1
BTK	32 ± 1	24 ± 5	0 ± 1.2	1 ± 0.2	28 ± 0.1
LYN	30 ± 7.5	34 ± 6.8	5 ± 0.9	57 ± 0.7	15 ± 1.5
LCK	49 ± 3	48 ± 4.7	2 ± 0.6	50 ± 28	39 ± 1.5
YES	41 ± 2.1	58 ± 0.8	1 ± 0.3	50 ± 5.5	25 ± 0.3
FYN	54 ± 6.1	45 ± 7.2	1 ± 0.8	74 ± 8.2	5 ± 0.9
ITK	51 ± 0.5	51 ± 3.4	3 ± 1.8	87 ± 2	10 ± 1
FLT3	96 ± 2.8	66 ± 5.8	20 ± 0.2	89 ± 1.7	7 ± 0.2

Kinase residual activity (%)	
	≤ 20%
	> 20% ≤ 50%
	> 50%

5.3. Characterization of malignant T-cell lines and assessment of TCR signaling functionality

To study the *in vitro* effect of our ZAP-70 inhibitors candidates, IQS117 and IQS141, on the viability, proliferation, and TCR signaling of several malignant T-cell lines, the cell lines under examination must have a functional surface TCR complex and associated signaling components, CD3 and/or CD28. Therefore, we conducted an initial immunophenotypic analysis (complete immunophenotype in Appendix Tables 2-3) on five malignant T-cell lines: Jurkat (T-ALL), OCI-Ly13.2 (ALK-negative ALCL), OCI-Ly12, SMZ-1 and T8ML-1 (PTCL, NOS). These cell lines represented different subtypes of T-cell leukemia and lymphomas (**Table 8**), where four out of the five were of non-commercial origin (T8ML-1, OCI-Ly13.2, OCI-Ly12 and SMZ-1), underscoring the necessity for additional characterization.

Regarding the immunophenotype of the cell lines (**Table 8**), Jurkat, OCI-Ly13.2 and T8ML-1 showed surface CD3, CD28 and TCRαβ, confirming their

suitability for further study. However, OCI-Ly12 and SMZ-1 exhibited no surface expression of CD3, CD28, TCRαβ or TCRγδ. Subsequently, we conducted further analysis to confirm the presence of cytoplasmic CD3 and TCRαβ in OCI-Ly12 and SMZ-1 cell lines, indicative of intracellular retention. Additionally, all cell lines exhibited CD30 expression, a characteristic marker associated with the ALCL subtype, a percentage of PTCL, NOS cases, and a third of T-ALL cases (184,213). Regarding CD4 and CD8 expression, Jurkat and SMZ-1 were CD4+, while T8ML-1 and OCI-Ly12 were CD8+. OCI-Ly13.2 was characterized as CD4- CD8-.

Table 8. Phenotypic characterization of malignant human T-cell lines. Cell line selection based on surface expression of CD3, CD28 and TCRαβ or TCRγδ. Jurkat, OCI-Ly13.2 and T8ML-1 cell lines exhibited surface expression of CD3, CD28 and TCRαβ while OCI-Ly12 and SMZ-1 cell lines did not expressed surface CD3, CD28, TCRαβ, or TCRγδ. Additional CD4, CD8 and CD30 expression shown for each cell line.

Cell line	Subtype	Immunophenotype								
		CD3	cytCD3	CD28	TCRαβ	cytTCRαβ	TCRγδ	CD4	CD8	CD30
Jurkat	T-ALL	+		+	+		-	+	-	+
OCI-Ly13.2	ALK-negative ALCL	+		+	+		-	-	-	+
T8ML-1	PTCL, NOS	+		+	+		-	-	+	+
OCI-Ly12	PTCL, NOS	-	+	-	-	+	-	-	+	+
SMZ-1	PTCL, NOS	-	+	-	-	+	-	+	-	+

ALCL, anaplastic large cell lymphoma; Cyt, cytoplasm; PTCL, NOS, peripheral T-cell lymphoma, not otherwise specified; T-ALL, T-cell acute lymphoblastic leukemia.

To further elucidate the functionality of the TCR signaling pathways within the studied malignant T-cell lines, we initially treated each cell line with hydrogen peroxidase (H_2O_2) and sodium pervanadate (Na_3VO_4). This treatment is known to inhibit tyrosine phosphatases, thereby intensifying and prolonging tyrosine phosphorylation events, including the activation of ZAP-70 and subsequent downstream TCR signaling (214). As a negative control for ZAP-70 expression, we used the Burkitt B-cell lymphoma line, Ramos. Importantly, unlike the Ramos cell line, all five malignant T-cell lines evaluated expressed ZAP-70 (**Figure 16A,B**).

Among the T-cell lines, Jurkat, T8ML-1 and OCI-Ly13.2 exhibited phosphorylation at both ZAP-70 activating residues, Y319 and Y493, along with downstream activation of PLCγ1 and ERK1/2 (**Figure 16A**). Conversely, SMZ-1 and OCI-Ly12 displayed no ZAP-70 phosphorylation or downstream activation of PLCγ1, accompanied by weaker ERK1/2 activation (**Figure 16B**). This observation aligns with previously described ZAP-70-independent activation of ERK1/2 in ZAP-70-negative Jurkat T cells (215).

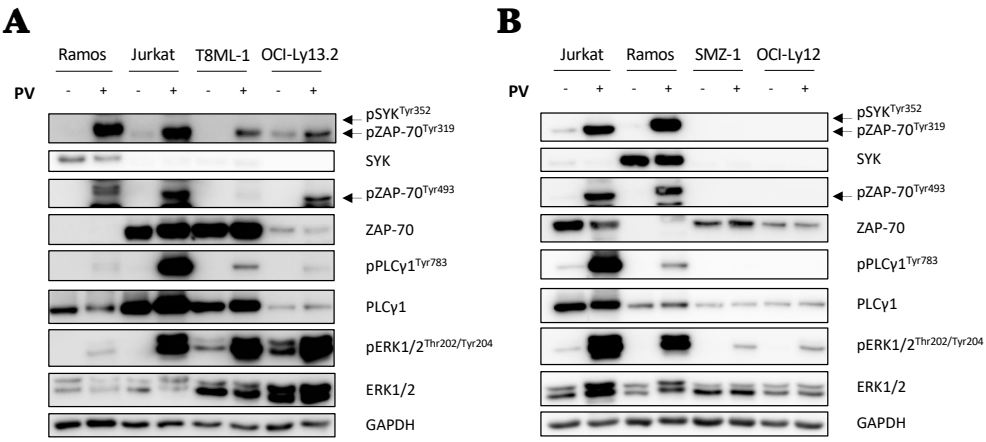

Figure 16. Assessment of TCR signaling functionality in malignant T-cell lines following pervanadate treatment. Each cell line was incubated with 100 mM sodium pervanadate (Na_3VO_4) and 300 mM hydrogen peroxide (H_2O_2) for 5 min. Western Blot analysis was performed to assess phosphorylation and total protein levels of SYK, ZAP-70, PLCγ1 and ERK1/2. **(A)** Jurkat, T8ML-1 and OCI-Ly13.2 cell lines demonstrated active TCR signaling, characterized by ZAP-70 activation and downstream pathway activity. **(B)** SMZ-1 and OCI-Ly13.2 cell lines exhibited impaired TCR signaling, as evidenced by the absence of ZAP-70 and PLCγ1 activation. Ramos cells were used as a ZAP-70 negative control cell line. Jurkat cells were included in both blots as a positive control for pervanadate treatment and antibody specificity. PV, pervanadate treatment.

Taking into consideration the specific immunophenotype required for further antigen-dependent TCR stimulation and the functionality of TCR signaling pathways, we selected Jurkat, T8ML-1 and OCI-Ly13.2 cell lines for subsequent experiments. Additionally, since T8ML-1 and OCI-Ly13.2 were non-commercial cell lines, we performed STR profile to validate their identity (Appendix Table 4).

5.4. ZAP-70 inhibitor candidates, IQS117 and IQS141, suppress the proliferation and viability of malignant T-cell lines in a dose-dependent manner

We initially assessed the sensitivity of malignant T-cell leukemia and lymphoma cell lines to the ZAP-70 inhibitor candidates IQS117 and IQS141. Jurkat, OCI-Ly13.2, and T8ML-1 cells were treated with escalating doses of each compound for 48 h. Cell proliferation was quantified using the CellTiter96™ Cell Proliferation Assay, and viable cells were identified as the Annexin V-negative/PI-negative population through flow cytometry (representative gating images are provided in Appendix Figures 1 and 2).

Our results unveiled a dose-dependent inhibitory effect of both IQS117 and IQS141 on all malignant T-cell lines evaluated (**Figure 17A,B**). Remarkably, both IQS117 and IQS141 demonstrated a similar effect on cell proliferation and viability, with IC50 values falling within the micromolar range (**Figure 17C,D**). However, cells tended to exhibit greater sensitivity to IQS117 treatment, as evidenced by consistently lower IC50 values compared to those observed with IQS141 treatment.

These results validated the efficiency of these two compounds decreasing the proliferation and viability of malignant T-cells *in vitro* and highlight their potential as therapeutic strategy for treatment of T-cell malignancies.

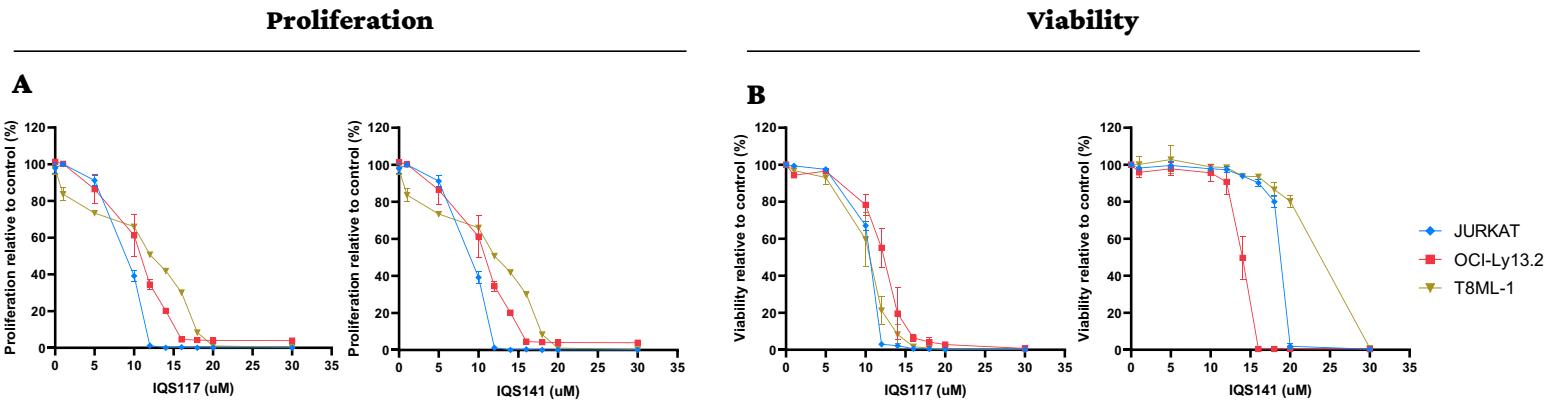

C

Cell line	Compound			
	IQS117		IQS141	
	IC50 (µM)	95% CI	IC50 (µM)	95% CI
Jurkat	9.80	9.58-10.02	16.71	15.80-17.68
OCI-Ly13.2	9.74	9.12-10.41	13.98	13.86-14.10
T8ML-1	11.78	10.85-12.79	19.94	17.03-23.36

D

Cell line	Compound			
	IQS117		IQS141	
	IC50 (µM)	95% CI	IC50 (µM)	95% CI
Jurkat	10.32	10.25-10.39	18.52	18.20-18.84
OCI-Ly13.2	12.03	11.59-12.48	13.94	13.72-14.17
T8ML-1	10.43	10.05-10.82	22.45	21.37-23.59

Figure 17. Dose-dependent inhibition of malignant T-cell lines proliferation and viability by IQS117 and IQS141. Jurkat, OCI-Ly13.2 and T8ML-1 cell lines were exposed to a range of concentrations (1-30 µM) of IQS117 and IQS141 for 48 h. Cell proliferation was assessed using the CellTiter96™ Cell Proliferation Assay, while cell viability was determined by assessing the Annexin V-negative/PI-negative population using Annexin V and PI staining, followed by flow cytometry analysis. Data are represented as percentages (%) relative to the DMSO control. **(A-B)** Dose-response curves illustrating the effect of IQS117 and IQS141 treatment on cell lines proliferation **(A)** and viability **(B)** plotted in a linear scale. Graphs show mean ± SEM. **(C-D)** Summary table of the half-maximal inhibitory concentrations (IC50) calculated for each treatment and cell line based on dose-response graphs plotted in logarithmic scale for proliferation **(C)** and viability **(D)**.

5.5. IQS117 and IQS141 antagonize antigen-mediated TCR signaling on malignant T cells

To better understand the *in vitro* on-target inhibition of IQS117 and IQS141 on ZAP-70 and their consequent impact on TCR signaling in response to TCR stimulation in cellular models, we treated Jurkat and OCI-Ly13.2 cell lines with increasing doses of IQS117 or IQS141 for 6 h. After treatment, we stimulated TCR signaling with soluble anti-CD3 and anti-CD28 antibodies for 1 min, followed by whole protein extraction and Western blotting analysis. We analyzed their effect on ZAP-70 phosphorylation, its immediate downstream targets (SLP-76 and LAT), and downstream signaling pathways (PLCγ1, ERK1/2 and AKT), as depicted in **Figure 18**. This analysis was conducted in Jurkat and OCI-Ly13.2 cell lines, as our efforts to optimize TCR stimulation for T8ML-1 cells were unsuccessful (data not shown).

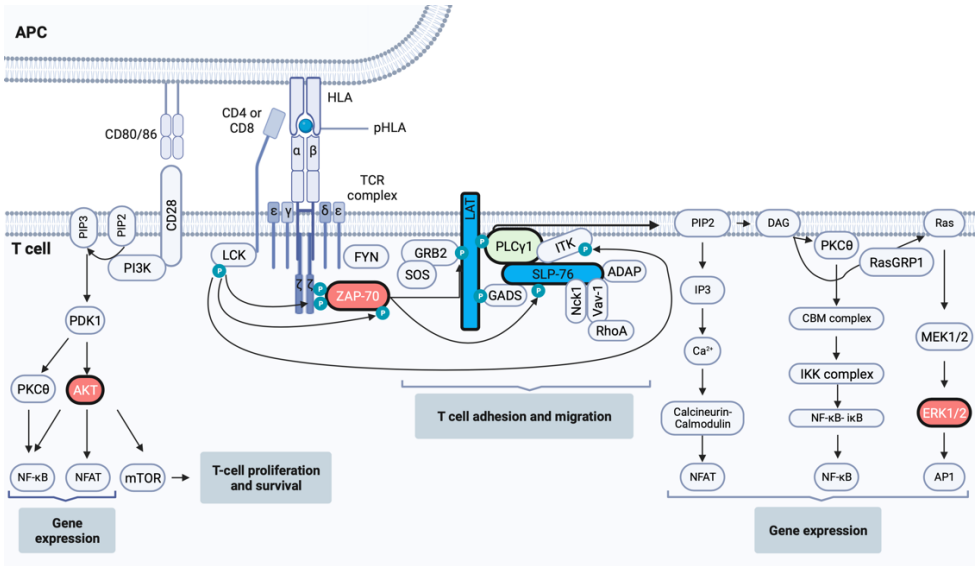

Figure 18. TCR signaling pathway scheme highlighting analyzed targets via Western blotting analysis following IQS117 and IQS141 treatment. Assessment of phosphorylation and total protein levels of ZAP-70, LAT, SLP-76, PLCγ1, ERK1/2 and AKT (indicated with bold black borders) in Jurkat and OCI-Ly13.2 cell lines following ZAP-70 inhibitor treatment and TCR stimulation.

5.5.1. IQS117 and IQS141 suppress the activation of ZAP-70 and its immediate TCR signaling targets

Our initial evaluation focused on the on-target effect of IQS117 and IQS141 on ZAP-70 activation and its immediate downstream targets, SLP-76 and LAT. To accomplish this, we examined the inhibitory influence of IQS117 and IQS141 on activating phosphorylation sites within ZAP-70, SLP-76, and LAT in TCR-stimulated Jurkat and OCI-Ly13.2 cells.

In Jurkat cells, TCR stimulation upregulated the phosphorylation of ZAP-70 at Y319, along with phosphorylated SLP-76 at Y128, and phosphorylated LAT at Y171 (**Figure 19A**). Remarkably, both compounds dose-dependently inhibited the phosphorylation of ZAP-70, SLP-76, and LAT, most notably at the highest dose evaluated. Interestingly, a transient increase in ZAP-70 phosphorylation at Y319 was observed at the lowest concentration tested for each compound.

Conversely, in OCI-Ly13.2 cells, TCR stimulation led to increased phosphorylation of ZAP-70 at Y319 and downstream phosphorylation of LAT at Y171, without any discernible phosphorylation of SLP-76 in Y128 (**Figure 19B**). IQS117 treatment demonstrated a dose-dependent inhibition of phosphorylated ZAP-70 and LAT, while IQS141 most prominently decreased the phosphorylation of ZAP-70 and LAT at the highest concentration tested.

Collectively, these results indicated that IQS117 and IQS141 effectively targeted ZAP-70 activation, further validated by the inhibition of its direct targets, SLP-76 and LAT in Jurkat cells and LAT in OCI.Ly13.2 cells.

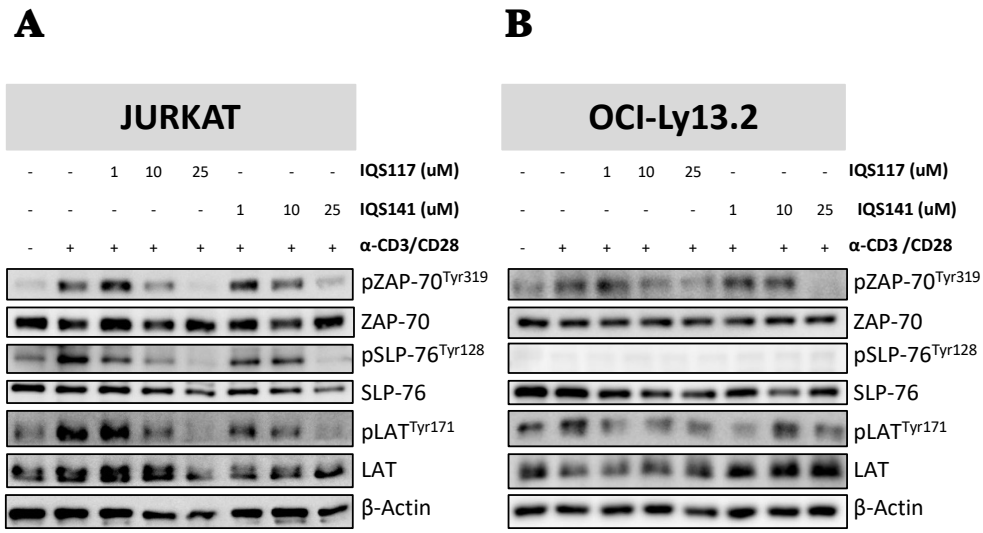

Figure 19. IQS117 and IQS141 decrease ZAP-70 activation and its downstream targets in Jurkat and OCI-Ly13.2 cells. (A-B) Western Blot analysis of phosphorylation and total protein levels of ZAP-70, SLP-76 and LAT in Jurkat **(A)** and OCI-Ly13.2 **(B)** cells. Cells were incubated with increasing doses of IQS117 and IQS141 for 6 h and stimulated with soluble anti-CD3 and anti-CD28 antibodies for 1 min. In each experiment, Jurkat or OCI-Ly13.2 treated with pervanadate served as positive controls for antibody specificity. Given the high intensity of these controls, they were incubated separately to prevent masking of other bands and they are not shown in the images.

5.5.2. IQS117 and IQS141 decrease ZAP-70 activation and distal TCR signaling

To gain further insight into the impact of ZAP-70 inhibition on downstream TCR signaling pathways, we evaluated the effect of IQS117 and IQS141 on the phosphorylation of several activating phosphorylation sites, including phosphorylated ZAP-70 at Y319 and Y493, phosphorylated PLCγ1 at Y783, phosphorylated AKT at S473 and phosphorylated ERK1/2 at T202/Y204, all in response to TCR stimulation (**Figure 20**).

In Jurkat cells, TCR stimulation led to increased phosphorylation in ZAP-70 Y319 and Y493, PLCγ1 Y783, ERK1/2 T202/Y204 and AKT S473 (**Figure 20A**). IQS117 treatment resulted in a dose-dependent reduction in the phosphorylation of ZAP-70 PLCγ1, ERK1/2 and AKT (**Figure 20A**). Conversely, IQS141 exhibited a dose-dependent

reduction in the phosphorylation of ZAP-70, PLCγ1, ERK1/2, while showing no impact on AKT phosphorylation.

In OCI-Ly13.2 cells, TCR stimulation led to increased phosphorylation in ZAP-70 Y319 and Y493 and ERK1/2 T202/Y204 (**Figure 20B**). No phosphorylation of PLCγ1 Y783 was observed, and AKT S473 phosphorylation remained similar. While IQS117 treatment induced a dose-dependent inhibitory effect on ZAP-70 at Y319, ERK1/2 and AKT, IQS141 treatment exerted a dose-dependent inhibitory effect on ZAP-70 Y319 and Y493 and ERK1/2. Similarly, IQS141 did not decreased AKT phosphorylation (**Figure 20B**).

Our findings consistently revealed a dose-dependent inhibition of ZAP-70 and downstream TCR signaling in both cell lines when treated with IQS117 or IQS141, compared to the TCR stimulation control. Besides, these results collectively suggested that IQS117 and IQS141 exerted their inhibitory effects on TCR signaling through different mechanistic pathways, with IQS141 showing limited AKT inhibition and IQS117 inhibition AKT.

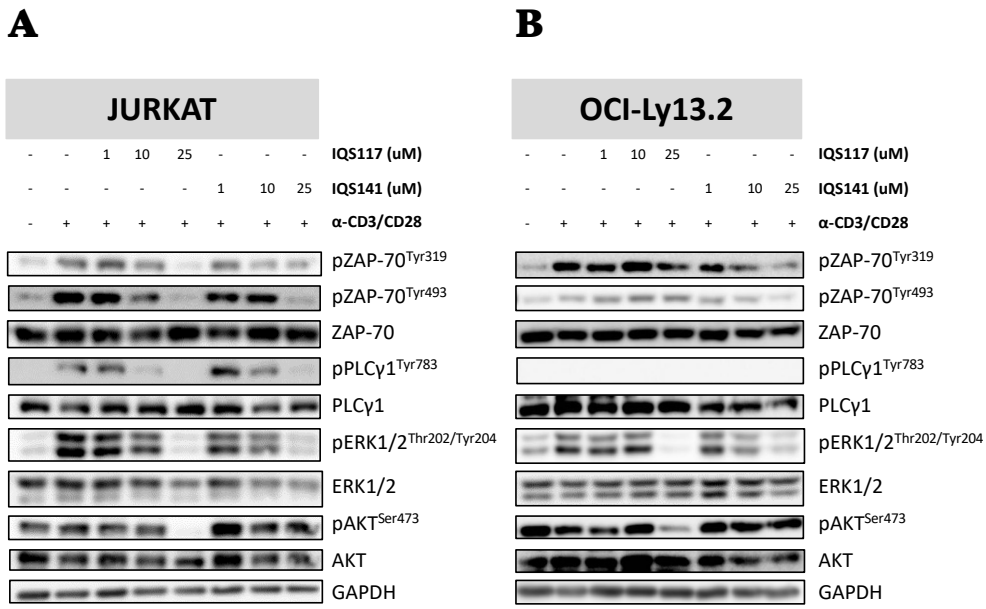

Figure 20. ZAP-70 inhibition by IQS117 and IQS141 downregulates distal TCR signaling in Jurkat and OCI-Ly13.2 cells. (A-B) Western Blot analysis of phosphorylation and total protein levels of ZAP-70, PLCγ1, ERK1/2 and AKT in Jurkat **(A)** and OCI-Ly13.2 **(B)** cells. Cells were incubated with increasing doses of IQS117 and IQS141 for 6 h and stimulated with soluble anti-CD3 and anti-CD28 antibodies for 1 min. In each experiment, Jurkat or OCI-Ly13.2 treated with pervanadate served as positive controls for antibody specificity. Given the high intensity of these controls, they were incubated separately to prevent masking of other bands and they are not shown in the images.

5.6. IQS117 and IQS141 exhibit no *in vivo* acute toxicity effects

Building upon the promising *in vitro* results of IQS117 and IQS141 on malignant T-cell lines, we proceeded to investigate their *in vivo* efficiency. For that, our initial step involved assessing the potential acute toxicity of the ZAP-70 inhibitor compounds, IQS117 and IQS141, as well as the control group (vehicle-treated), utilizing two administration routes: oral gavage (p.o.) and intraperitoneal injection (i.p.), as illustrated in **Figure 21A**. Each test group consisted of four mice, ensuring an equal distribution with 50% male and 50% females, for each drug and route of administration evaluated.

Following the OECD Fixed Dose Procedure guideline for single-dose acute toxicity (196), which recommends a starting dose of 300 mg/kg in the absence of previous *in vivo* data for the tested compound, we administered a 300 mg/kg dose to one mouse per compound. We closely monitored their appearance and behaviour for 30 min, and no discernible alterations in the mice aspect or behaviour were observed. Subsequently, the remaining mice underwent the same treatment regimen, and we attentively observed them for a duration of 14 days. Throughout this observation period, no mortality was recorded in either the treatment groups or the vehicle group.

Furthermore, our investigation revealed that IQS117 and IQS141, administered via both p.o. and i.p., did not produced changes in body weight when compared to the mice treated with the vehicle (**Figure 21C**). Additionally, no abnormal behaviours or signs of dehydration were noted in any of the mice throughout the study duration. On day 14 of the study, we sacrificed the mice and conducted a thorough gross examination of the organs that revealed no abnormalities in any organ. Moreover, histopathological evaluation of tissue sections obtained from the small intestine, liver, lung, lymph node, spleen, bone marrow and kidney exhibited no morphological changes at the 300 mg/kg dose, regardless of administration route, compared to the vehicle-treated controls (**Figure 21B**).

In summary, our acute toxicity assay for the ZAP-70 inhibitors IQS117 and IQS141, administered via p.o. or i.p. routes, demonstrated no adverse effects on mouse behaviour, body weight, organ gross examination, or histopathological characteristics at the specified dose of 300 mg/kg when compared to the vehicle group. Because we observed no acute toxic effects at this 300 mg/kg dose, further doses evaluations were not conducted.

Figure 21 (next page). Absence of acute toxicity effects following single-dose oral and intraperitoneal administration of IQS117 and IQS141. (A) Scheme representing mice treatment and monitoring strategy. **(B)** Histopathological assessment of oral gavage (p.o.) or intraperitoneal injection (i.p.) administration of IQS117 or IQS141 at a dose of 300 mg/kg on multiple organs (small intestine, liver, lung, lymph node, spleen, bone marrow and kidney) at day 14 post-administration, compared to vehicle-treated mice. Hematoxylin and eosin staining. Scale bar represents 1000 µm. **(C)** Impact of p.o. and i.p. administration of IQS117, IQS141, and vehicle on mice body weight.

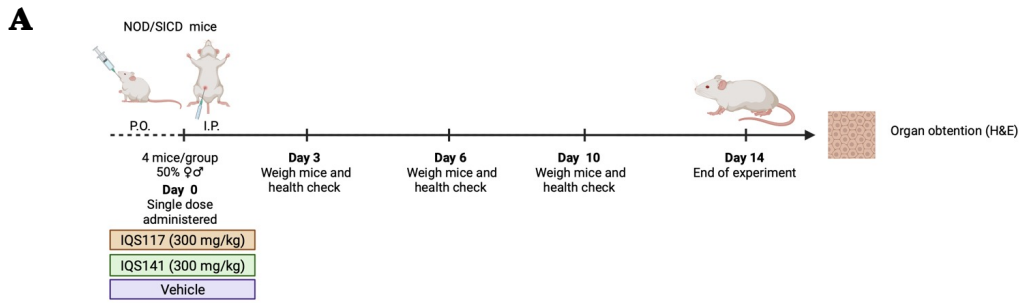
A
NOD/SICD mice
P.O.
I.P.
4 mice/group
50% ♀♂
Day 0
Single dose
administered
IQS117 (300 mg/kg)
IQS141 (300 mg/kg)
Vehicle
Day 3
Weigh mice and
health check
Day 6
Weigh mice and
health check
Day 10
Weigh mice and
health check
Day 14
End of experiment
Organ obtention (H&E)

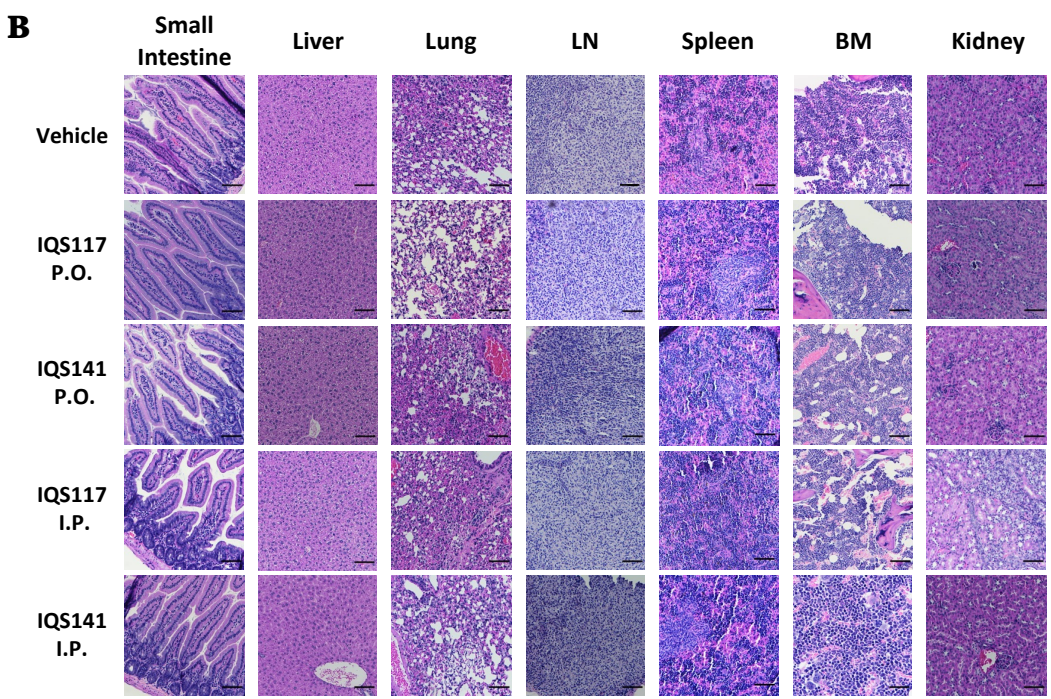
B
Small Intestine
Liver
Lung
LN
Spleen
BM
Kidney
Vehicle
IQS117 P.O.
IQS141 P.O.
IQS117 I.P.
IQS141 I.P.

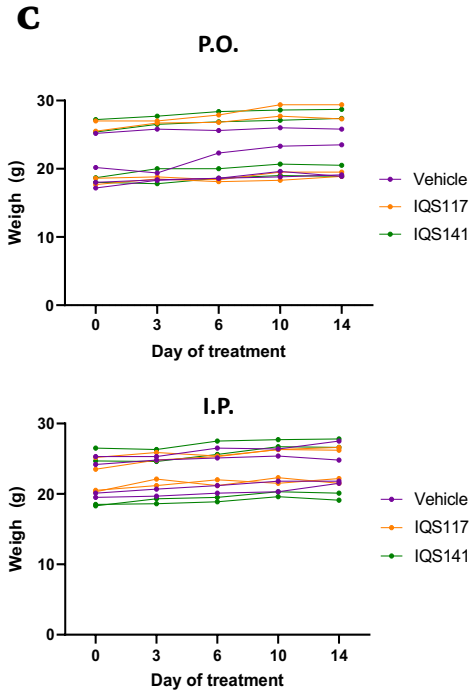
C
P.O.
Weigh (g)
Day of treatment
Vehicle
IQS117
IQS141
I.P.
Weigh (g)
Day of treatment
Vehicle
IQS117
IQS141

5.7. Improved pharmacokinetic profiles with oral administration of IQS117 and IQS141 in comparison to intraperitoneal route *in vivo*

Given the absence of observed toxic effects at the initial dose of 300 mg/kg, for the *in vivo* pharmacokinetic evaluation of IQS117 and IQS141, we made the decision to reduce the drug dosage to 50 mg/kg, the subsequent lower dose recommended by OECD guidelines and commonly used in *in vivo* experiments with tyrosine kinase inhibitors (216,217). To determine the optimal route of administration between oral gavage (p.o.) and intraperitoneal injection (i.p.) for IQS117 and IQS141, we conducted a single-dose pharmacokinetic study at 50 mg/kg (**Figure 22**). Both drugs were detected in mice plasma following p.o. and i.p. administration. However, p.o. administration exhibited a longer half-life ($t_{1/2}$) and improved total drug exposure over time ($AUC_{0-\infty}$) for IQS117 and IQS141 compared to their respective i.p. values (**Figure 22C**). Specifically, p.o. administration of IQS117 resulted in a higher peak blood concentration (C_{max}) occuring at a delayed time (T_{max}), a slower elimination rate (K_{el}) compared to i.p. administration. Conversely, p.o. administration of IQS141 yielded a lower C_{max} at a longer time (T_{max}) in comparison to i.p. administration, along with a reduced elimination rate (K_{el}).

In summary, the pharmacokinetic evaluation in mice indicated that p.o. administration is the optimal route for IQS117 and IQS141, characterized by longer half-lives and extended total drug exposure compared to i.p. administration, making it more suitable for subsequent *in vivo* experiments.

A

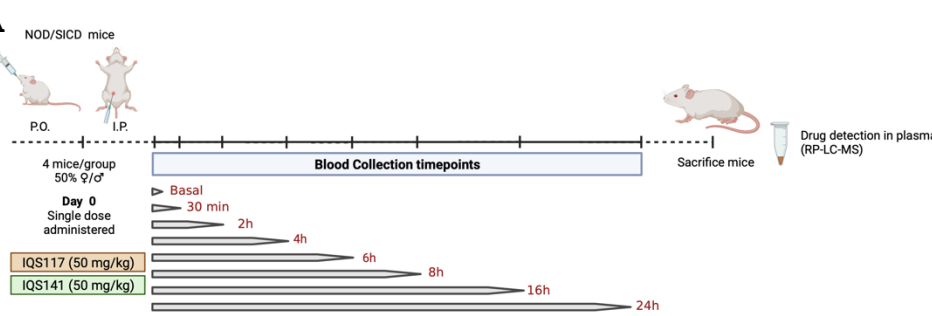

B

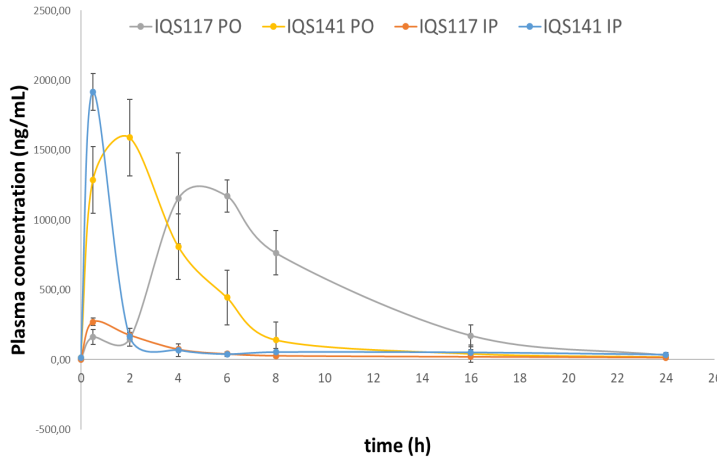

C

Parameter	IQS117 (50 mg/kg)		IQS141 (50 mg/kg)	
	P.O.	I.P.	P.O.	I.P.
$T_{1/2}$ (h)	3,5±0,6	2,5±1,2	2,3±0,6	1±0,06
T_{max} (h)	5±1,2	0,5±0,0	2±0,0	0,5±0,0
C_{max} (ng/mL)	1277,2±142,4	259,2±33,3	1597±267,4	1918±132
K_{el} (h^{-1})	0,2±0,04	0,32±0,1	0,31±0,1	0,68±0,04
$AUC_{0-\infty}$ ($h \cdot ng \cdot mL^{-1}$)	11152,1±1468,5	1204,8±167,4	7784±2301,1	3803,9±1028,7

Figure 21. Enhanced pharmacokinetic efficiency of IQS117 and IQS141 upon oral gavage administration compared to intraperitoneal injection in mice. (A) Experimental design scheme: A single 50 mg/kg dose of IQS117 or IQS141 was administered via oral gavage (p.o.) or intraperitoneal injection (i.p.). Mice were sacrificed at various time points, and plasma samples were collected from intracardiac blood for drug detection using reversed-phase liquid chromatography-tandem mass spectrometry (RP-LC-MS). **(B)** Plasma concentration-time profiles following a single p.o. or i.p. dose for each compound. **(C)** Pharmacokinetic parameters calculated from plasma concentration-time profiles. Data are reported as mean ± SD.

5.8. IQS117 and IQS141 exhibit no influence on tumor growth or mice survival in subcutaneous models of T-cell leukemia and T-cell lymphoma *in vivo*

Given the limited availability of established models for studying T-cell malignancies in preclinical research, we initially aimed to develop subcutaneous xenograft models using Jurkat and OCI-Ly13.2 cell lines to evaluate the impact of ZAP-70 inhibition *in vivo*. Previous studies have successfully generated xenograft models with Jurkat cells in athymic mice and OCI-Ly13.2 cells in NOD/SICD mice (218,219). To precisely monitor tumor growth, Jurkat and OCI-Ly13.2 cell lines were transfected with a lentiviral vector to express luciferase, allowing the assessment of tumor progression by *in vivo* bioluminescence imaging (BLI). The luciferase signal, which is proportional to the tumor burden, was quantified using the IVIS-Spectrum to determine the average radiance per mouse over the course of the experiment.

However, our initial pilot study in NOD/SCID mice, which lack functional T and B cells, yielded inconsistent tumor development (data not shown). Consequently, we decided to transition to the NSG immunodeficient mice strain, which is characterized by the absence of functional B and T cells, as well as a compromised innate immune system with defective macrophage and dendritic cells and non-functional NK cells. NSG mice are widely recognized as a valuable model for establishing xenograft models from various tumor types (220,221). Based on the consistent tumor growth observed in the pilot study in both Jurkat-Luc and OCI-Ly13.2-Luc xenograft models in NSG mice (data not shown), we subsequently assessed the effect of ZAP-70 inhibitors in this mouse strain.

Subsequently, we subcutaneously injected Jurkat-Luc or OCI-Ly13.2-Luc cells into the right flank of each NSG mice (**Figure 23A**). Fourteen days following cell injection, all animals from both models developed detectable tumors restricted to the injection site (**Figure 23B,F**). The animals were then randomized to receive either

IQS117, IQS141 or vehicle for both the Jurkat-Luc model (vehicle, n=8, mean radiance = $2.53x10^{10}$ p/s/cm^2/sr ± $2.02x10^9$; IQS117, n=8, mean radiance = $2.64x10^{10}$ p/s/cm^2/sr ± $4.67x10^9$; IQS141, n=8, mean radiance = $2.23x10^{10}$ p/s/cm^2/sr ± $1.8x10^9$) and the OCI-Ly13.2-Luc model (vehicle, n=8, mean radiance = $2.47x10^{10}$ p/s/cm^2/sr ± $7.35x10^9$; IQS117, n=8, mean radiance = $1.51x10^{10}$ p/s/cm^2/sr ± $3.57x10^9$; IQS141, n=8, mean radiance = $1.24x10^{10}$ p/s/cm^2/sr ± $1.79x10^9$). On day fifteen post-cell injection, mice were dosed with 50 mg/kg of IQS117, IQS141 or vehicle in the drinking water until the end of the experiment.

Tumor growth was monitored non-invasively through weekly BLI measurement (**Figure 23C,G**), and additionally, tumor volume was measured with a caliper every seven to ten days (**Figure 23D,H**). Mice treated with ZAP-70 inhibitors exhibited no significant differences in BLI signal or tumor size by day 36 (Jurkat-Luc) (**Figure 23B,C,D**) and day 56 (OCI-Ly13.2-Luc) (**Figure 23F,G,H**). Furthermore, there was no survival benefit in the treatment groups compared to the vehicle-treated group in Jurkat-Luc and OCI-Ly13.2-Luc xenografts (**Figure 23E,I**).

In summary, this initial approach demonstrated no discernible advantages in subcutaneous mice treated with ZAP-70 inhibitors.

Figure 23 (next page). Treatment with IQS117 or IQS141 treatment does not impair tumor growth or prolong mice survival in subcutaneous malignant T-cell xenografts. (A) Schematic representation of mice treatment and monitoring strategy. **(B,F)** Representative images of NSG mice engrafted with Jurkat-Luc **(B)** or OCI-Ly13.2-Luc **(F)** cells before the first day of treatment (day 14) or imaged after treatment on the days noted within each image panel. **(C,G)** Tumor size represented as the average radiance (photons/second per cm^2/sr) measured by bioluminescence imaging (BLI) for Jurkat-Luc **(C)** and OCI-Ly13.2-Luc **(G)** xenografts. **(D,H)** Tumor volume measurements taken every seven to ten days. Data displayed until day 36 for Jurkat-Luc **(D)** and day 56 for OCI-Ly13.2-Luc **(H)** xenografts, representing the last day when all animals were still alive. Graphs depict mean ± SEM of 8 mice/group. BLI and tumor volume analyzed using two-way ANOVA for Jurkat-Luc ($P > 0.05$) and OCI-Ly13.2-Luc ($P > 0.05$). The black arrow indicates the initiation of treatment (day 15 post-cell injection). **(E,I)** Kaplan-Meier survival curves, statistically compared using the log-rank test for Jurkat-Luc **(E)** and OCI-Ly13.2-Luc **(I)** xenograft.

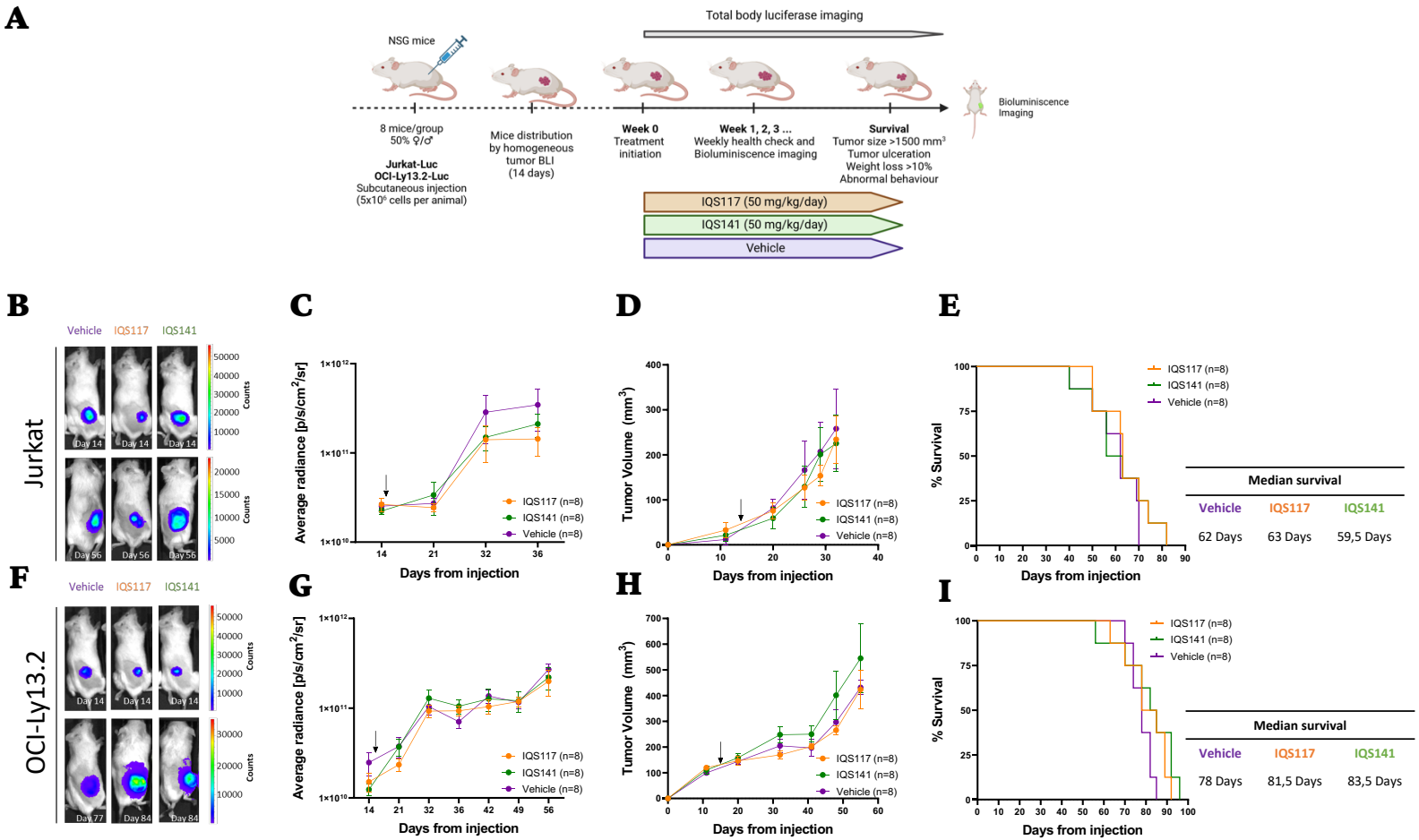
A
Total body luciferase imaging
NSG mice
8 mice/group
50% ♀/♂
Jurkat-Luc
OCI-Ly13.2-Luc
Subcutaneous injection
(5x10⁶ cells per animal)
Mice distribution
by homogeneous
tumor BLI
(14 days)
Week 0
Treatment
initiation
Week 1, 2, 3 ...
Weekly health check and
Bioluminiscence imaging
Survival
Tumor size >1500 mm³
Tumor ulceration
Weight loss >10%
Abnormal behaviour
Bioluminiscence
Imaging
IQS117 (50 mg/kg/day)
IQS141 (50 mg/kg/day)
Vehicle
B
Vehicle
IQS117
IQS141
Jurkat
Day 14
Day 56
Counts
C
Average radiance [p/s/cm²/sr]
Days from injection
IQS117 (n=8)
IQS141 (n=8)
Vehicle (n=8)
D
Tumor Volume (mm³)
Days from injection
E
% Survival
Median survival
Vehicle
IQS117
IQS141
62 Days
63 Days
59,5 Days
F
OCI-Ly13.2
Day 77
Day 84
G
H
I
78 Days
81,5 Days
83,5 Days

5.9. Minimal transcriptomic alterations in subcutaneous tumors from malignant T-cell xenograft models treated with IQS117 or IQS141

To assess potential transcriptome alterations in subcutaneous tumors derived from OCI-Ly13.2 and Jurkat xenograft models, we conducted an end-point experiment following a one-week treatment with ZAP-70 inhibitors or vehicle in a separate cohort from the survival experiment.

To achieve this, we subcutaneously injected Jurkat and OCI-Ly13.2 cells into the right flank of each mouse. We then waited until day twenty-eight post-injection, when tumor size reached approximately 200-250 mm^3 to ensure we had sufficient tumor material in both xenograft models. On day twenty-eight post-injection, we uniformly distributed the mice based on tumor size (Jurkat: Vehicle, 181 $mm^3 \pm 44.2$; IQS117, 161.6 $mm^3 \pm 43.9$; IQS141: 202.7 $mm^3 \pm 19.7$; OCI-Ly13.2: Vehicle, 243.1 $mm^3 \pm 11.6$, IQS117 240.5 $mm^3 \pm 15.8$, IQS141, 247.7 $mm^3 \pm 13.5$). Subsequently, mice were subjected to a seven-day treatment regimen with either IQS117, IQS141, or the vehicle, administered at a dose of 50 mg/kg in the drinking water. Following treatment, all mice were sacrificed, and RNA was extracted from the tumor tissue for RNA sequencing (RNAseq) analysis (**Figure 24A**).

In our RNAseq data analysis, we employed principal component analysis (PCA) to discern the major sources of variation. Notably, we found that the primary source of variation was attributed to the specific cell line under examination (**Figure 24B**). However, when we compared the treated groups to the vehicle group within both Jurkat (**Figure 24C**) or OCI-Ly13.2 (**Figure 24D**) models, we did not discern distinct clusters.

Furthermore, the results obtained from the differential expression analysis, which compared all treatment groups for Jurkat and OCI-Ly13.2 models, were in

accordance with the PCA findings. In both cell lines, there were no significant changes in gene expression between treated and vehicle groups (adjusted P value > 0.05).

To further substantiate these findings, we calculated Euclidean distances for the Jurkat (**Figure 24E)** and OCI-Ly13.2 (**Figure 24F**) models, confirming the absence of any discernible clustering pattern in response to ZAP-70 inhibitors or vehicle treatment.

Given the lack of conclusive findings from the analysis of individual significant genes, we conducted a gene set enrichment analysis (GSEA) against the Reactome database for each treatment comparison in both Jurkat and OCI-Ly13.2 models. However, our results indicated the absence of significant overlapping gene sets associated with ZAP-70 inhibitors (data not shown).

These collective results suggested that the lack of a survival benefit from ZAP-70 inhibitor treatment in subcutaneous malignant T-cell xenograft models may be attributed to inadequate drug delivery to the tumor site, as evidenced by the absence of significant transcriptomic changes and the lack of enriched gene sets related to each treatment.

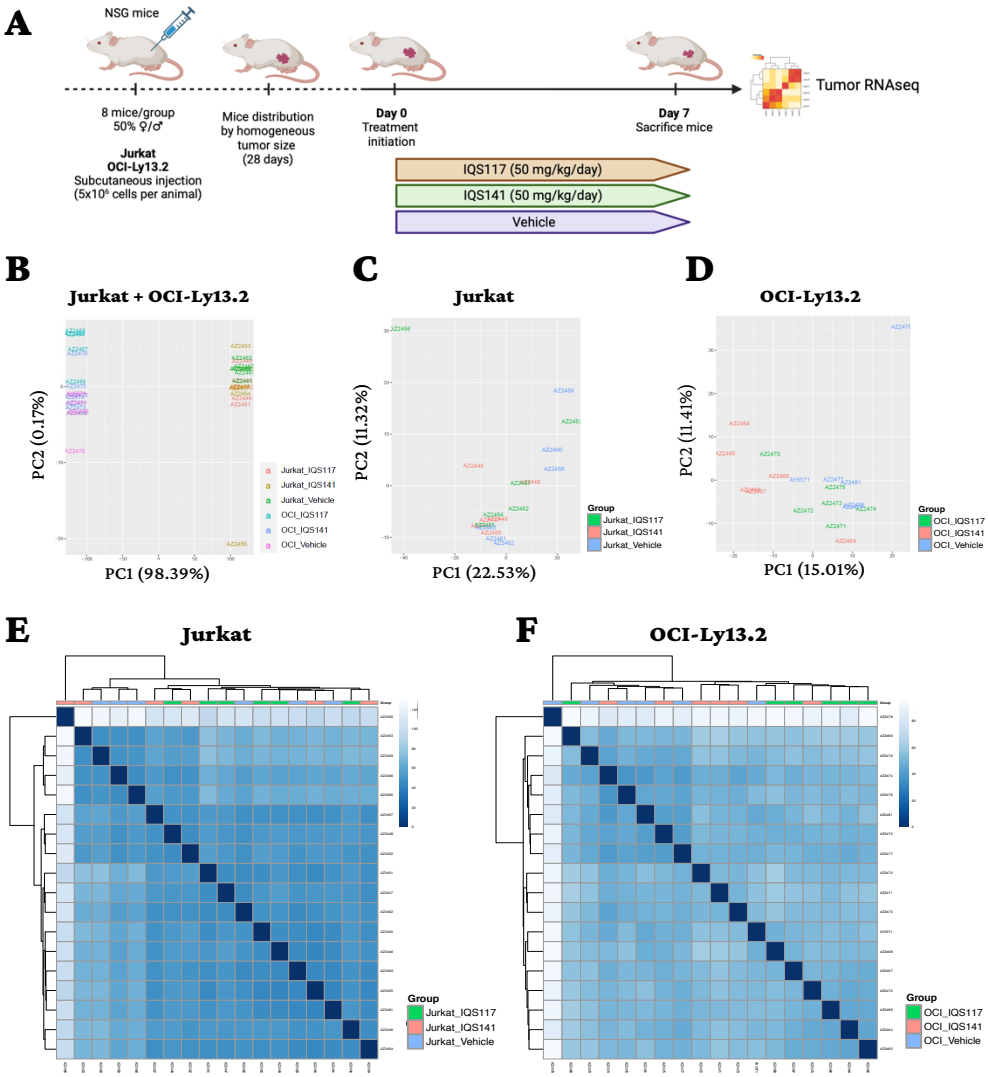

Figure 22. Absence of distinct differential gene regulation in subcutaneous tumors from OCI-Ly13.2 and Jurkat xenograft models upon ZAP-70 inhibitors treatment. (A) Schematic overview of mice treatment and monitoring. **(B-D)** Principal component analysis (PCA) of the first two principal components (PC1 and PC2) using RNA sequencing data from subcutaneous tumors in OCI-Ly13.2 and Jurkat xenograft models. The plot illustrates the clustering of samples comparing cell lines **(B)** and among treatment groups for each Jurkat **(C)** and OCI-Ly13.2 model **(D)**, with each point representing an individual sample. **(E,F)** Euclidean distance values heatmaps comparing Jurkat **(E)** and OCI-Ly13.2 **(F)** samples in response to ZAP-70 inhibitor or vehicle. The color scale represents normalized Euclidean distances, with dark blue signifying greater similarity and light blue indicating lower similarity.

5.10. Lack of survival benefit or tumor growth suppression in intravenous malignant T-cell xenografts treated with IQS117 and IQS141

Given the lack of observable effects of ZAP-70 inhibitors in the subcutaneous xenograft models, we decided to shift our focus to intravenous xenograft models derived from malignant T-cell lines in NSG mice. Intravenous models have proven effective for establishing Jurkat xenograft models in pre-clinical studies (151,222). To proceed with this investigation, we conducted a pilot study with the primary objectives of optimizing cell density and assessing mouse survival following cell injection of Jurkat-Luciferized (Jurkat-Luc) and OCI-Ly13.2-Luciferized (OCI-Ly13.2-Luc) cells via tail vein. Importantly, the results from this pilot study revealed that all mice developed the disease (data not shown), validating the engraftment efficiency to further explore the impact of ZAP-70 inhibition in both xenograft models.

For that, Jurkat-Luc or OCI-Ly13.2-Luc cells were injected via tail vein into six mice per treatment group or vehicle control (**Figure 25A**). Subsequently, BLI imaging performed fourteen days after Jurkat-Luc cell injection and twenty-one days after OCI-Ly13.2-Luc cell injection, revealing that two Jurkat-Luc mice did not develop tumors and were consequently excluded from the analysis. Additionally, two OCI-Ly13.2-Luc mice were excluded due to deaths following manipulation. Notably, both models exhibited widespread dissemination to various anatomical sites within the animals (**Figure 25B,E**). Specifically, the leukemic cell line, Jurkat-Luc, disseminated throughout the mice, including the bone marrow, lymph nodes and lungs (**Figure 25B**). In contrast, the lymphoma cell line, OCI-Ly13.2-Luc, displayed a distinct distribution profile, primarily detected in the spleen and liver (**Figure 25E**).

Then, mice were randomized to receive either IQS117, IQS141, or the vehicle in both the Jurkat-Luc xenograft model (vehicle, n=6, mean radiance = 7.62×10^7 p/s/cm^2/sr $\pm$ 7.11×10^6; IQS117, n=5, mean radiance = 1.23×10^8 p/s/cm^2/sr $\pm$ 4.40×10^7;

IQS141, n=5, mean radiance = $2.60x10^8$ p/s/cm^2/sr ± $9.49x10^7$) and the OCI-Ly13.2-Luc xenograft model (vehicle, n=6, mean radiance = $4.05x10^7$ p/s/cm^2/sr ± $2.16x10^7$; IQS117, n=5, mean radiance = $3.93x10^7$ p/s/cm^2/sr ± $1.09x10^7$; IQS141, n=5, mean radiance = $4.04x10^7$ p/s/cm^2/sr ± $1.19x10^7$). Daily oral gavage dosing with 50 mg/kg of IQS117, IQS141, or vehicle was administered. Tumor growth was monitored through weekly BLI measurement (**Figure 25C,F**).

In the Jurkat-Luc model, at day 15 after treatment initiation, a significant increase in tumor growth was observed in IQS141-treated Jurkat-Luc xenograft mice compared to the vehicle group (two-way ANOVA $P < 0.0001$; IQS141 mean radiance = $2.54x10^{10}$ p/s/cm^2/sr ± $6.32x10^9$ vs $1.44x10^{10}$ p/s/cm^2/sr ± $2.15x10^9$ for vehicle; $P = 0.046$) (**Figure 25C**). However, despite the statistical significance, this did not translate into a meaningful survival disadvantage, with similar median survival values of 36 days for IQS141 and 34 days for the vehicle group (**Figure 25D**). Conversely, IQS117-treated mice in the Jurkat-Luc xenograft model did not exhibit significant differences in terms of BLI or survival observed over time (**Figure 25C,D**).

In the case of the OCI-Ly13.2-Luc xenograft model, despite the absence of significant differences in BLI results, a statistically significant difference between IQS117 and IQS141 in terms of survival was observed (**Figure 25F,G**). However, these differences might not be attributed to the efficacy of the drugs, as the median survival value of 58 days for IQS117-treated mice was lower than the median survival value for IQS141 and the vehicle groups, which exhibited similar survival durations of 66 days and 64 days, respectively.

Upon necropsy, we performed flow cytometry analysis on the spleen and bone marrow samples obtained from the Jurkat-Luc xenograft model, as well as spleen and liver samples from the OCI-Ly13.2-Luc xenograft model to identify the presence of human malignant T cells. Analysis of samples from Jurkat-Luc xenograft mice revealed the presence of human malignant T cells in the spleen and predominantly in the bone marrow (**Figure 26B,C**). Furthermore, all OCI-Ly13.2-Luc xenograft mice exhibited splenomegaly and hepatomegaly (**Figure 26A**), with malignant T cells detected in the liver and spleen irrespectively of the treatment

group (**Figure 26D,E**). No statistical differences were observed in the number of malignant T cells in the groups treated with ZAP-70 inhibitors compared to the vehicle-treated groups for both the Jurkat-Luc and OCI-Ly13.2-Luc xenograft models.

Collectively, the findings from intravenous malignant T-cell xenograft models indicate that IQS117 and IQS141 treatments do not significantly affect tumor growth and mice survival. This observation raises the possibility that additional factors or mechanisms beyond the drugs efficacy might be influencing the observed survival and BLI disparities, indicating the need for further investigation.

Figure 23 (next page). Limited impact of IQS117 and IQS141 on tumor growth in intravenous malignant T-cell xenografts. (A) Schematic representation of mice treatment and monitoring strategy. **(B,E)** Representative images of NSG mice engrafted with Jurkat-Luc **(B)** and OCI-Ly13.2-Luc **(E)** cells prior to the initiation of treatment and post-treatment on the indicated days in each image panel. **(C,F)** Tumor size displayed as the average radiance (photons/second per cm^2/sr) measured by BLI imaging for Jurkat-Luc **(C)** and OCI-Ly13.2-Luc **(F)** xenografts. Data are shown until day 29 (Jurkat-Luc) and day 56 (OCI-Ly13.2-Luc), the last day with a minimum of 4 animals per group still alive. Graphs depict mean ± SEM of 5-6 mice per group. Two-way ANOVA analysis for Jurkat-Luc ($P < 0.05$) and OCI-Ly13.2-Luc ($P > 0.05$); * $P < 0.05$; from Bonferroni Post-hoc analysis. Asterisks indicate comparisons between IQS117 and vehicle (first asterisk) and IQS141 and vehicle (second asterisk). Black arrow indicates the treatment initiation (day 15 for Jurkat-Luc; day 22 for OCI-Ly13.2-Luc). **(D,G)** Kaplan-Meier survival curves for Jurkat-Luc **(D)** and OCI-Ly13.2-Luc **(G)** xenografts, with statistical comparisons using the log-rank test of;* $P < 0.05$. ns, not significant.

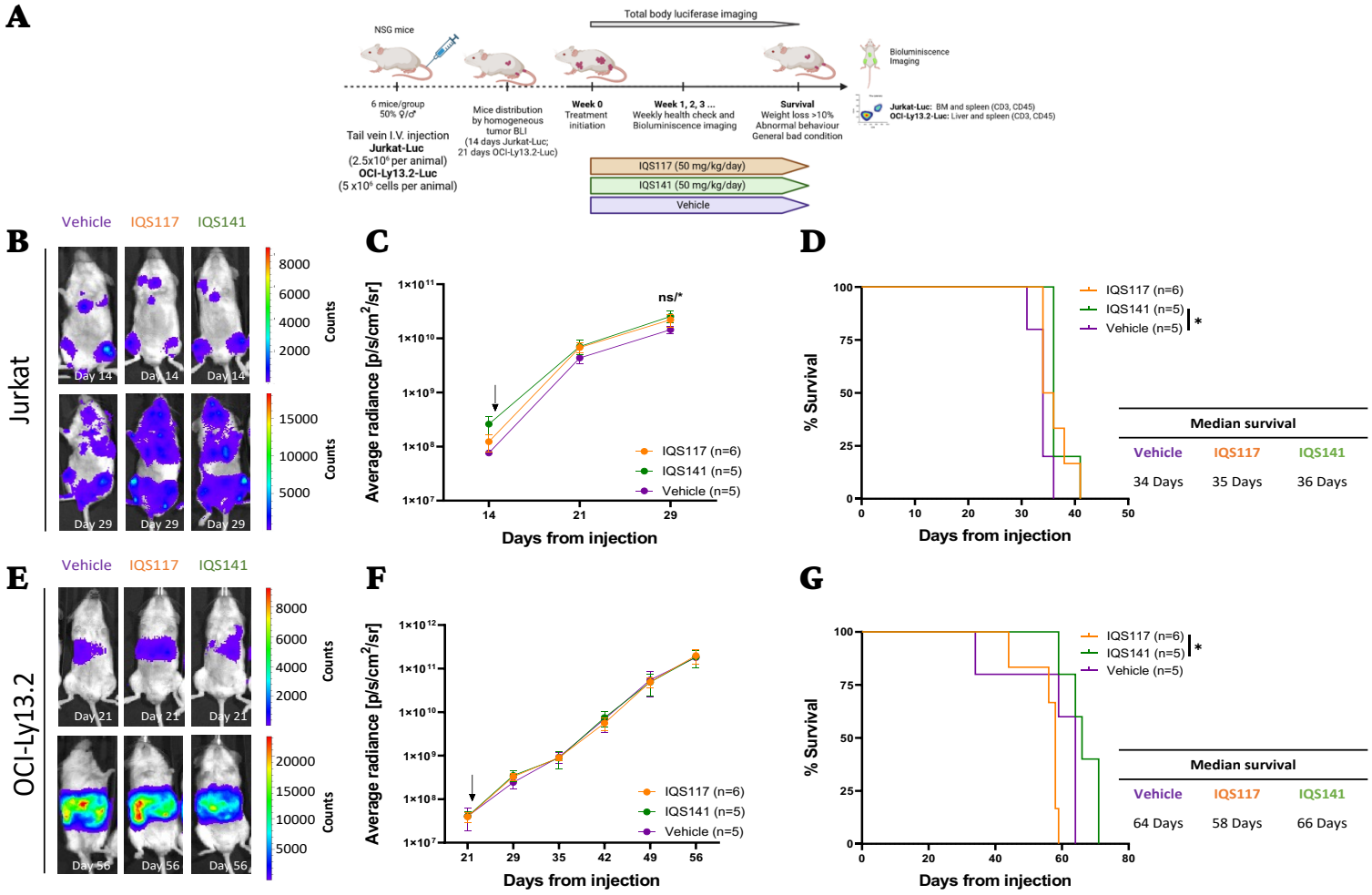
A
NSG mice
Total body luciferase imaging
Bioluminiscence Imaging
6 mice/group 50% ♀/♂
Tail vein I.V. injection
Jurkat-Luc (2.5x10⁶ per animal)
OCI-Ly13.2-Luc (5 x10⁶ cells per animal)
Mice distribution by homogeneous tumor BLI (14 days Jurkat-Luc; 21 days OCI-Ly13.2-Luc)
Week 0 Treatment initiation
Week 1, 2, 3 ... Weekly health check and Bioluminiscence imaging
Survival Weight loss >10% Abnormal behaviour General bad condition
Jurkat-Luc: BM and spleen (CD3, CD45)
OCI-Ly13.2-Luc: Liver and spleen (CD3, CD45)
IQS117 (50 mg/kg/day)
IQS141 (50 mg/kg/day)
Vehicle
B
Vehicle IQS117 IQS141
Jurkat
Day 14
Day 29
Counts
C
Average radiance [p/s/cm²/sr]
ns/*
IQS117 (n=6)
IQS141 (n=5)
Vehicle (n=5)
Days from injection
D
% Survival
IQS117 (n=6)
IQS141 (n=5)
Vehicle (n=5)
*
Median survival
Vehicle IQS117 IQS141
34 Days 35 Days 36 Days
Days from injection
E
Vehicle IQS117 IQS141
OCI-Ly13.2
Day 21
Day 56
Counts
F
Average radiance [p/s/cm²/sr]
IQS117 (n=6)
IQS141 (n=5)
Vehicle (n=5)
Days from injection
G
% Survival
IQS117 (n=6)
IQS141 (n=5)
Vehicle (n=5)
*
Median survival
Vehicle IQS117 IQS141
64 Days 58 Days 66 Days
Days from injection

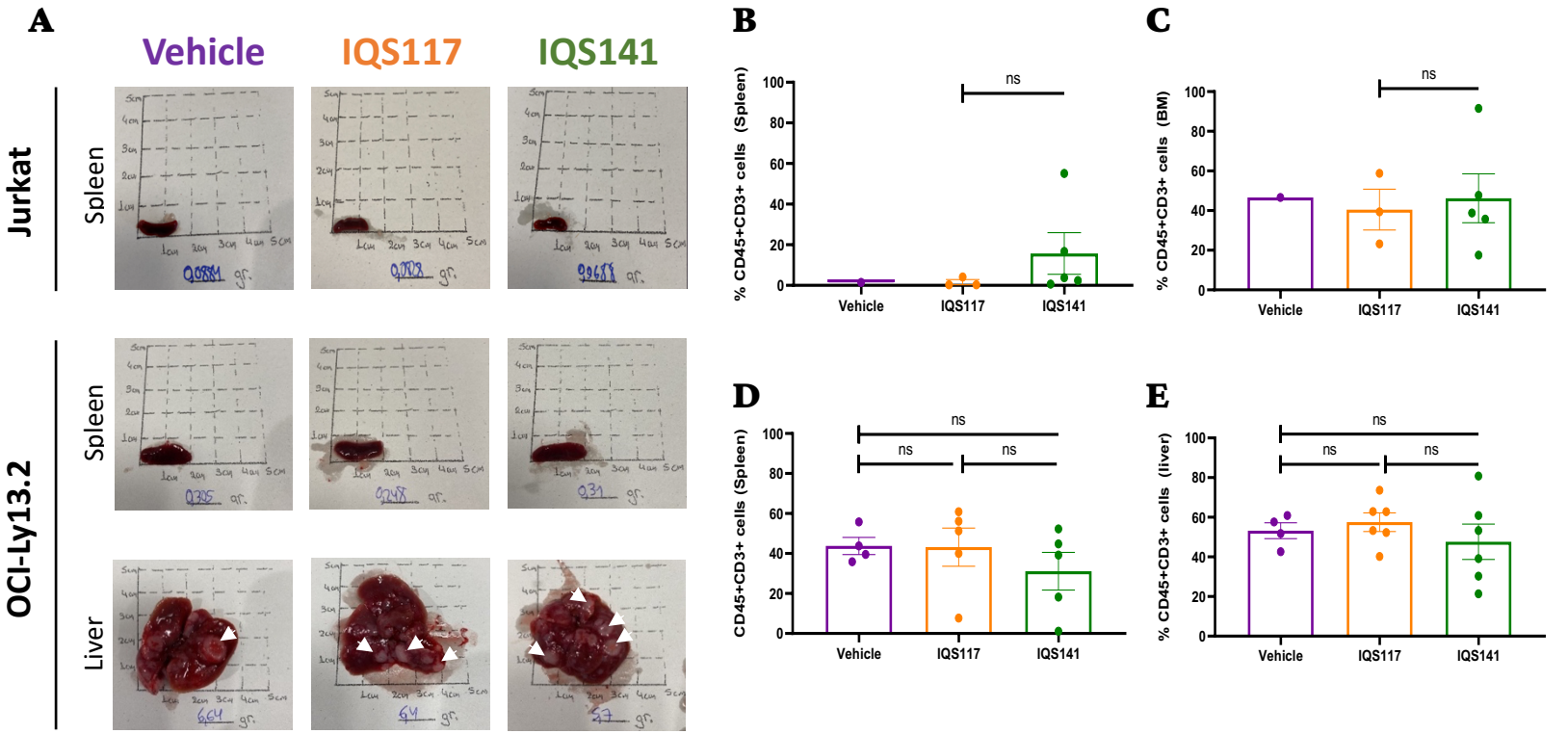

Figure 24. Unchanged organ size and malignant T-cell percentages on the spleen and liver of intravenous malignant T-cell xenografts following treatment with IQS117 and IQS141. **(A)** Representative organ images from mice treated with IQS117, IQS141 and vehicle in Jurkat-Luc and OCI-Ly13.2-Luc xenograft models. White arrows indicate tumor masses in the liver. **(B)** Flow cytometry quantification of human malignant T cells in the spleen **(B)** and bone marrow **(C)** for the Jurkat-Luc xenograft model, and in the spleen **(D)** and liver **(E)** for the OCI-Ly13.2-Luc xenograft model. Human malignant T cells were identified as CD45-positive CD3-positive cells. (*, $P < 0.05$; ns, not significant, Mann Whitney test).

6. Discussion

The clinical and biological heterogeneity of T-cell malignancies has made it challenging to develop effective treatment strategies, especially given the suboptimal responses to first-line anthracycline-based chemotherapy regimens on prevalent subtypes, where 5-year OS rates range from 32-49% (73–75). This underscores the pressing need for more tailored and efficacious treatment approaches for treating T-cell malignancies.

T-cell malignancies frequently exhibit epigenetic dysregulation and mutations within the TCR signaling pathways (34,37–42,46,49,54,61,65,66,128). However, many of these identified mutations are rare, making it difficult to develop targeted therapies (34). Furthermore, emerging evidence underscores the importance of TCR signaling in the pathogenesis of T-cell malignancies (186), whose inhibition has shown potential to impact chemotherapy response (146) and resistance (152,153). It is noteworthy that there are currently no FDA-approved drugs specifically targeting TCR signaling pathways in T-cell malignancies.

A hypothesis that has gained importance is the reliance of T-cell malignancies on TCR signaling for survival, evident in the ubiquitous expression of TCR signaling proteins (223). In this context, a key player is ZAP-70, a crucial kinase primarily expressed in T cells and NK cells, essential for proximal TCR signaling pathway and T-cell development (123). Certain T-cell malignancy subtypes, like nTFHL-AI and PTCL, NOS, maintain ZAP-70 expression (185). Moreover, a substantial portion of nTFHL-AI cases exhibit constitutive activation of ZAP-70 (152), suggesting its role in disease pathogenesis. In addition, ZAP-70 knockdown has been shown to reduce cell proliferation and induce apoptosis in T-ALL and CTCL cell lines (187). Preclinical studies have demonstrated the sensitivity of T-cell malignancies to the inhibition of various kinases within the TCR signaling cascade, including SYK (224), PI3K (225), ITK (152) and PKC (226), which function downstream of ZAP-70. However, the inhibition of LCK, an upstream kinase of ZAP-70, was insufficient in inhibiting malignant T-cell proliferation or inducing apoptosis (151). Significantly, studies focusing on selective ZAP-70 inhibitors in T-cell malignancies are lacking.

To explore the therapeutic potential of inhibiting ZAP-70 kinase activity and its impact on TCR signaling in T-cell malignancies, we developed a library of 27 novel pyrido[2,3-d]pyrimidine derivative compounds targeting the kinase domain of ZAP-70. Among these compounds, IQS117 and IQS141 were the most potent and selective inhibitors against a panel of kinases, reducing ZAP-70 kinase activity to 17% and 11%, respectively, at 10 µM, while maintaining an approximate three-fold selectivity for ZAP-70 over SYK, a structurally homologous B-cell kinase (227). Our analysis revealed no significant decrease (< 20%) in kinase activity for other kinases treated with IQS117 and IQS141, although both compounds exhibited moderate inhibitory effects (21-50% residual kinase activity) on proximal BCR signaling kinases (BTK and LYN) and members of the Src family (LCK, YES, and FYN), mainly expressed on T cells, at 10 µM. To optimize the optimal dosage for a balanced ZAP-70 kinase inhibition and minimized off-target effects, it is crucial to conduct lower-dose evaluations of IQS117 and IQS141 against the same kinase panel. This approach gains support from our findings on TAK-659, a SYK/FLT3 inhibitor previously reported to have on-target activity in the low nanomolar range and 23-fold selectivity for SYK over ZAP-70 in a cell-free assay (228). Notably, in our panel, TAK-659 showed a lack of selectivity against most evaluated kinases at 10 µM. Furthermore, this approach would enable the comparison with RDN2150, a recently reported potent ZAP-70 inhibitor achieving 98.3% inhibition of kinase activity at 1 µM with an eighteen-fold selectivity for ZAP-70 over SYK (190). Importantly, the specificity of RDN2150 toward key proximal TCR signaling kinases, such as FYN, LCK, and ITK, remains undocumented, necessitating further *in vitro* validation experiments to elucidate its impact on malignant T cell lines.

Subsequent *in vitro* analysis of the antitumoral effect of IQS117 and IQS141 on the proliferation and viability of Jurkat, OCI-Ly13.2 and T8ML-1 malignant T-cell lines revealed a dose-dependent inhibition of cell proliferation and viability within the micromolar range in all cell lines. Both inhibitors also dose-dependently inhibited the phosphorylation of ZAP-70, its immediate downstream effectors (LAT and SLP-76), and downstream signaling pathways (PLCγ1, ERK1/2 and AKT) in Jurkat and OCI-Ly13.2 cell lines. Notably, OCI-Ly13.2 cells exhibited a

lack of activation in SLP-76 and PLCγ1, while ERK1/2 activation persisted. This observation raises the possibility for ERK1/2 activation through alternative GEFs, such as SOS, in the absence of SLP-76/PLCγ1/RasGRP1 activation (230,231). Notably, IQS117 exhibited additionally inhibitory effects on AKT in Jurkat and OCI-Ly13.2 cell lines compared to IQS141. However, our kinase inhibition panel revealed that both IQS117 and IQS141 had minimal impact on AKT kinase activity. Since AKT activation in T cells is primarily regulated by PI3K and PDK1, which were not included in our kinase panel, the observed AKT inhibition could be a consequence from off-target effects on these upstream kinases. Additional Western blotting analysis of these kinases would provide clarity. Given the pivotal role of AKT in regulating cell survival, proliferation, and differentiation in both normal and malignant cells (232–234), AKT inhibition by IQS117 may explain the generally lower IC50 values for proliferation and viability in IQS117-treated cells compared to IQS141-treated cells.

Building upon our promising *in vitro* results, we evaluated the safety and pharmacokinetic profiles of IQS117 and IQS141 in immunodeficient mice. While conventional protocols typically involve immunocompetent mice or rats (190,196,229,235), we opted for immunodeficient mice for our initial studies to align with our malignant T-cell xenografts model background. We observed no significant changes in body weight or acute organ histopathology following a single-dose of 300 mg/kg of IQS117 or IQS141 compared to the vehicle-treated mice, regardless of the administration route. Notably, oral administration of IQS117 and IQS141 at a lower dose of 50 mg/kg resulted in longer half-lives, higher C_{max} and prolonged total drug exposure in mice compared to the intraperitoneal administration, leading to the choice of oral administration for pharmacological *in vivo* experiments. However, it is essential to consider that, while these results are promising, they may not fully represent the potential toxicity pharmacokinetic profiles in immunocompetent mice, given the potential impact of the immune system activation on drug metabolism and toxicity. Therefore, the absence of observed toxicity in immunodeficient mice primarily suggests limited direct toxicity effects of the drugs on the organ microenvironment.

To validate our results from cellular models, IQS117 and IQS141 were orally administered to luciferase-expressing Jurkat and OCI-Ly13.2 subcutaneous and intravenous xenograft models, with a control group receiving a vehicle treatment. Notably, there were no significant differences in tumor growth and survival in the subcutaneous xenograft models upon IQS117 and IQS141 treatment compared to the vehicle treatment group. This led us to conduct another experiment to evaluate potential transcriptomic changes in subcutaneous tumors derived from OCI-Ly13.2 and Jurkat xenograft models after seven days of oral treatment with IQS117, IQS141, and vehicle. However, this analysis did not reveal distinct transcriptome changes associated with ZAP-70 inhibition when compared to the vehicle-treated group.

These results raised concerns about the effective delivery of the compounds to the subcutaneous tumor site, despite their detection in mouse plasma during the previous pharmacokinetic assay. Subsequently, we shifted our focus to intravenous xenograft models to assess the impact of the drugs in a disseminated disease context. However, not significant differences were observed in tumor growth or survival in the intravenous Jurkat-Luc and OCI-Ly13.2 xenograft models. Furthermore, there were no significant differences in the percentage of malignant T cells in the spleen or BM in the Jurkat-Luc or in the liver and spleen in the OCI-Ly13.2-Luc models between IQS117- and IQS141-treated mice compared to the vehicle group.

To further assess whether IQS117 and IQS141 effectively reach the tumor site, Western blotting analysis and IHQ staining for phospho-ZAP-70 should be conducted to shed light on the activation status of ZAP-70 in IQS117 and IQS141-treated mice compared to the vehicle group. Another potential approach to improve drug delivery could involve synthesizing the salt form of each compound, a strategy that has previously proven effective in improving *in vivo* drug efficacy (229).

In conclusion, our findings emphasize the potential of ZAP-70 inhibition in T-cell malignancies. Nevertheless, further investigations are required to bridge

the gap between promising *in vitro* results and *in vivo* efficacy, particularly regarding drug delivery to the tumor site. This additional insight will be crucial to optimize the structure of more efficient ZAP-70 inhibitors.

7. Conclusions

1. IQS117 and IQS141 demonstrate the highest efficacy and selectivity in inhibiting ZAP-70 kinase activity among the synthesized compounds.

2. IQS117 and IQS141 effectively suppress the proliferation and viability of malignant T-cell lines.

3. IQS117 and IQS141 exert potent inhibitory effects on ZAP-70 activation, effectively disrupting TCR signaling in malignant T-cell lines.

4. In immunodeficient mice, the absence of acute toxicity associated with IQS117 and IQS141 administered via oral gavage and intraperitoneal injection underscores their favourable safety profiles *in vivo*.

5. After oral gavage administration, both IQS117 and IQS141 exhibit prolonged half-lives and increased total drug exposure in the bloodstream of immunodeficient mice compared to intraperitoneal injection.

6. IQS117 and IQS141 do not significantly improve the survival of subcutaneous and intravenous T-ALL and ALK-negative ALCL xenograft models of malignant T-cell lines, nor do they induce substantial transcriptomic changes in subcutaneous tumors, indicating the necessity for further research to enhance their efficacy in these models.

8. Future Research Opportunities

Our study elucidates the challenges associated with treating heterogeneous T-cell malignancies while highlighting the therapeutic potential of ZAP-70 inhibition. To deepen our understanding and develop effective therapies, we propose several avenues for future research. Firstly, we intend to expand our kinase panel to encompass a diverse array of kinases at several doses, with a particular emphasis on those relevant to various cellular subtypes within the immune system. This expanded evaluation will allow us to delve deeper into the selectivity profile of our ZAP-70 inhibitors.

Secondly, building upon the observed *in vitro* effects of our ZAP-70 inhibitors on proliferation, viability, and TCR signaling in malignant T-cell lines, we will expand our study to include a more extensive range of cellular models, representing other T-cell malignancy subtypes. Furthermore, we will assess their impact on healthy T cells. Additionally, we will include malignant B-cell lines to discern the potential off-target effects identified in the kinase inhibition panel. This approach will facilitate a more comprehensive understanding of the therapeutic potential of ZAP-70 inhibitors on T-cell malignancies. Thirdly, the on-target effects observed with pharmacological ZAP-70 inhibition need validation via genetic ZAP-70 knockdown in malignant T-cell lines. Fourthly, we plan to explore transcriptomic alterations in malignant T cells following treatment with ZAP-70 inhibitors, alongside the identification of potential synergistic therapeutic targets for combined administration with ZAP-70 inhibitors.

In fifth place, we plan to expand our i*n vivo* studies to include assessments of both acute and chronic exposure in various mouse models, including immunodeficient and immunocompetent mice. This approach will provide valuable insights into potential safety concerns and variations in pharmacokinetics related to the presence of a functional immune response. Lastly, we aim to conduct an acute treatment experiment of ZAP-70 inhibitors in intravenous xenograft models of malignant T-cells. This experimental setup will not only involve addressing transcriptomic changes following ZAP-70 inhibition treatment but will also address the issue of drug delivery to the tumor site. Given the lack of a significant impact on the survival of intravenous xenograft models of

malignant T-cells in response to ZAP-70 inhibitors, we will employ LC-MS to quantitatively measure drug delivery to the tumor sites. Specifically, we will focus on evaluating drug delivery in the spleen and BM for the Jurkat-Luc model, and the spleen and liver OCI-Ly13.2-Luc model.

In summary, our findings underscore the therapeutic potential of ZAP-70 inhibition and emphasize the need for further research to optimize ZAP-70 inhibitors for clinical use, addressing critical aspects such as safety, pharmacokinetics, and drug delivery to enhance their efficacy and clinical utility.

9. Bibliography

1. Abbas KA, Lichtman HA. Cellular and Molecular Immunology. 9th ed. Philadelphia, PA: Elsevier; 2017. 229 p.

2. Jagannathan-Bogdan M, Zon LI. Hematopoiesis. Development. 2013;140(12):2463–7.

3. Cheng H, Zheng Z, Cheng T. New paradigms on hematopoietic stem cell differentiation. Protein Cell. 2020;11(1):34–44.

4. Laurenti E, Göttgens B. From haematopoietic stem cells to complex differentiatoin landscapes. Nature. 2018;553(7689):418–26.

5. Kumar B V, Connors T, Farber DL. Human T cell development, localization, and function throughout life. Immunity. 2018;48(2):202–13.

6. Germain RN. t-cell development and the CD4-CD8 lineage decision. Nat Rev Immunol. 2002;2(5):309–22.

7. García-Mariscal A, Blanco B del, Hernández-Munain C. Generation of lymphocyte antigen receptor diversity: Validation of the "accessibility model" in controlling V(D)J recombination. Inmunología. 2013;32(2):57–69.

8. Franchini DM, Benoukraf T, Jaeger S, Ferrier P, Payer-Bornet D. Initiation of V(D)J Recombination by Dβ-Associated Recombination Signal Sequences: A critical Control Point in TCRβ Gene Assembly. PLoS One. 2009;4(2):e4575.

9. Rothenberg E V., Moore JE, Yui MA. Launching the T-cell-lineage developmental programme. Nat Rev Immunol. 2008;8(1):9–21.

10. Magali I. Instructive Cues of Thymic T Cell Selection. Annu Rev Immunol. 2022;40:95–119.

11. Gaud G, Lesourne R, Love PE. Regulatory mechanisms in T cell receptor signalling. Nat Rev Immunol. 2018;18(8):485–97.

12. Klein L, Kyewski B, Allen PM, Hogquist KA. Positive and negative selection of the T cell repertoire: what thymocytes see and don't see. Nat Rev Immunol. 2014;14(6):377–91.

13. Neefjes J, Jongsma MLM, Paul P, Bakke O. Towards a systems understanding of MHC class l and MHC class II antigen presentation. Nat Rev Immunol. 2011;11(12):823–36.

14. Parkin J, Cohen B. An overview of the immune system. Lancet. 2001;357(9270):P1777–89.

15. Alaggio R, Amador C, Anagnostopoulos I, Attygalle AD, Araujo IB de O, Berti E, et al. The 5th edition of the World Health Organization Classification of Haematolymphoid Tumours: Lymphoid Neoplasms. Leukemia. 2022;36(7):1720–48.

16. Harris NL, Jaffe ES, Stein H, Banks PM, Chan JKC, Cleary ML, et al. A revised European-American classification of lymphoid neoplasms: A proposal from the International Lymphoma Study Group. Blood. 1994;84(5):1361–92.

17. Jaffe ES, Harris NL, Stein H, Vardiman JW. World Health Organization Classification of Tumours. Pathology and Genetics of Tumours of Haematopoietic and Lymphoid Tissues. 3rd ed. Lyon: IARCPress; 2001.

18. Campo E, Jaffe ES, Cook JR, Quintanilla-Martinez L, Swerdlow SH, Anderson KC, et al. The International Consensus Classification of Mature Lymphoid Neoplasms: a report from the Clinical Advisory Committee. Blood. 2022;140(11):1229–53.

19. Siegel RL, Miller KD, Wagle NS, Jemal A. Cancer statistics, 2023. CA Cancer J Clin. 2023;73(1):17–48.

20. Fiore D, Cappelli LV, Broccoli A, Zinzani PL, Chan WC, Inghirami G. Peripheral T cell lymphomas: from the bench to the clinic. Nat Rev Cancer. 2020;20(6):323–42.

21. Vose JM, Neumann M, Harris ME. International peripheral T-cell and natural killer/T-cell lymphoma study: Pathology findings and clinical outcomes international T-cell lymphoma project. J Clin Oncol. 2008;26(25):4124–30.

22. Adams S V., Newcomb PA, Shustov AR. Racial patterns of peripheral T-Cell lymphoma incidence and survival in the United States. J Clin Oncol. 2016;34(9):963–71.

23. Yoon SE, Song Y, Kim SJ, Yoon DH, Chen TY, Koh Y, et al. Comprehensive analysis of peripheral T-cell and natural killer/T-cell lymphoma in Asian patients: A multinational, multicenter, prospective registry study in Asia. Lancet Reg Heal - West Pacific. 2021;10:100126.

24. Guru Murthy GS, Pondaiah SK, Abedin S, Atallah E. Incidence and survival of T-cell acute lymphoblastic leukemia in the United States. Leuk Lymphoma. 2019;60(5):1171–8.

25. Hanbali A, Kotb A, Fakih R El, Alfraih F, Shihata N, Rasheed W, et al. Improved survival of adolescents and young adults patients with T-cell acute lymphoblastic leukemia. Int J Hematol Oncol. 2023;12(1).

26. El-Sharkawi D, Attygalle A, Dearden C. Mature T-Cell leukemias: Challenges in Diagnosis. Front Oncol. 2022;12:777066.

27. Redaelli A, Laskin BL, Stephens JM, Botteman MF, Pashos CL. A systematic literature review of the clinical and epidemiological burden of acute lymphoblastic leukaemia (ALL). Eur J Cancer Care (Engl). 2005;14(1):53–62.

28. Mohammed Saleh MF, Kotb A, Abdallah GEM, Muhsen IN, El Fakih R, Aljurf M. Recent advances in diagnosis and therapy of angioimmunoblastic T cell lymphoma. Curr Oncol. 2021;28(6):5480–98.

29. Phan A, Veldman R, Lechowicz MJ. T-cell Lymphoma Epidemiology: the Known and Unknown. Curr Hematol Malig Rep. 2016;11(6):492–503.

30. de Leval L, Feldman AL, Pileri S, Nakamura S, Gaulard P. Extranodal T- and NK-cell lymphomas. Virchows Arch. 2022;482(1):245–64.

31. Pileri SA, Tabanelli V, Fiori S, Calleri A, Melle F, Motta G, et al. Peripheral t-cell lymphoma, not otherwise specified: Clinical manifestations, diagnosis, and future treatment. Vol. 13, Cancers. 2021.

32. Shustov A, Soma L. Anaplastic large cell lymphoma: Contemporary concepts and optimal management. Vol. 176, Cancer Treatment and Research. Springer International Publishing; 2019. 127–144 p.

33. Soldini D, Campo E. New insights into the diagnosis of lymphomas. Ann Oncol. 2012;23(SUPPL. 10):83–8.

34. Cortés JR, Palomero T. Biology and molecular pathogenesis of mature t-cell lymphomas. Cold Spring Harb Perspect Med. 2021;11(5):1–20.

35. De Leval L, Rickman DS, Thielen C, De Reynies A, Huang YL, Delsol G, et al. The gene expression profile of nodal peripheral T-cell lymphoma demonstrates a molecular link between angioimmunoblastic T-cell lymphoma (AITL) and follicular helper T (TFH) cells. Blood. 2007;109(11):4952–63.

36. Quivoron C, Couronné L, Della Valle V, Lopez CK, Plo I, Wagner-Ballon O, et al. TET2 Inactivation Results in Pleiotropic Hematopoietic Abnormalities in Mouse and Is a Recurrent Event during Human Lymphomagenesis. Cancer Cell. 2011;20(2):276.

37. Couronné L, Bastard C, Bernard OA. TET2 and DNMT3A Mutations in Human T-Cell Lymphoma . N Engl J Med. 2012;366(1):95–6.

38. Cairns RA, Iqbal J, Lemonnier F, Kucuk C, De Leval L, Jais JP, et al. IDH2 mutations are frequent in angioimmunoblastic T-cell lymphoma. Blood. 2012;119(8):1901–3.

39. Palomero T, Couronné L, Khiabanian H, Kim MY, Ambesi-Impiombato A, Perez-Garcia A, et al. Recurrent mutations in epigenetic regulators, RHOA and FYN kinase in peripheral T cell lymphomas. Nat Genet. 2014;46(2):166–70.

40. Sakata-Yanagimoto M, Enami T, Yoshida K, Shiraishi Y, Ishii R, Miyake Y, et al. Somatic RHOA mutation in angioimmunoblastic T cell lymphoma. Nat Genet. 2014;46(2):171–5.

41. Marques-Piubelli ML, Amador C, Vega F. Pathologic and molecular insights in nodal T-follicular helper cell lymphomas. Front Oncol. 2023;13(January):1–10.

42. Lemonnier F, Couronné L, Parrens M, Jaïs JP, Travert M, Lamant L, et al. Recurrent TET2 mutations in peripheral T-cell lymphomas correlate with TFH-like features and adverse clinical parameters. Blood. 2012;120(7):1466–9.

43. Moran-Crusio K, Reavie L, Shih A, Abdel-Wahab O, Ndiaye-Lobry D, Lobry C, et al. Tet2 Loss Leads to Increased Hematopoietic Stem Cell Self-Renewal and Myeloid Transformation. Cancer Cell. 2011;20(1):11–24.

44. Steensma DP, Ebert BL. Clonal hematopoiesis as a model for premalignant changes during aging. Exp Hematol. 2020;83(December):48–56.

45. Fujisawa M, Nguyen TB, Abe Y, Suehara Y, Fukumoto K, Suma S, et al. Clonal germinal center B cells function as a niche for T-cell lymphoma. Blood. 2022;140(18):1937–50.

46. Cortés JR, Palomero T. The curious origins of angioimmunoblastic T-cell lymphoma. Curr Opin Hematol. 2016;23(4):434–43.

47. Leca J, Lemonnier F, Meydan C, Foox J, El Ghamrasni S, Mboumba DL, et al. IDH2 and TET2 mutations synergize to modulate T Follicular Helper cell functional interaction with the AITL microenvironment. Cancer Cell. 2023;41(2):323-339.e10.

48. Jaffe AB, Hall A. RHO GTPASES: Biochemistry and Biology. Annu Rev Cell Dev Biol. 2005;21:247–69.

49. Yoo HY, Sung MK, Lee SH, Kim S, Lee H, Park S, et al. A recurrent inactivating mutation in RHOA GTPase in angioimmunoblastic T cell lymphoma. Nat Genet. 2014;46(4):371–5.

50. Ng SY, Brown L, Stevenson K, DeSouza T, Aster JC, Louissaint A, et al. RhoA G17V is sufficient to induce autoimmunity and promotes T-cell lymphomagenesis in mice. Blood. 2018;132(9):935–47.

51. Cortes JR, Ambesi-Impiombato A, Couronné L, Quinn SA, Kim CS, Almeida AC da S, et al. RHOA G17V induces T follicular helper cell specification and promotes lymphomagenesis. Cancer Cell. 2018;33(2):259–73.

52. Hapgood G, Savage KJ. The biology and management of systemic anaplastic large cell lymphoma. Blood. 2015;126(1):17–25.

53. Rimokh R, Magaud JP, Berger F, Samarut J, Coiffier B, Germain D, et al. A translocation involving a specific breakpoint (q35) on chromosome 5 is characteristic of anaplastic large cell lymphoma ('Ki-1 lymphoma'). Br J Haematol. 1989;71(1):31–6.

54. Hathuc V, Kreisel F. Genetic Landscape of Peripheral T-Cell Lymphoma. Life. 2022;12(3).

55. Crescenzo R, Abate F, Lasorsa E, Tabbo' F, Gaudiano M, Chiesa N, et al. Convergent mutations and kinase fusions lead to oncogenic STAT3 activation in anaplastic large cell lymphoma. Cancer Cell. 2015;27(4):516–32.

56. Vasmatzis G, Johnson SH, Knudson RA, Ketterling RP, Braggio E, Fonseca R, et al. Genome-wide analysis reveals recurrent structural abnormalities of TP63 and other p53-related genes in peripheral T-cell lymphomas. Blood. 2012;120(11):2280–9.

57. Feldman AL, Dogan A, Smith DI, Law ME, Ansell SM, Johnson SH, et al. Discovery of recurrent t(6;7) (p25.3;q32.3) translocations in ALK-negative anaplastic large cell lymphomas by massively parallel genomic sequencing. Blood. 2011;117(3):915–9.

58. Piccaluga PP, Agostinelli C, Califano A, Rossi M, Basso K, Zupo S, et al. Gene expression analysis of peripheral T cell lymphoma, unspecified, reveals distinct profiles and new potential therapeutic targets. J Clin Invest. 2007;117(3):823–34.

59. Iqbal J, Weisenburger DD, Greiner TC, Vose JM, McKeithan T, Kucuk C, et al. Molecular signatures to improve diagnosis in peripheral T-cell lymphoma and prognostication in angioimmunoblastic T-cell lymphoma. Blood. 2010;115(5):1026–36.

60. Iqbal J, Wright G, Wang C, Rosenwald A, Gascoyne RD, Weisenburger DD, et al. Gene expression signatures delineate biological and prognostic subgroups in peripheral T-cell lymphoma. Blood. 2014;123(19):2915–23.

61. Vallois D, Dobay MPD, Morin RD, Lemonnier F, Missiaglia E, Juilland M, et al. Activating mutations in genes related to TCR signaling in angioimmunoblastic and other follicular helper T-cell-derived lymphomas. Blood. 2016;128(11):1490–502.

62. Amador C, Greiner TC, Heavican TB, Smith LM, Galvis KT, Lone W, et al. Reproducing the molecular subclassification of peripheral T-cell lymphoma–NOS by immunohistochemistry. Blood. 2019;134(24):2159–70.

63. Zain JM, Hanona P. Aggressive T-cell lymphomas: 2021 Updates on diagnosis, risk stratification and management. Am J Hematol. 2021;96(8):1027–46.

64. Gianni F, Belver L, Ferrando A. The genetics and mechanisms of T-cell acute lymphoblastic leukemia. Cold Spring Harb Perspect Med. 2020;10(3):1–28.

65. Bardelli V, Arniani S, Pierini V, Di Giacomo D, Pierini T, Gorello P, et al. T-cell acute lymphoblastic leukemia: Biomarkers and their clinical usefulness. Genes (Basel). 2021;12(8):1–20.

66. De Smedt R, Morscio J, Goossens S, Van Vlierberghe P. Targeting steroid resistance in T-cell acute lymphoblastic leukemia. Blood Rev. 2019;38:100591.

67. Weng AP, Ferrando AA, Lee W, Morris IV JP, Silverman LB, Sanchez-Irizarry C, et al. Activating mutations of NOTCH1 in human T cell acute lymphoblastic leukemia. Science (80-). 2004;306(5694):269–71.

68. Liu R Bin, Guo JG, Liu TZ, Guo CC, Fan XX, Zhang X, et al. Meta-analysis of the clinical characteristics and prognostic relevance of NOTCH1 and FBXW7 mutation in T-cell acute lymphoblastic leukemia. Oncotarget. 2017;8(39):66360–70.

69. Ferrando AA, Neuberg DS, Staunton J, Loh ML, Huard C, Raimondi SC, et al. Gene expression signatures define novel oncogenic pathways in T cell acute lymphoblastic leukemia. Cancer Cell. 2002;1(1):75–87.

70. Chan SH, Chiang J, Ngeow J. CDKN2A germline alterations and the relevance of genotype-phenotype associations in cancer predisposition. Hered Cancer Clin Pract. 2021;19(1):1–9.

71. Litzow MR, Raetz EA. Clinical Management of Acute Lymphoblastic Leukemia: From Bench to Bedside. Clinical Management of Acute Lymphoblastic Leukemia: From Bench to Bedside. 2022. 1–437 p.

72. National Comprehensive Cancer Network. T-Cell Lymphomas (Version 1.2023) [Internet]. [cited 2023 Jan 5]. Available from: https://www.nccn.org/professionals/physician_gls/pdf/t-cell.pdf

73. Ellin F, Landström J, Jerkeman M, Relander T. Real-world data on prognostic factors and treatment in peripheral T-cell lymphomas: A study from the Swedish Lymphoma Registry. Blood. 2014;124(10):1570–7.

74. Carson KR, Horwitz SM, Pinter-brown LC, Rosen ST, Pro B, Hsi ED, et al. A Prospective Cohort Study of Patients with Peripheral T-Cell Lymphoma in the United States. Cancer. 2017;123(7):1174–83.

75. Savage KJ, Harris NL, Vose JM, Ullrich F, Jaffe ES, Connors JM, et al. ALK-anaplastic large-cell lymphoma is clinically and immunophenotypically different from both ALK+ ALCL and peripheral T-cell lymphoma, not otherwise specified: Report from the International Peripheral T-Cell Lymphoma Project. Blood. 2008;111(12):5496–504.

76. Park SI, Horwitz SM, Foss FM, Brown LCP, Carson KR, Rosen ST, et al. The Role of Autologous Stem Cell Transplantation in Patients With Nodal Peripheral T-Cell Lymphomas in First Complete Remission: Report From COMPLETE, a Prospective, Multicenter Cohort Study. Cancer. 2019;125(9):1507–17.

77. Brink M, Meeuwes FO, Poel MWM van der, Kersten MJ, Wondergem M, Mutsaers PGNJ, et al. Impact of etoposide and ASCT on survival among patients aged <65 years with stage II to IV PTCL: a population-based cohort study. Blood. 2022;140(9):1009–19.

78. Abeyakoon C, van der Weyden C, Harrop S, Khot A, Dickinson M, Yannakou CK, et al. Role of haematopoietic stem cell transplantation in peripheral T-cell lymphoma. Cancers (Basel). 2020;12(11):1–24.

79. Zing NPiC, Fischer T, Zain J, Federico M, Rosen ST. Peripheral T-Cell Lymphomas: Incorporating New Developments in Diagnostics, Prognostication, and Treatment Into Clinical Practice-PART 1: PTCL-NOS, FTCL, AITL, ALCL. Oncol Willist Park. 2018;32(7):e74–82.

80. Sibon D. Peripheral T-Cell Lymphomas : Therapeutic Approaches. Cancers (Basel). 2022;14:2332.

81. Wulf GG, Altmann B, Ziepert M, D'Amore F, Held G, Greil R, et al. Alemtuzumab plus CHOP versus CHOP in elderly patients with peripheral T-cell lymphoma: the DSHNHL2006-1B/ACT-2 trial. Leukemia. 2021;35(1):143–55.

82. Bachy E, Camus V, Thieblemont C, Sibon D, Casasnovas RO, Ysebaert L, et al. Romidepsin Plus CHOP Versus CHOP in Patients With Previously Untreated Peripheral T-Cell Lymphoma: Results of the Ro-CHOP Phase III Study (Conducted by LYSA). J Clin Oncol. 2022;40(3):242–51.

83. Pro B, Horwitz SM, Prince HM, Foss FM, Sokol L, Greenwood M, et al. Romidepsin induces durable responses in patients with relapsed or refractory angioimmunoblastic T-cell lymphoma. Hematol Oncol. 2017;35(4):914–7.

84. Ghione P, Faruque P, Mehta-Shah N, Seshan V, Ozkaya N, Bhaskar S, et al. T follicular helper phenotype predicts response to histone deacetylase inhibitors in relapsed/refractory peripheral T-cell lymphoma. Blood Adv. 2020;4(19):4640–7.

85. Horwitz S, O'Connor OA, Pro B, Trümper L, Iyer S, Advani R, et al. The ECHELON-2 Trial: 5-year results of a randomized, phase III study of brentuximab vedotin with chemotherapy for CD30-positive peripheral T-cell lymphoma. Ann Oncol. 2022;33(3):288–98.

86. Carobolante F, Chiaretti S, Skert C, Bassan R. Practical guidance for the management of acute lymphoblastic leukemia in the adolescent and young adult population. Ther Adv Hematol. 2020;11:1–25.

87. National Comprehensive Cancer Network. Acute Lymphoblastic leukemia (Version 2.2023) [Internet]. [cited 2023 Jul 28]. Available from: https://www.nccn.org/professionals/physician_gls/pdf/all.pdf

88. Malard F, Mohty M. Acute Lymphoblastic Leukaemia. Lancet. 2020;395(10230):1146–62.

89. Mitchell CD, Richards SM, Kinsey SE, Lilleyman J, Vora A, Eden TOB. Benefit of dexamethasone compared with prednisolone for childhood acute lymphoblastic leukaemia: Results of the UK Medical Research Council ALL97 randomized trial. Br J Haematol. 2005;129(6):734–45.

90. Möricke A, Zimmermann M, Valsecchi MG, Stanulla M, Biondi A, Mann G, et al. Dexamethasone vs prednisone in induction treatment of pediatric ALL: results of the randomized trial AIEOP-BFM ALL 2000. Blood. 2016;127(17):2101–12.

91. Mak V, Hamm J, Chhanabhai M, Shenkier T, Klasa R, Sehn LH, et al. Survival of patients with peripheral T-cell lymphoma after first relapse or progression: Spectrum of disease and rare long-term survivors. J Clin Oncol. 2013;31(16):1970–6.

92. O'Connor OA, Pro B, Pinter-Brown L, Bartlett N, Popplewell L, Coiffier B, et al. Pralatrexate in patients with relapsed or refractory peripheral T-cell lymphoma: Results from the pivotal PROPEL study. J Clin Oncol. 2011;29(9):1182–9.

93. Coiffier B, Pro B, Prince HM, Foss F, Sokol L, Greenwood M, et al. Romidepsin for the treatment of relapsed/refractory peripheral T-cell lymphoma: Pivotal study update demonstrates durable responses. J Hematol Oncol. 2014;7(1):1–9.

94. Pro B, Advani R, Brice P, Bartlett NL, Rosenblatt JD, Illidge T, et al. Brentuximab vedotin (SGN-35) in patients with relapsed or refractory systemic anaplastic large-cell lymphoma: Results of a phase II study. J Clin Oncol. 2012;30(18):2190–6.

95. O'Connor OA, Horwitz S, Masszi T, Van Hoof A, Brown P, Doorduijn J, et al. Belinostat in patients with relapsed or refractory peripheral T-cell lymphoma: Results of the pivotal phase II BELIEF (CLN-19) study. J Clin Oncol. 2015;33(23):2492–9.

96. Merino M, Kasamon Y, Li H, Ma L, Leong R, Zhou J, et al. FDA approval summary: Crizotinib for pediatric and young adult patients with relapsed or refractory systemic anaplastic large cell lymphoma. Pediatr Blood Cancer. 2022;69:e29602.

97. Foster JH, Voss SD, Hall D, Minard CG, Balis FM, Wilner K, et al. Activity of Crizotinib in Patients with ALK-aberrant Relapsed/ Refractory Neuroblastoma: A Children's Oncology Group Study (ADVL0912). Clin Cancer Res. 2021;27(13):3543–8.

98. Lemonnier F, Dupuis J, Sujobert P, Tournillhac O, Cheminant M, Sarkozy C, et al. Treatment with 5-azacytidine induces a sustained response in patients with angioimmunoblastic T-cell lymphoma. Blood. 2018;132(21):2305–9.

99. Reismüller B, Attarbaschi A, Peters C, Dworzak MN, Pötschger U, Urban C, et al. Long-term outcome of initially homogenously treated and relapsed childhood acute lymphoblastic leukaemia in Austria - A population-based report of the Austrian Berlin-Frankfurt-Münster (BFM) Study Group. Br J Haematol. 2009;144(4):559–70.

100. Thomas DA, Kantarjian H, Smith TL, Koller C, Cortes J, O'Brien S, et al. Primary refractory and relapsed adult acute lymphoblastic leukemia: characteristics, treatment results, and prognosis with salvage therapy. Cancer. 1999;86(7):1216–30.

101. Cohen MH, Johnson JR, Justice R, Pazdur R. FDA Drug Approval Summary: Nelarabine (Arranon®) for the Treatment of T-Cell Lymphoblastic Leukemia/Lymphoma. Oncologist. 2008;13(6):709–14.

102. Berg SL, Blaney SM, Devidas M, Lampkin TA, Murgo A, Bernstein M, et al. Phase II study of nelarabine (compound 506U78) in children and young adults with refractory T-cell malignancies: A report from the children's oncology group. J Clin Oncol. 2005;23(15):3376–82.

103. DeAngelo DJ, Yu D, Johnson JL, Coutre SE, Stone RM, Stopeck AT, et al. Nelarabine induces complete remissions in adults with relapsed or refractory T-lineage acute lymphoblastic leukemia or lymphoblastic lymphoma: Cancer and Leukemia Group B study 19801. Blood. 2007;109(12):5136–42.

104. Dunsmore KP, Winter SS, Devidas M, Wood BL, Esiashvili N, Chen Z, et al. Children's oncology group AALL0434: A phase III randomized clinical trial testing nelarabine in newly diagnosed t-cell acute lymphoblastic leukemia. J Clin Oncol. 2020;38(28):3282–93.

105. Ferrando AA. The role of NOTCH1 signaling in T-ALL. Hematology. 2009 Jan 1;2009(1):353–61.

106. Deangelo DJ, Stone RM, Silverman LB, Stock W, Attar EC, Dallob IF, et al. A phase I clinical trial of the Notch inhibitor MK-0752 in patients with T-cell acute lymphoblastic leukemia/lymphoma (T-ALL) and other leukemias. J Clin Oncol. 2006;24(18):6585.

107. Pullarkat VA, Lacayo NJ, Jabbour E, Rubnitz JE, Bajel A, Laetsch TW, et al. Venetoclax and Navitoclax in Combination with Chemotherapy in Patients with Relapsed or Refractory Acute Lymphoblastic Leukemia and Lymphoblastic Lymphoma. Cancer Discov. 2021 Jun 1;11(6):1440–53.

108. Ofran Y, Ringelstein-Harlev S, Slouzkey I, Zuckerman T, Yehudai-Ofir D, Henig I, et al. Daratumumab for eradication of minimal residual disease in high-risk advanced relapse of T-cell/CD19/CD22-negative acute lymphoblastic leukemia. Leukemia. 2020;34(1):293–5.

109. Bride KL, Vincent TL, Im SY, Aplenc R, Barrett DM, Carroll WL, et al. Preclinical efficacy of daratumumab in T-cell acute lymphoblastic leukemia. Blood. 2018 Mar 1;131(9):995–9.

110. Lu P, Hill HA, Navsaria LJ, Wang ML. CAR-T and other adoptive cell therapies for B cell malignancies. J Natl Cancer Cent. 2021;1(3):88–96.

111. Luo L, Zhou X, Zhou L, Liang Z, Yang J, Tu S, et al. Current state of CAR-T therapy for T-cell malignancies. Ther Adv Hematol. 2022;13:1–21.

112. Patel J, Gao X, Wang H. An Update on Clinical Trials and Potential Therapeutic Strategies in T-Cell Acute Lymphoblastic Leukemia. Int J Mol Sci. 2023;24(8).

113. An J, Tan Y, Wang G, Deng B, Ling Z, Song W, et al. Donor-Derived CD7 Chimeric Antigen Receptor T Cells for T-Cell Acute Lymphoblastic Leukemia: First-in-Human, Phase I Trial. J Clin Oncol. 2021;39:3340–51.

114. Tai Y, Wang Q, Korner H, Zhang L, Wei W. Molecular mechanisms of T cells activation by dendritic cells in autoimmune diseases. Front Pharmacol. 2018;9(JUN):1–10.

115. Gorentla BK, Zhong XP. T cell Receptor Signal Transduction in T lymphocytes. J Clin Cell Immunol. 2012;Suppl 12:5.

116. Brownlie RJ, Zamoyska R. T cell receptor signalling networks: Branched, diversified and bounded. Nat Rev Immunol. 2013;13(4):257–69.

117. Courtney AH, Lo WL, Weiss A. TCR signaling: Mechanisms of Initiation and Propagation. Trends Immunol. 2018;43(2):108–23.

118. Shah K, Al-Haidari A, Sun J, Kazi JU. T cell receptor (TCR) signaling in health and disease. Signal Transduct Target Ther. 2021;6:412.

119. Mariuzza RA, Agnihotri P, Orban J. The structural basis of T-cell receptor (TCR) activation: An enduring enigma. J Biol Chem. 2019;295(4):914–25.

120. Chylek LA, Akimov V, Dengjel J, Rigbolt KTG, Hu B, Hlavacek WS, et al. Phosphorylation site dynamics of early T-cell receptor signaling. PLoS One. 2014;9(8).

121. Palacios EH, Weiss A. Function of the Src-family kinases, Lck and Fyn, in T-cell development and activation. Oncogene. 2004;23(7):7990–8000.

122. Appleby MW, Gross JA, Cooke MP, Levin SD, Qian X, Perlmutter RM. Defective T cell receptor signaling in mice lacking the thymic isoform of p59fyn. Cell. 1992;70(5):751–63.

123. Au-Yeung BB, Shah NH, Shen L, Weiss A. ZAP-70 in Signaling, Biology, and Disease. Annu Rev Immunol. 2018;36:127–56.

124. Balagopalan L, Kortum RL, Coussens NP, Barr VA, Samelson LE. The linker for activation of T Cells (LAT) signaling hub: From signaling complexes to microclusters. J Biol Chem. 2015;290(44):26422–9.

125. Devkota S, Joseph RE, Min L, Bruce Fulton D, Andreotti AH. Scaffold Protein SLP-76 Primes PLCγ1 for Activation by ITK-Mediated Phosphorylation. J Mol Biol. 2015;427(17):2734–47.

126. Berridge MJ. Inositol trisphosphate and calcium signalling mechanisms. Biochim Biophys Acta - Mol Cell Res. 2009;1793(6):933–40.

127. Hwang JR, Byeon Y, Kim D, Park SG. Recent insights of T cell receptor-mediated signaling pathways for T cell activation and development. Exp Mol Med. 2020;52(5):750–61.

128. Liu X, Ning J, Liu X, Chan WC. Mutations Affecting Genes in the Proximal T-Cell Receptor Signaling Pathway in Peripheral T-Cell Lymphoma. Cancers (Basel). 2022;14(15):1–19.

129. Debackere K, Marcelis L, Demeyer S, Vanden Bempt M, Mentens N, Gielen O, et al. Fusion transcripts FYN-TRAF3IP2 and KHDRBS1-LCK hijack T cell receptor signaling in peripheral T-cell lymphoma, not otherwise specified. Nat Commun. 2021;12(1).

130. Moon CS, Reglero C, Cortes JR, Quinn SA, Alvarez S, Zhao J, et al. FYN–TRAF3IP2 induces NF-κB signaling-driven peripheral T-cell lymphoma. Nat Cancer. 2021;2(1):98–113.

131. De Keersmaecker K, Porcu M, Cox L, Girardi T, Vandepoel R, De Beeck JO, et al. NUP214-ABL1-mediated cell proliferation in T-cell acute lymphoblastic leukemia is dependent on the LCK kinase and various interacting proteins. Haematologica. 2014;99(1):85–93.

132. Boddicker RL, Razidlo GL, Dasari S, Zeng Y, Hu G, Knudson RA, et al. Integrated mate-pair and RNA sequencing identifies novel, targetable gene fusions in peripheral T-cell lymphoma. Blood. 2016 Sep 1;128(9):1234–45.

133. Abate F, Da Silva-Almeida AC, Zairis S, Robles-Valero J, Couronne L, Khiabanian H, et al. Activating mutations and translocations in the guanine exchange factor VAV1 in peripheral T-cell lymphomas. Proc Natl Acad Sci U S A. 2017;114(4):764–9.

134. Watatani Y, Sato Y, Miyoshi H, Sakamoto K, Nishida K, Gion Y, et al. Molecular heterogeneity in peripheral T-cell lymphoma, not otherwise specified revealed by comprehensive genetic profiling. Leukemia. 2019;33(12):2867–83.

135. Fujisawa M, Sakata-Yanagimoto M, Nishizawa S, Komori D, Gershon P, Kiryu M, et al. Activation of RHOA-VAV1 signaling in angioimmunoblastic T-cell lymphoma. Leukemia. 2018;32(3):694–702.

136. Cortes JR, Filip I, Albero R, Patiño-Galindo JA, Quinn SA, Lin WHW, et al. Oncogenic Vav1-Myo1f induces therapeutically targetable macrophage-rich tumor microenvironment in peripheral T cell lymphoma. Cell Rep. 2022;39(3).

137. Yu DD, Zhang J. Update on recurrent mutations in angioimmunoblastic T-cell lymphoma. Int J Clin Exp Pathol. 2021;14(12):1108.

138. Huang Y, Moreau A, Dupuis J, Streubel B, Petit B, Gouill S Le, et al. Peripheral T-cell lymphomas with a follicular growth pattern are derived from follicular helper T cells (TFH) and may show overlapping features with angioimmunoblastic T-cell lymphomas. Am J Surg Pathol. 2009;33(5):682–90.

139. Timmins MA, Wagner SD, Ahearne MJ. The new biology of PTCL-NOS and AITL: current status and future clinical impact. Br J Haematol. 2020;189(1):54–66.

140. Pechloff K, Holch J, Ferch U, Schweneker M, Brunner K, Kremer M, et al. The fusion kinase ITK-SYK mimics a T cell receptor signal and drives oncogenesis in conditional mouse models of peripheral T cell lymphoma. J Exp Med. 2010;207(5):1031–44.

141. Kataoka K, Nagata Y, Kitanaka A, Shiraishi Y, Shimamura T, Yasunaga JI, et al. Integrated molecular analysis of adult T cell leukemia/lymphoma. Nat Genet. 2015;47(11):1304–15.

142. Bongiovanni D, Saccomani V, Piovan E. Aberrant signaling pathways in t-cell acute lymphoblastic leukemia. Int J Mol Sci. 2017;18(9):1–29.

143. Thorpe LM, Yuzugullu H, Zhao JJ. PI3K in cancer: divergent roles of isoforms, modes of. Nat Rev Cca. 2015;15(1):7–24.

144. Chinen Y, Kuroda J, Shimura Y, Nagoshi H, Kiyota M, Yamamoto-Sugitani M, et al. Phosphoinositide protein kinase PDPK1 is a crucial cell signaling mediator in multiple myeloma. Cancer Res. 2014;74(24):7418–29.

145. Brammer JE, Zinzani PL, Zain J, Mead M, Casulo C, Jacobsen ED, et al. Duvelisib in Patients with Relapsed/Refractory Peripheral T-Cell Lymphoma from the Phase 2 Primo Trial: Results of an Interim Analysis. Blood. 2021;138:2456.

146. Magni M, Biancon G, Rizzitano S, Cavanè A, Paolizzi C, Dugo M, et al. Tyrosine kinase inhibition to improve anthracycline-based chemotherapy efficacy in T-cell lymphoma. Br J Cancer. 2019;121(7):567–77.

147. Wieduwilt MJ. Ph+ ALL in 2022: is there an optimal approach? Hematology. 2022 Dec 9;2022(1):206–12.

148. Crombet O, Lastrapes K, Zieske A, Morales-Arias J. Complete morphologic and molecular remission after introduction of dasatinib in the treatment of a pediatric patient with t-cell acute lymphoblastic leukemia and ABL1 amplification†. Pediatr Blood Cancer. 2012;59(2):333–4.

149. Soverini S, Colarossi S, Gnani A, Castagnetti F, Rosti G, Bosi C, et al. Resistance to dasatinib in Philadelphia-positive leukemia patients and the presence or the selection of mutations at residues 315 and 317 in the BCR-ABL kinase domain. Haematologica. 2007;92(3):401–4.

150. Wöhrle FU, Halbach S, Aumann K, Schwemmers S, Braun S, Auberger P, et al. Gab2 signaling in chronic myeloid leukemia cells confers resistance to multiple Bcr-Abl inhibitors. Leukemia. 2013;27(1):118–29.

151. Laukkanen S, Veloso A, Yan C, Oksa L, Alpert EJ, Do D, et al. Therapeutic targeting of LCK tyrosine kinase and mTOR signaling in T-cell acute lymphoblastic leukemia. Blood. 2022;140(17):1891–906.

152. Liu Y, Wang X, Deng L, Ping L, Shi Y, Zheng W, et al. ITK inhibition induced in vitro and in vivo anti-tumor activity through downregulating TCR signaling pathway in malignant T cell lymphoma. Cancer Cell Int. 2019;19(1):1–19.

153. Wang T, Lu Y, Polk A, Chowdhury P, Zamalloa CM, Suemori K, et al. T-cell receptor signalling activates an ITK/NF-κB/GATA-3 axis in T-cell lymphomas facilitating resistance to chemotherapy. 2017;23(10):2506–15.

154. Horwitz SM, Feldman TA, Hess BT, Khodadoust MS, Kim YH, Munoz J, et al. The Novel SYK/JAK Inhibitor Cerdulatinib Demonstrates Good Tolerability and Clinical Response in a Phase 2a Study in Relapsed/Refractory Peripheral T-Cell Lymphoma and Cutaneous T-Cell Lymphoma. Blood. 2018 Nov 29;132(Supplement 1):1001.

155. Chan AC, Irving BA, Fraser JD, Weiss A. The ζ chain is associated with a tyrosine kinase and upon T-cell antigen receptor stimulation associates with ZAP-70, a 70-kDa tyrosine phosphoprotein. Proc Natl Acad Sci U S A. 1991;88(20):9166–70.

156. Chan AC, Iwashima M, Turck CW, Weiss A. ZAP-70: A 70 kd protein-tyrosine kinase that associates with the TCR ζ chain. Cell. 1992;71(4):649–62.

157. Vivier E, da Silva AJ, Ackerly M, VivierOovo E, da SilvaovA AJ, Ackerly M, et al. Association of a 70-kDa tyrosine phosphoprotein with the CD16: c: y complex expressed in human natural killer cells* Division Of “hmor 1mmuno10gy9 Dana-Farber Cancer Institute, and Departments Of Patholow” and. Eur J Immunol. 1993;23:1872–6.

158. Crespo M, Villamor N, Giné E, Muntañola A, Colomer D, Marafioti T, et al. ZAP-70 expression in normal Pro/Pre B cells, mature B cells, and in B-cell acute lymphoblastic leukemia. Clin Cancer Res. 2006;12(3 I):726–34.

159. Chan AC. Syk Family of Protein Tyrosine Kinases. 2004;4:139–45.

160. Ashouri JF, Lo WL, Nguyen TTT, Shen L, Weiss A. ZAP70, too little, too much can lead to autoimmunity. Immunol Rev. 2022;307(1):145–60.

161. Zhao Q, Williams BL, Abraham RT, Weiss A. Interdomain B in ZAP-70 Regulates but Is Not Required for ZAP-70 Signaling Function in Lymphocytes. Mol Cell Biol. 1999;19(1):948–56.

162. Kaur M, Singh M, Silakari O. Insight into the therapeutic aspects of ' Zeta-Chain Associated Protein Kinase 70 kDa ' inhibitors : A review. Cell Signal. 2014;26(11):2481–92.

163. Katz ZB, Blount A, Biophotonics WA, Jolla L. A cycle of ZAP70 kinase activation and release from the TCR amplifies and disperses Antigenic Stimuli. Nat Immunol. 2017;18(1):86–95.

164. Rao N, Lupher ML, Ota S, Reedquist KA, Druker BJ, Band H. The Linker Phosphorylation Site Tyr292 Mediates the Negative Regulatory Effect of Cbl on ZAP-70 in T Cells. J Immunol. 2000;164(9):4616–26.

165. Mège D, Di Bartolo V, Germain V, Tuosto L, Michel F, Acuto O. Mutation of tyrosines 492/493 in the kinase domain of ZAP-70 affects multiple T-cell receptor signaling pathway. J Biol Chem. 1996;271(51):32644–52.

166. Wang H, Kadlecek TA, Au-Yeung BB, Goodfellow HES, Hsu LY, Freedman TS, et al. ZAP-70: an essential kinase in T-cell signaling. Cold Spring Harb Perspect Biol. 2010;2(5):1–17.

167. Cheng AM, Negishi I, Anderson SJ, Chan AC, Bolen J, Loh DY, et al. The Syk and ZAP-70 SH2-containing tyrosine kinases are implicated in pre-T cell receptor signaling. Proc Natl Acad Sci U S A. 1997;94(18):9797–801.

168. Palacios EH, Weiss A. Distinct roles for Syk and ZAP-70 during early thymocyte development. J Exp Med. 2007;204(7):1703–15.

169. Chan AC, Van Oers NS, Tran A, Turka L, Law C, Ryan J, et al. Differential expression of ZAP-70 and Syk protein tyrosine kinases, and the role of this family of protein tyrosine kianses in TCR signaling. J Immunol. 1994;152(10):4758–66.

170. Carreras J, Villamor N, Colomo L, Moreno C, Ramón y Cajal S, Crespo M, et al. Immunohistochemical analysis of ZAP-70 expression in B-cell lymphoid neoplasms. J Pathol. 2005;205(4):507–13.

171. Chen J, Moore A, Ringshausen I. ZAP-70 Shapes the Immune Microenvironment in B Cell Malignancies. Front Oncol. 2020;10(October):1–8.

172. Bosch F, Dalla-Favera R. Chronic lymphocytic leukaemia: from genetics to treatment. Nat Rev Clin Oncol. 2019;16(11):684–701.

173. Hamblin TJ, Davis Z, Gardiner A, Oscier DG, Stevenson FK. Unmutated Ig VH Genes Are Associated With a More Aggressive Form of Chronic Lymphocytic Leukemia. Blood. 1999 Sep 15;94(6):1848–54.

174. Crespo M, Bosch F, Villamor N, Bellosillo B, Colomer D, Rozman M, et al. ZAP-70 Expression as a Surrogate for Immunoglobulin-Variable-Region Mutations in Chronic Lymphocytic Leukemia. N Engl J Med. 2003;348(18):1764–75.

175. Wiestner A, Rosenwald A, Barry TS, Wright G, Davis RE, Henrickson SE, et al. ZAP-70 expression identifies a chronic lymphocytic leukemia subtype with unmutated immunoglobulin genes, inferior clinical outcome, and distinct gene expression profile. Blood. 2003;101(12):4944–51.

176. Chen L, Widhopf G, Huynh L, Rassenti L, Rai KR, Weiss A, et al. Expression of ZAP-70 is associated with increased B-cell receptor signaling in chronic lymphocytic leukemia. Blood. 2002;100(13):4609–14.

177. Gobessi S, Laurenti L, Longo PG, Sica S, Leone G, Efremov DG. ZAP-70 enhances B-cell-receptor signaling despite absent or inefficient tyrosine kinase activation in chronic lymphocytic leukemia and lymphoma B cells. Blood. 2007;109(5):2032–9.

178. Chen L, Huynh L, Apgar J, Tang L, Rassenti L, Weiss A, et al. ZAP-70 enhances IgM signaling independent of its kinase activity in chronic lymphocytic leukemia. Blood. 2008;111(5):2685–92.

179. Richardson SJ, Matthews C, Catherwood MA, Alexander HD, Carey BS, Farrugia J, et al. ZAP-70 expression is associated with enhanced ability to respond to migratory and survival signals in B-cell chronic lymphocytic leukemia (B-CLL). Blood. 2006;107(9):3584–92.

180. Calpe E, Codony C, Baptista MJ, Abrisqueta P, Carpio C, Purroy N, et al. ZAP-70 enhances migration of malignant B lymphocytes toward CCL21 by inducing CCR7 expression via IgM-ERK1/2 activation. Blood. 2011;118(16):4401–10.

181. Chen J, Sathiaseelan V, Moore A, Tan S, Chilamakuri CSR, Roamio Franklin VN, et al. ZAP-70 constitutively regulates gene expression and protein synthesis in chronic lymphocytic leukemia. Blood. 2021;137(26):3629–40.

182. Sadras T, Martin M, Kume K, Robinson ME, Saravanakumar S, Lenz G, et al. Developmental partitioning of SYK and ZAP70 prevents autoimmunity and cancer. Mol Cell. 2021;81(10):2094–111.

183. Bonzheim I, Geissinger E, Roth S, Zettl A, Marx A, Rosenwald A, et al. Anaplastic large cell lymphomas lack the expression of T-cell receptor molecules or molecules of proximal T-cell receptor signaling. Blood. 2004;104(10):3358–60.

184. Bisig B, de Reyniès A, Bonnet C, Sujobert P, Rickman DS, Marafioti T, et al. CD30-positive peripheral T-cell lymphomas share molecular and phenotypic features. Haematologica. 2013;98(8):1250–8.

185. Rodriguez-Pinilla SM, Sanchez MEC, Rodriguez J, Garcia JF, Sanchez-Espiridion B, Lamana LF, et al. Loss of TCR-beta F1 and/or EZRIN expression is associated with unfavorable prognosis in nodal peripheral T-cell lymphomas. Blood Cancer J. 2013;3(4).

186. Warner K, Weit N, Crispatzu G, Admirand J, Jones D, Herling M. T-cell receptor signaling in peripheral T-cell lymphoma - A review of patterns of alterations in a central growth regulatory pathway. Curr Hematol Malig Rep. 2013;8(3):163–72.

187. Liu Y, Ding N, Wang X, Deng L, Ping L, Shi Y, et al. The Intracellular TCR Signaling Pathway As a Novel Therapeutic Target in AITL Patients. Blood. 2017;130(Suplement 1):1461.

188. de Mel S, Mustafa N, Selvarajan V, Azaman MI, Jaynes PW, Venguidessane S, et al. T and NK cell lymphoma cell lines do not rely on ZAP-70 for survival. PLoS One. 2022;17(1 1).

189. Rao D, Li H, Ren X, Sun Y, A CW, Zheng M, et al. Discovery of a potent, selective, and covalent ZAP-70 kinase inhibitor. Eurpean J Med Chem. 2021;219:113393.

190. Rao D, Yang T, Feng H, An Q, Zhang S, Yu J, et al. Discovery and Structural Optimization of Covalent ZAP-70 Kinase inhibitors against Psoriasis. J Med Chem. 2023;Online ahead of print.

191. Visperas PR, Wilson CG, Winger JA, Yan Q, Lin K, Arkin MR, et al. Identification of inhibitors of the association of ZAP-70 with the T cell receptor by high-throughput screen. SLAS Discov. 2017;22(3):324–31.

192. Levin SE, Zhang C, Kadlecek TA, Shokat KM, Weiss A. Inhibition of ZAP-70 kinase activity via an analog-sensitive allele blocks T cell receptor and CD28 superagonist signaling. J Biol Chem. 2008;283(22):15419–30.

193. Wong NML, Wong WW. Engineering a Dual Small Molecule Gated ZAP70 Switch in T Cells. ACS Synth Biol. 2018;7(4):969–77.

194. Krimbrel EA, Davis TN, Bradner JE, Kung AL. In vivo pharmacodynamic imaging of proteasome inhibition. Mol Imaging. 2009;8(3):140–7.

195. Dull T, Zufferey R, Kelly M, Mandel RJ, Nguyen M, Trono D, et al. A Third-Generation Lentivirus Vector with a Conditional Packaging System. J Virol. 1998;72(11):8463–71.

196. OECD. OECD Publishing. 2002. Test No. 420: Acute Oral Toxicity - Fixed Dose Procedure, OECD Guidelines for the Testing of Chemicals, Section 4.

197. Dobin A, Davis CA, Schlesinger F, Drenkow J, Zaleski C, Jha S, et al. STAR: ultrafast universal RNA-seq aligner. Bioinformatics. 2013;29(1):15–21.

198. Li B, Dewey CN. RSEM: accurate transcript quantification from RNA-Seq data with or without a reference genome. BMC Bioinformatics. 2011;12:323.

199. Ritchie ME, Phipson B, Wu D, Hu Y, Law CW, Shi W, et al. Limma powers differential expression analyses for RNA-sequencing and microarray studies. Nucleic Acids Res. 2015;43(7):e47.

200. Robinson MD, Oshlack A. A scaling normalization method for differential expression analysis of RNA-seq data. Genome Biol. 2010;11(3):R25.

201. Korotkevich G, Sukhov V, Budin N, Shpak B, Artyomov MN, Sergushichev A. Fast gene set enrichment analysis. 2021;

202. Gillespie M, Jassal B, Stephan R, Milacic M, Rothfels K, Senff-Ribeiro A, et al. The reactome pathway knowledgebase 2022. Nucleic Acids Res. 2022;50(D1):D687–92.

203. Kumar A, Bhagat KK, Singh AK, Singh H, Angre T, Verma A, et al. Medicinal chemistry perspective of pyrido[2,3-d]pyrimidines as anticancer agents. RSC Adv. 2023;13(10):6872–908.

204. Puig De La Bellacasa R, Roué G, Balsas P, Pérez-Galán P, Teixidó J, Colomer D, et al. 4-Amino-2-arylamino-6-(2,6-dichlorophenyl)-pyrido[2,3- d]pyrimidin-7-(8 H)-ones as BCR kinase inhibitors for B lymphoid malignancies. Eur J Med Chem. 2014;86:664–75.

205. Jin L, Pluskey S, Petrella EC, Cantin SM, Gorga JC, Rynkiewicz MJ, et al. The three-dimensional structure of the ZAP-70 kinase domain in complex with staurosporine: Implications for the design of selective inhibitors. J Biol Chem. 2004;279(41):42818–25.

206. Masip V, Lirio Á, Sánchez-López A, Cuenca AB, de la Bellacasa RP, Abrisqueta P, et al. Expanding the Diversity at the C-4 Position of Pyrido[2,3-d]pyrimidin-7(8H)-ones to Achieve Biological Activity against ZAP-70. Pharmaceuticals. 2021;14(12).

207. Gordon LI, Karmali R, Kaplan JB, Popat R, Burris HA, Ferrari S, et al. Spleen tyrosine kinase/FMS-Like tyrosine kinase-3 inhibition in relapsed/refractory B-cell lymphoma, including diffuse large B-cell lymphoma: updated data with mivavotinib (TAK-659/ CB-659. Oncotarget. 2023;14(1):57–70.

208. Pratz KW, Kaplan J, Levy M, Bixby D, Burke PW, Erba H, et al. A phase Ib trial of mivavotinib (TAK-659), a dual SYK/FLT3 inhibitor, in patients with relapsed/refractory acute myeloid leukemia. Haematologica. 2023;108(3):705–16.

209. Abbas HA, Wierda WG. Acalabrutinib: A Selective Bruton Tyrosine Kinase Inhibitor for the Treatment of B-Cell Malignancies. Front Oncol. 2021;11(May).

210. Shirley M. Bruton Tyrosine Kinase Inhibitors in B-Cell Malignancies: Their Use and Differential Features. Target Oncol. 2022;17(1):69–84.

211. Dubovsky JA, Beckwith KA, Natarajan G, Woyach JA, Jaglowski S, Zhong Y, et al. Ibrutinib is an irreversible molecular inhibitor of ITK driving a Th1-selective pressure in T lymphocytes. Blood. 2013;122(15):2539–49.

212. Herman SEM, Montraveta A, Niemann CU, Mora-Jensen H, Gulrajani M, Krantz F, et al. The Bruton Tyrosine Kinase (BTK) Inhibitor Acalabrutinib Demonstrates Potent On-Target Effects and Efficacy in Two Mouse Models of Chronic Lymphocytic Leukemia. Clin Cancer Res. 2017;23(11):2831–41.

213. Zheng W, Medeiros JL, Young KH, Goswami M, Powers L, Kantarjian HH, et al. CD30 Expression in Acute Lymphoblastic Leukemia as Assessed by Flow Cytometry Analysis. Leuk Lymphoma. 2014;55(3):624–7.

214. Griffith CE, Zhang W, Wange RL. ZAP-70-dependent and -independent activation of Erk in Jurkat T cells: Differences in signaling induced by H2O2 and CD3 cross-linking. J Biol Chem. 1998;273(17):10771–6.

215. Shan X, Balakir R, Criado G, Wood JS, Seminario MC, Madrenas J, et al. ZAP-70-Independent Ca 2+ Mobilization and Erk Activation in Jurkat T Cells in Response to T-Cell Antigen Receptor Ligation . Mol Cell Biol. 2001;21(21):7137–49.

216. Marcos-Jiménez A, Carvoeiro DC, Ruef N, Cuesta-Mateos C, Roy-Vallejo E, Gómez-García de Soria V, et al. Dasatinib-induced spleen contraction leads to transient lymphocytosis. Blood Adv. 2023;7(11):2418–30.

217. Muqbil I, Chaker M, Aboukameel A, Mohammad RM, Azmi AS, Ramchandren R. Pre-clinical anti-tumor activity of Bruton's Tyrosine Kinase inhibitor in Hodgkin's Lymphoma cellular and subcutaneous tumor model. Heliyon. 2019;5(8):e02290.

218. Cayrol F, Praditsuktavorn P, Fernando TM, Kwiatkowski N, Marullo R, Calvo-Vidal MN, et al. THZ1 targeting CDK7 suppresses STAT transcriptional activity and sensitizes T-cell lymphomas to BCL2 inhibitors. Nat Commun. 2017;8(May 2016):1–11.

219. Mezencev R, Mcdonald JF. Subcutaneous xenografts of Human T-Lineage Acute Lymphoblastic Leukemia Jurkat Cells in Nude Mice. In Vivo (Brooklyn). 2011;25:603–8.

220. Gill RPK, Gantchev J, Villarreal AM, Ramchatesingh B, Netchiporouk E, Akilov OE, et al. Understanding Cell Lines, Patient-Derived Xenograft and Genetically Engineered Mouse Models Used to Study Cutaneous T-Cell Lymphoma. Cells. 2022;11(4):593.

221. Kanaji N, Tadokoro A, Susaki K, Yokokura S, Ohmichi K, Haba R, et al. Higher susceptibility of NOD / LtSz- scid Il2rg - / - NSG mice to xenotransplanted lung cancer cell lines. Cancer Manag Res. 2014;6:431–6.

222. Chen KH, Wada M, Firor AE, Pinz KG, Jares A, Liu H, et al. Novel anti-CD3 chimeric antigen receptor targeting of aggressive T cell malignancies. Oncotarget. 2016;7:56219–32.

223. Wilcox RA. A three-signal model of T-cell lymphoma pathogenesis. Am J Hematol. 2016;91(1):113–22.

224. Wilcox RA, Sun DX, Novak A, Dogan A, Ansell SM, Feldman AL. Inhibition of Syk protein tyrosine kinase induces apoptosis and blocks proliferation in T-cell non-Hodgkin lymphoma cell lines. Leukemia. 2010;24(1):229–32.

225. Horwitz SM, Koch R, Porcu P, Oki Y, Moskowitz A, Perez M, et al. Activity of the PI3K-δ,γ inhibitor duvelisib in a phase 1 trial and preclinical models of T-cell lymphoma. Blood. 2018;131(8):888–98.

226. Querfeld C, Rizvi MA, Kuzel TM, Guitart J, Rademaker A, Sabharwal SS, et al. The selective protein kinase C β inhibitor enzastaurin induces apoptosis in cutaneous T-cell lymphoma cell lines through the AKT pathway. J Invest Dermatol. 2006;126(7):1641–7.

227. Gangopadhyay K, Manna B, Roy S, Kumari S, Debnath O, Chowdhury S, et al. An allosteric hot spot in the tandem-SH2 domain of ZAP-70 regulates T-cell signaling. Biochem J. 2020;477(7):1287–308.

228. Lam B, Arikawa Y, Cramlett J, Dong Q, Jong R De, Feher V, et al. Discovery of TAK-659 an Orally Available Investigational Inhibitor of Spleen Tyrosine Kinase (SYK). Bioorganic Med Chem Lett. 2016;26(24):5947–50.

229. Balsas P, Esteve-Arenys A, Roldán J, Jiménez L, Rodríguez V, Valero JG, et al. Activity of the novel BCR kinase inhibitor IQS019 in preclinical models of B-cell non-Hodgkin lymphoma. J Hematol Oncol. 2017;10(1):1–14.

230. Perley JP, Mikolajczak J, Harrison ML, Buzzard GT, Rundell AE. Multiple Model-Informed Open-Loop Control of Uncertain Intracellular Signaling Dynamics. PLoS Comput Biol. 2014;10(4).

231. Schubbert S, Shannon K, Bollag G. Hyperactive Ras in developmental disorders and cancer. Nat Rev Cancer. 2007;7(4):295–308.

232. Coffer PJ, Jin J, Woodgett JR. Protein kinase B (c-Akt): a multifunctional mediator of phosphatidylinositol 3-kinase activation. Biochem J. 1998;335:1–13.

233. Genot EM, Arrieumerlou C, Ku G, Burgering BMT, Weiss A, Kramer IM. The T-Cell Receptor Regulates Akt (Protein Kinase B) via a Pathway Involving Rac1 and Phosphatidylinositide 3-Kinase. Mol Cell Biol. 2000;20(15):5469–78.

234. Fillmore GC, Wang Q, Carey MJ, Kim CH, Elenitoba-Johnson KSJ, Lim MS. Expression of Akt (protein kinase B) and its isoforms in malignant lymphomas. Leuk Lymphoma. 2005;46(12):1765–73.

235. Bhatt HD, McClain SA, Lee HM, Zimmerman T, Deng J, Johnson F, et al. The Maximum-Tolerated Dose and Pharmacokinetics of a Novel Chemically Modified Curcumin in Rats. J Exp Pharmacol. 2022;14(January):73–85.

10. Appendix

Appendix Table 1. Kinase inhibition profile of ZAP-70 inhibitor candidates and commercial drugs (Ibrutinib, Acalabrutinib and TAK-659) determined by measuring residual kinase activity (%) at a concentration of 10 µM of each candidate against a panel of 26 kinases.

Compound ID	IQS117	IQS123	IQS129	IQS134	IQS135	IQS138
AKT1 aa106-480	101 ± 17.2	83 ± 9.7	82 ± 10.5	83 ± 4.5	93 ± 16.4	84 ± 3.3
AKT2 aa107-481	76 ± 4.4	75 ± 5.9	76 ± 5.9	75 ± 2.4	78 ± 2.1	82 ± 3.1
AKT3 aa106-479	102 ± 2.4	91 ± 0.6	94 ± 7	91 ± 2.2	95 ± 1.1	94 ± 9.4
BRAF	80 ± 5.9	83 ± 8.3	117 ± 1.4	99 ± 12.7	104 ± 11.5	97 ± 11.9
BTK	32 ± 1	65 ± 6.4	30 ± 0	41 ± 1.8	43 ± 2.5	60 ± 6.5
CHK1	96 ± 5.4	90 ± 2.3	91 ± 4.2	90 ± 5.2	87 ± 7.1	87 ± 7.2
CHK2	70 ± 1.9	78 ± 8	91 ± 6.2	87 ± 6.4	90 ± 7.1	9013.1
CSF1R	59 ± 6.3	79 ± 13.5	52 ± 5.6	58 ± 3.5	75 ± 19.9	57 ± 1.9
FLT3	96 ± 2.8	82 ± 8.4	72 ± 0.3	71 ± 0.6	71 ± 5.2	84 ± 8.8
FYN	54 ± 6.1	71 ± 9.8	62 ± 1.1	68 ± 6.7	68 ± 3.6	68 ± 1.2
IRAK4	57 ± 3	75 ± 4.3	75 ± 8.9	81 ± 11.1	78 ± 12.7	77 ± 14.2
ITK	51 ± 0.5	73 ± 2.1	66 ± 2.1	67 ± 3.7	68 ± 6.1	65 ± 1.6
JAK3	84 ± 2.1	74 ± 5.8	83 ± 0.5	88 ± 2.3	80 ± 4.6	102 ± 8.4
JNK3	92 ± 20.6	84 ± 23.2	103 ± 11.3	97 ± 15.3	96 ± 16.8	96 ± 12.2
LCK	49 ± 3	45 ± 3.4	48 ± 1.3	60 ± 4.9	64 ± 2.7	102 ± 5.1
LYN	30 ± 7.5	69 ± 0.2	43 ± 3.6	41 ± 3.5	57 ± 3.7	81 ± 7.4
MAP4K2	84 ± 0.4	79 ± 3.9	84 ± 2.3	91 ± 8.5	84 ± 0.4	95 ± 6.6
MAP4K5	89 ± 1	95 ± 5.5	90 ± 3.3	91 ± 3.4	88 ± 3.6	95 ± 7.5
MET	101 ± 12.5	90 ± 4.4	88 ± 13.5	91 ± 3.5	84 ± 2.8	91 ± 3.7
SRC	80 ± 5	82 ± 3	48 ± 2	61 ± 1.8	66 ± 5.7	77 ± 16.5
SYK	62 ± 3.3	81 ± 5	48 ± 2.1	64 ± 6.7	56 ± 5.6	80 ± 17.3
VEGFR1	94 ± 1.3	80 ± 4.4	71 ± 8.1	68 ± 1.4	75 ± 3.2	89 ± 7.3
VEGFR2	107 ± 13.8	77 ± 5.9	42 ± 1.6	62 ± 1.6	56 ± 2.9	90 ± 32
VEGFR3	90 ± 0.7	83 ± 7.5	63 ± 9.6	72 ± 2.4	72 ± 2.1	83 ± 7.7
YES	41 ± 2.1	75 ± 5.1	49 ± 1.6	73 ± 20.9	53 ± 1.3	74 ± 6.1
ZAP70	17 ± 1.6	83 ± 2.9	40 ± 5	49 ± 3.7	65 ± 7.3	70 ± 11.3

Kinase residual activity (%)

	≤ 20%		> 20% ≤ 50%		> 50%

Compound ID	IQS139	IQS141	IQS142	IQS143	IQS144	IQS145
AKT1 aa106-480	88 ± 17.9	95 ± 0.5	97 ± 5.3	97 ± 6.2	92 ± 10.1	87 ± 6.9
AKT2 aa107-481	82 ± 4.6	73 ± 9.2	77 ± 14.4	77 ± 11.5	76 ± 5.6	84 ± 4.3
AKT3 aa106-479	91 ± 1.7	97 ± 11.4	96 ± 9	90 ± 7.5	92 ± 9.4	98 ± 10.2
BRAF	123 ± 36	80 ± 6.2	77 ± 3.9	90 ± 17.7	89 ± 10	98 ± 6.6
BTK	72 ± 8.4	24 ± 5	82 ± 7.8	91 ± 11.9	43 ± 0.9	78 ± 22
CHK1	93 ± 4	85 ± 2.9	93 ± 4.3	93 ± 11.9	86 ± 5.8	90 ± 9.8
CHK2	87 ± 3.4	69 ± 1.1	84 ± 10.3	94 ± 2	90 ± 1.6	94 ± 7.8
CSF1R	60 ± 6	44 ± 12.2	77 ± 11.1	60 ± 7.7	57 ± 5	75 ± 31.7
FLT3	94 ± 8.9	66 ± 5.8	78 ± 2.7	78 ± 8	73 ± 4.9	81 ± 0.1
FYN	69 ± 7.5	45 ± 7.2	105 ± 9.8	84 ± 18.4	71 ± 16.2	74 ± 5.5
IRAK4	79 ± 2.9	82 ± 24.3	93 ± 16.5	83 ± 4.7	80 ± 15.7	94 ± 12
ITK	69 ± 9.4	51 ± 3.4	86 ± 6.5	86 ± 6.6	75 ± 6.3	85 ± 27.3
JAK3	98 ± 8.8	78 ± 4.7	94 ± 3.2	97 ± 10.8	91 ± 7.5	100 ± 11.8
JNK3	95 ± 9.6	71 ± 8.2	76 ± 4.4	88 ± 13.2	95 ± 10.4	93 ± 5.1
LCK	85 ± 7	48 ± 4.7	91 ± 11.1	94 ± 4.2	58 ± 5.1	101 ± 4.2
LYN	69 ± 9.3	34 ± 6.8	92 ± 10.8	71 ± 8.6	55 ± 10.1	91 ± 12.1
MAP4K2	110 ± 13.4	77 ± 3	91 ± 7.3	91 ± 8.7	98 ± 1.2	93 ± 4.1
MAP4K5	92 ± 3.5	95 ± 4.1	101 ± 1.3	95 ± 2.8	94 ± 2.8	94 ± 5.8
MET	106 ± 5.1	81 ± 6.1	102 ± 3.1	96 ± 12.7	89 ± 7.4	87 ± 8.8
SRC	67 ± 6.4	51 ± 8.6	87 ± 22.6	85 ± 6	67 ± 4.2	81 ± 15.6
SYK	77 ± 12.4	41 ± 9.2	85 ± 10.7	92 ± 8.7	66 ± 10.1	80 ± 7.2
VEGFR1	86 ± 9.7	59 ± 3	90 ± 16	94 ± 12	98 ± 39.7	86 ± 9
VEGFR2	83 ± 13.8	58 ± 6	83 ± 9.2	85 ± 10.1	75 ± 5.3	88 ± 0.9
VEGFR3	82 ± 9	62 ± 9	84 ± 16.5	82 ± 10	77 ± 0.1	85 ± 3
YES	76 ± 20.7	58 ± 0.8	77 ± 0.1	89 ± 9.5	76 ± 13.2	64 ± 10.2
ZAP70	70 ± 31.2	11 ± 0.5	69 ± 17.1	87 ± 13.3	50 ± 2.7	65 ± 0.3

Kinase residual activity (%)

	≤ 20%		> 20% ≤ 50%		> 50%

Compound ID	IQS146	IQS147	IQS148	IQS149	IQS150	IQS151
AKT1 aa106-480	105 ± 22.5	92 ± 6.1	99 ± 1.3	97 ± 1.9	115 ± 25.9	91 ± 0.1
AKT2 aa107-481	91 ± 6.3	93 ± 10.7	78 ± 9.7	79 ± 6.6	75 ± 8.1	75 ± 4
AKT3 aa106-479	86 ± 4.3	105 ± 11.6	90 ± 7.2	86 ± 4.3	94 ± 7.1	85 ± 4.2
BRAF	92 ± 3	100 ± 7.5	75 ± 4.8	73 ± 6.2	68 ± 1.9	85 ± 4.9
BTK	94 ± 4.1	101 ± 7.1	74 ± 8.9	79 ± 1	83 ± 8	34 ± 3.6
CHK1	90 ± 7.1	91 ± 9.4	91 ± 6.5	94 ± 9.4	87 ± 9.2	80 ± 0.5
CHK2	102 ± 0.8	98 ± 12.2	80 ± 7.7	79 ± 1.4	85 ± 7	82 ± 9.6
CSF1R	73 ± 1.5	82 ± 33.3	74 ± 9.2	79 ± 21.3	87 ± 1	54 ± 4.3
FLT3	95 ± 3.8	110 ± 3.2	93 ± 5.9	79 ± 12.1	88 ± 0.7	74 ± 0.8
FYN	82 ± 2.7	79 ± 17.8	73 ± 1.1	80 ± 12.4	93 ± 32.2	64 ± 13.4
IRAK4	93 ± 12.5	98 ± 10.9	82 ± 1.8	78 ± 12.7	83 ± 6.1	100 ± 2.1
ITK	84 ± 5.2	85 ± 17.9	80 ± 6.9	85 ± 7.6	90 ± 2.1	66 ± 3.1
JAK3	101 ± 18.9	102 ± 8.1	91 ± 13.3	96 ± 19.8	96 ± 15.8	72 ± 11.7
JNK3	89 ± 9.8	95 ± 5.6	69 ± 6.4	70 ± 11.9	80 ± 28.7	93 ± 15.4
LCK	76 ± 10	98 ± 8.7	90 ± 18.1	98 ± 14	96 ± 21	64 ± 6.3
LYN	71 ± 7.4	100 ± 20.6	72 ± 3.6	67 ± 10.7	78 ± 3.9	51 ± 5.4
MAP4K2	92 ± 5	121 ± 7.6	76 ± 4	83 ± 10.1	93 ± 2.5	89 ± 5.2
MAP4K5	89 ± 0.3	102 ± 1.8	98 ± 3.4	95 ± 1.2	97 ± 3.5	92 ± 6.4
MET	92 ± 16.5	107 ± 8.3	102 ± 2.5	88 ± 14.3	99 ± 11.5	94 ± 7.2
SRC	90 ± 12	98 ± 11	85 ± 8.6	81 ± 10.8	87 ± 5.2	63 ± 10.3
SYK	90 ± 0.3	104 ± 9.4	89 ± 5.7	92 ± 3.4	82 ± 5.4	73 ± 11.8
VEGFR1	90 ± 4.4	104 ± 6.7	87 ± 8.8	80 ± 0.9	88 ± 5.3	102 ± 44.4
VEGFR2	89 ± 5.9	101 ± 4.4	94 ± 11.8	84 ± 2.8	79 ± 3	75 ± 7.5
VEGFR3	83 ± 9.7	99 ± 5.5	92 ± 10.1	89 ± 11	83 ± 10.1	74 ± 2.4
YES	98 ± 2.2	111 ± 5.4	82 ± 4.9	94 ± 22.2	79 ± 18.3	57 ± 9.8
ZAP70	84 ± 19	96 ± 5.6	81 ± 5.4	88 ± 5.3	83 ± 9.9	69 ± 1.9

Kinase residual activity (%)

	≤ 20%		> 20% ≤ 50%		> 50%

Compound ID	IQS152	IQS153	IQS154	IQS155	IQS156	IQS157
AKT1 aa106-480	99 ± 4.8	95 ± 3.7	93 ± 5.9	92 ± 4.3	103 ± 4.3	111 ± 25
AKT2 aa107-481	82 ± 4.4	84 ± 9.1	87 ± 5.9	81 ± 7.7	77 ± 6.7	74 ± 5.7
AKT3 aa106-479	93 ± 11	96 ± 6	94 ± 13.5	96 ± 12.7	89 ± 2.5	88 ± 7.8
BRAF	97 ± 0.8	94 ± 1.6	94 ± 8.6	102 ± 7.1	73 ± 9.3	74 ± 4.8
BTK	85 ± 3.2	63 ± 14.6	46 ± 15.8	51 ± 4.6	65 ± 4.9	78 ± 7.1
CHK1	88 ± 4.9	88 ± 7.8	82 ± 6	89 ± 3.4	89 ± 4.9	87 ± 5.9
CHK2	111 ± 1.1	94 ± 0.8	92 ± 3.7	86 ± 3.1	77 ± 4.8	81 ± 1.4
CSF1R	81 ± 21.9	121 ± 0.9	40 ± 0.7	66 ± 1.8	67 ± 2.3	84 ± 7.7
FLT3	92 ± 4.8	95 ± 9.8	83 ± 5.8	105 ± 12.1	97 ± 4.5	81 ± 6.6
FYN	79 ± 11.3	117 ± 8.7	60 ± 1.3	73 ± 4.6	62 ± 2.1	72 ± 4.4
IRAK4	104 ± 13.9	94 ± 6.7	73 ± 3	88 ± 6	86 ± 9.4	90 ± 1.6
ITK	94 ± 8.6	137 ± 6.9	71 ± 5.4	78 ± 6.4	74 ± 1.3	84 ± 11.8
JAK3	98 ± 11	85 ± 2.6	95 ± 2.9	77 ± 10.5	90 ± 10.7	84 ± 5.6
JNK3	86 ± 6.3	88 ± 4	92 ± 6.9	92 ± 8.8	71 ± 6.6	69 ± 5.3
LCK	96 ± 11.6	66 ± 8.4	53 ± 3.2	72 ± 3.7	61 ± 13	80 ± 11.2
LYN	90 ± 11.8	67 ± 5.5	45 ± 11.5	78 ± 13.8	41 ± 9.4	70 ± 10.5
MAP4K2	99 ± 5	104 ± 7.9	91 ± 8.9	107 ± 21.6	74 ± 11.5	81 ± 0.5
MAP4K5	98 ± 3.3	93 ± 2.3	92 ± 3.8	93 ± 3.3	101 ± 0.4	104 ± 0.2
MET	92 ± 15.1	94 ± 14.3	82 ± 2.6	95 ± 6.7	98 ± 8.8	92 ± 6.4
SRC	56 ± 10.9	83 ± 18.3	46 ± 0.7	85 ± 14.7	64 ± 6.5	92 ± 13.4
SYK	77 ± 4.6	68 ± 7	57 ± 8	60 ± 3.3	85 ± 7.6	86 ± 1.6
VEGFR1	97 ± 19.6	99 ± 6	76 ± 4.6	81 ± 4.6	73 ± 2.3	84 ± 9.7
VEGFR2	77 ± 7.2	85 ± 5.4	78 ± 44.6	85 ± 0.6	90 ± 8.6	82 ± 3.5
VEGFR3	80 ± 7.8	83 ± 5.4	62 ± 5.9	77 ± 1.1	79 ± 3.7	80 ± 2.7
YES	91 ± 12.3	58 ± 7	76 ± 14.9	67 ± 5.3	66 ± 9.8	81 ± 4.7
ZAP70	72 ± 28.8	86 ± 5.7	67 ± 5.5	81 ± 0.9	64 ± 9.3	85 ± 3

Kinase residual activity (%)

	≤ 20%		> 20% ≤ 50%		> 50%

Compound ID	IQS158	IQS159	IQS160	Acalabrutinib	Ibrutinib	TAK-659
AKT1 aa106-480	90 ± 5.8	104 ± 18.5	92 ± 0.5	87 ± 0.3	115 ± 6.9	88 ± 16
AKT2 aa107-481	70 ± 9.9	76 ± 7.6	78 ± 8.9	77 ± 1.4	84 ± 14.7	91 ± 4
AKT3 aa106-479	82 ± 12.3	90 ± 10.1	85 ± 5.2	84 ± 7.9	95 ± 8.6	70 ± 8.6
BRAF	76 ± 2.5	97 ± 1.6	83 ± 16.7	73 ± 11.8	31 ± 3.2	94 ± 10.9
BTK	21 ± 2.6	20 ± 1.6	96 ± 13.9	1 ± 0.2	0 ± 1.2	28 ± 0.1
CHK1	79 ± 0.9	87 ± 6.8	87 ± 8.3	85 ± 5.5	99 ± 8.6	5 ± 1.6
CHK2	68 ± 3.8	94 ± 0	102 ± 2.4	95 ± 7.8	70 ± 2.8	12 ± 3.4
CSF1R	47 ± 13.6	86 ± 12.9	76 ± 9.7	75 ± 2.2	50 ± 3	1 ± 0.6
FLT3	66 ± 7.4	87 ± 6.9	81 ± 9.8	89 ± 1.7	20 ± 0.2	7 ± 0.2
FYN	52 ± 6.7	82 ± 14.3	86 ± 17.2	74 ± 8.2	1 ± 0.8	5 ± 0.9
IRAK4	63 ± 10.3	79 ± 6.1	88 ± 4.9	87 ± 3.9	85 ± 12.4	10 ± 0.4
ITK	61 ± 1.8	83 ± 9.2	90 ± 14	87 ± 2	3 ± 1.8	10 ± 1
JAK3	82 ± 2.3	96 ± 10.3	91 ± 1	96 ± 9.7	4 ± 1.4	5 ± 0.3
JNK3	74 ± 19.5	79 ± 0.7	86 ± 7.3	88 ± 4.4	103 ± 8.9	80 ± 9.5
LCK	44 ± 5	89 ± 15.2	92 ± 6.3	50 ± 28	2 ± 0.6	39 ± 1.5
LYN	35 ± 5.9	78 ± 11.6	76 ± 2.2	57 ± 0.7	5 ± 0.9	15 ± 1.5
MAP4K2	79 ± 6.7	91 ± 12.2	89 ± 8.8	85 ± 11.7	132 ± 6.7	15 ± 1.2
MAP4K5	99 ± 0.6	96 ± 7.9	98 ± 1.5	73 ± 2.8	44 ± 0.6	3 ± 0.9
MET	89 ± 11.4	100 ± 6.7	90 ± 7.2	91 ± 10	64 ± 3.1	79 ± 8.1
SRC	39 ± 8.3	91 ± 1.5	83 ± 7.7	59 ± 6.2	6 ± 1.2	17 ± 0.1
SYK	33 ± 7.5	90 ± 10	94 ± 12.4	92 ± 5.3	81 ± 0.8	1 ± 0.1
VEGFR1	64 ± 1.9	84 ± 0.7	93 ± 5.6	82 ± 11	19 ± 0.7	13 ± 1.4
VEGFR2	39 ± 6.7	89 ± 2.5	91 ± 3	64 ± 0.1	7 ± 0.2	5 ± 0.8
VEGFR3	57 ± 3.6	88 ± 6.9	90 ± 0	76 ± 1.9	9 ± 0.8	3 ± 0.1
YES	43 ± 15	84 ± 5.3	102 ± 17.8	50 ± 5.5	1 ± 0.3	25 ± 0.3
ZAP70	23 ± 2.9	92 ± 8.5	93 ± 7.7	95 ± 2	76 ± 0	7 ± 0.6

Kinase residual activity (%)

	≤ 20%		> 20% ≤ 50%		> 50%

Appendix Table 2. Immunophenotypic surface staining of malignant T-cell lines

Cell line (subtype)	Surface Target																			
	TCRαβ	TCRγδ	CD2	CD3	CD4	CD5	CD7	CD8	CD10	CD19	CD25	CD27	CD28	CD30	CD45	CD45RA	CD45RO	CD197	CD279	HLA-DR
Jurkat (T-ALL)	+	-	+	+	+	+	+	-	-	-	-	+	+	+	+	+/-	-	-	-	-
OCI-Ly13.2 (ALK-negative ALCL)	+	-	+	+	-	-	+/-	-	-	-	-	+	+	+	+	+	-	+/-	+	+
OCI-Ly12 (PTCL, NOS)	-	-	+	-	-	-	-	+	-	-	+	-	-	+	+	-	+	+	+/-	+
T8ML-1 (PTCL, NOS)	+	-	+	+	-	-	-	+	-	-	+	-	+	+	+	-	+	+	-	+
SMZ-1 (PTCL, NOS)	-	-	+	-	+	+/-	-	-	-	-	+	+	-	+	+	-	+/-	+	-	+

Appendix Table 3. Immunophenotypic intracellular staining of malignant T-cell lines

Cell line (subtype)	Cytoplasmic Target	
	TCRαβ	CD3
OCI-Ly12 (PTCL, NOS)	+	+
SMZ-1 (PTCL, NOS)	+	+

Appendix Table 4. Short tandem repeat profiles (STR) of malignant T-cell lines. Genetic characterization and STR analysis of malignant T-cell lineage

Cell line (Subtype)		STR profile										
		D5S818	D13S317	D7S820	D16S539	VWA	TH01	AMEL	TPOX	CSF1PO	D21S11	Number of shared alleles (% match)
OCI-Ly13.2 (ALK-negative ALCL)	Expected profile	12,13	17	10	11,13	17	7	X	11	9,1	30, 30.2	18/18 (100%)
	Observed profile	12,13	17	10	11,13	17	7	X	11	9,1	30, 30.2	
T8ML-1 (PTCL, NOS)	Expected profile	13	8,11	12	10,11	16, 17	6,7	X	8,11	12	29,3	18/18 (100%)
	Observed profile	13	8,11	12	10,11	16, 17	6,7	X	8,11	12	29,3	

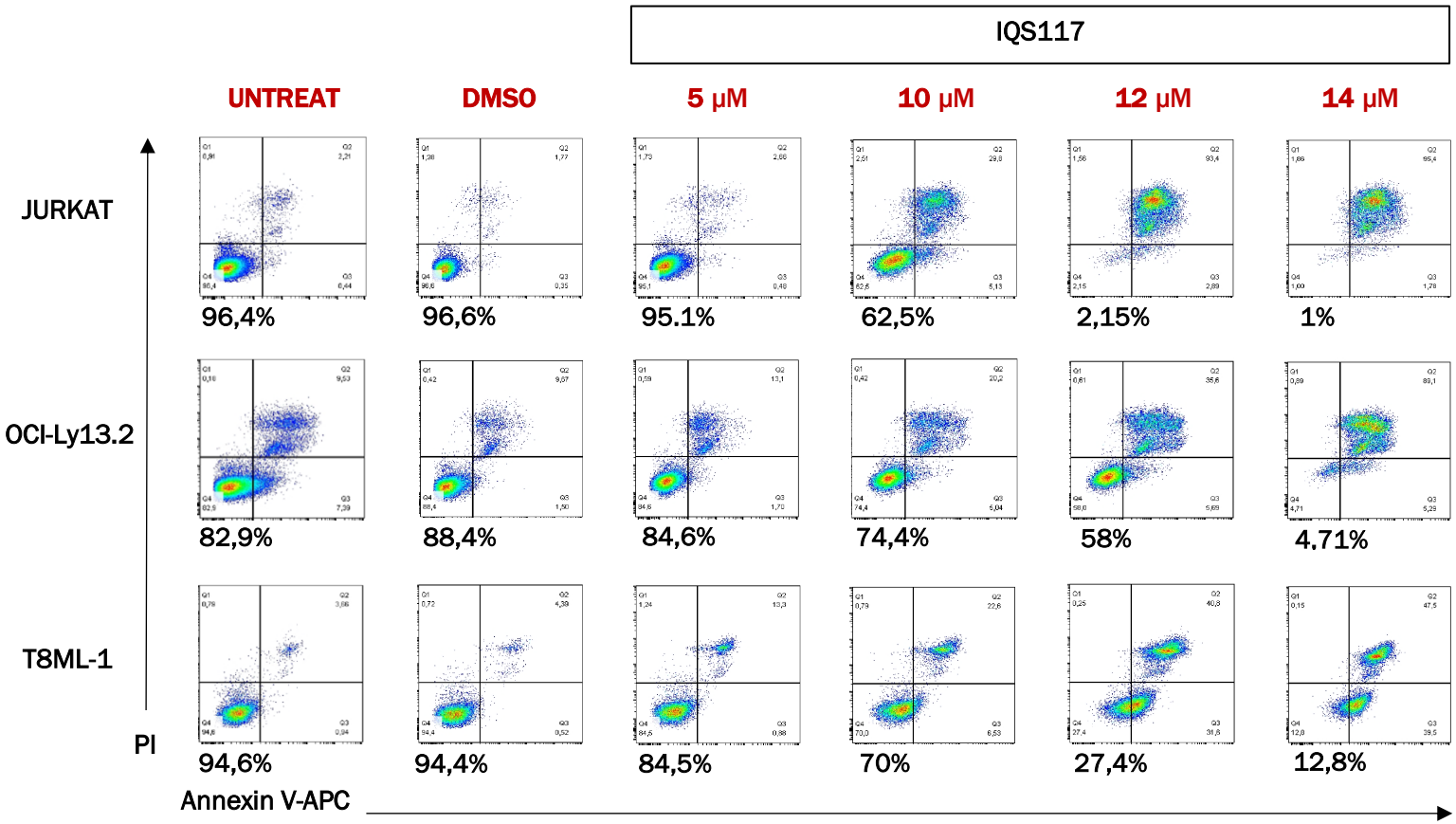

Appendix Figure 1. IQS141 dose-dependently inhibited malignant T-cells viability. Representative flow cytometry analysis demonstrating the effect of increasing doses of IQS141 on the viability of malignant T-cell lines after 48 h of treatment. Viable cells were identified as Annexin V-negative/PI-negative population.

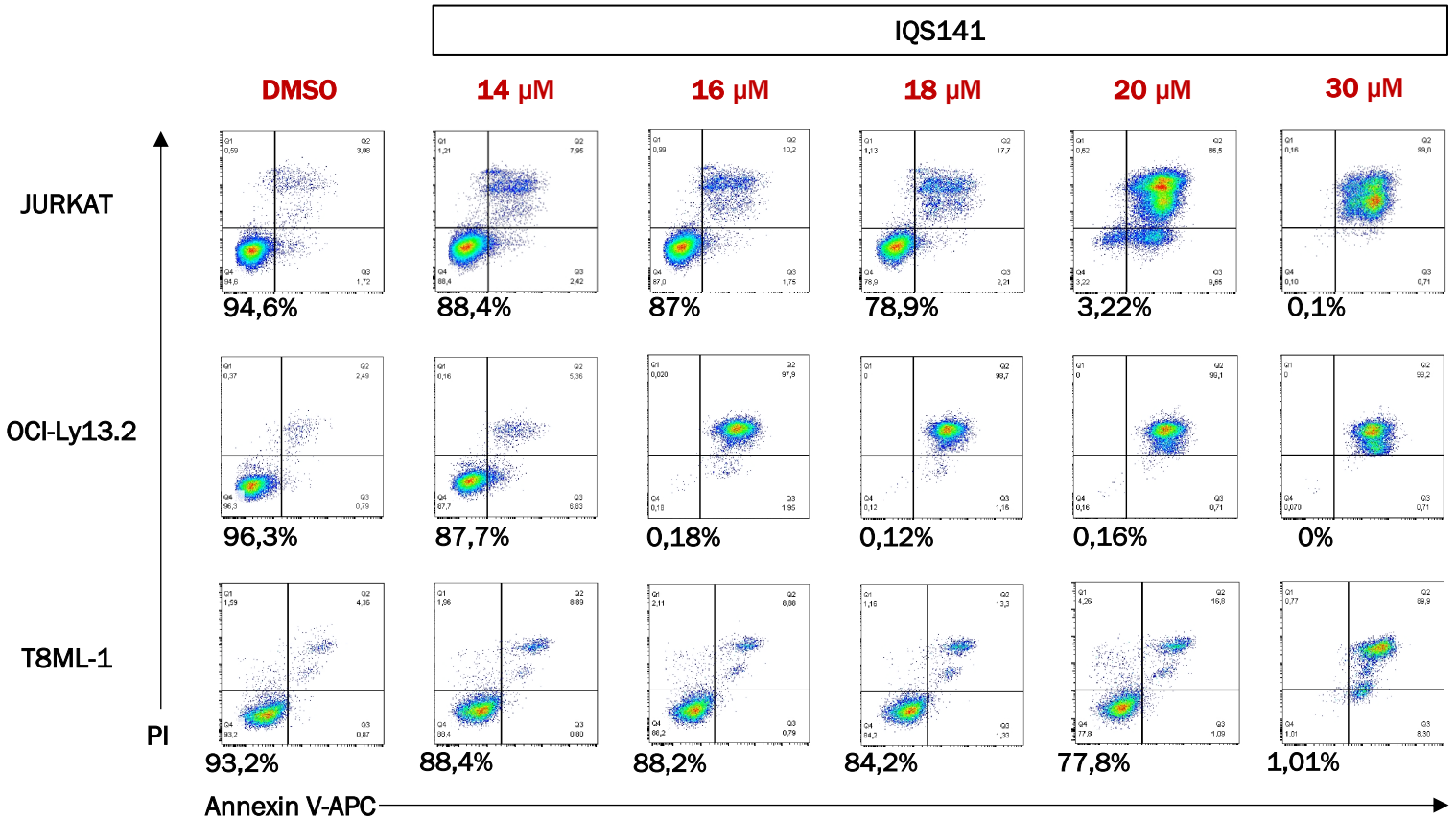

Appendix Figure 2. IQS141 dose-dependently inhibited malignant T-cells viability. Representative flow cytometry analysis demonstrating the effect of increasing doses of IQS141 on the viability of malignant T-cell lines after 48 h of treatment. Viable cells were identified as Annexin V-negative/PI-negative population.